UNIVERSIDADE FEDERAL DO RIO GRANDE DO SUL

INSTITUTO DE PESQUISAS HIDRÁULICAS

Pareamento Bacia - Lagoa usando modelagem hidrológica-hidrodinâmica e sensoriamento remoto

Andrés Mauricio Munar Samboní

Tese submetida ao Programa de Pós-Graduação em Recursos Hídricos e Saneamento Ambiental da Universidade Federal do Rio Grande do Sul como requisito parcial para a obtenção do título de Doutor em Recursos Hídricos e Saneamento Ambiental

Orientador:	**David da Motta-Marques**
Co-Orientadores:	**Carlos Ruberto Fragoso Júnior**
	Juan Martin Bravo

Banca Examinadora

Prof. Dr. Walter Collischonn	Instituto de Pesquisas Hidráulicas - UFRGS
Prof. Dra. Rutinéia Tassi.	Departamento de Engenharia Sanitária e Ambiental - UFSM
Prof. Dra. Marie Paule Bonnet	Institute of Research for Development - IRD/França

Porto Alegre, Dezembro de 2017

Pareamento Bacia - Lagoa usando modelagem hidrológica-hidrodinâmica e sensoriamento remoto

Andrés Mauricio Munar Samboní

Trabalho Aprovado. Porto Alegre, Dezembro de 2017

Banca Examinadora

Prof. Dr. David da Motta-Marques
Orientador

Prof. Dra. Marie Paule Bonnet
IRD/França

Prof. Dr. Carlos Ruberto Fragoso Júnior
Co-Orientador

Prof. Dr. Juan Martin Bravo
Co-Orientador

Prof. Dr. Walter Collischonn
Instituto de Pesquisas Hidráulicas - UFRGS

Prof. Dra. Rutinéia Tassi
Departamento de Engenharia Sanitária e Ambiental - UFSM

Agradecimentos

Registro aqui meus sinceros agradecimentos:

Primeiramente a Deus, que é o maior responsável pela realização deste trabalho.

Aos meus pais, Nelson Munar Penagos e Gloria Mercedes Samboní, pela confiança e apoio incondicional em cada passo que dou. A minha tia, Sandra Patricia Munar Penagos, que sempre me ilumina desde o céu e está sempre do meu lado. Aos meus irmãos Nelson Javier e Laura Camila, avôs, tios, primos e familiares pela confiança e apoio.

Ao meu professor orientador, David da Motta-Marques, por sempre apoiar com entusiasmo e acompanhar de perto o meu trabalho, e pela intensa transmissão de motivação na pesquisa do novo conhecimento. Aos professores Juan Martin Bravo e Carlos Ruberto Fragoso Jr, por serem excelentes professores e co-orientadores, sempre dispostos a conversar e ajudar, e que eu sei que sempre posso contar com eles.

Ao Instituto de Pesquisas Hidráulicas IPH como um todo, e ao Governo Federal na figura da CAPES, que concederam condições, estrutura física e a bolsa de estudo que me permitiram realizar este trabalho.

Aos meus colegas do grupo de pesquisa no IPH durante o período de Doutorado: Daniela, Vinícius, Juliana, Andressa, Mônica, Marla, Luana e especialmente aos meus amigos Rafael e Gláucia pela convivência excelente, por todos os debates e discussões de ideias, e por sempre me apoiar e me ajudar quando eu precisei. Finalmente, a galera de compatriotas colombianos: Nestor, Gabriel, Fernando, Carlos, Huber, Galileo e aos antigos e novos amigos que sempre me apoiam. Nunca serão esquecidos.

Resumo

Pareamento Bacia - Lagoa usando modelagem hidrológica-hidrodinâmica e sensoriamento remoto

Autor: Andrés Mauricio Munar Samboní
Orientadores: David da Motta-Marques, Juan Martin Bravo e C. Ruberto Fragoso Jr

A gestão de recursos hídricos tornou-se cada vez mais complexa devido ao rápido crescimento sócio-econômico e as mudanças ambientais nas bacias hidrográficas nas últimas décadas. Modelos computacionais são importantes ferramentas de suporte na gestão de recursos hídricos e tomada de decisões devido a sua funcionalidade, provendo informações importantes sobre os principais processos físicos, químicos e biológicos, e permitindo melhorar o entendimento desses processos, os quais ocorrem em diferentes escalas espaciais e temporais. Na presente tese, o objetivo foi compreender o funcionamento hidrológico do sistema integrado bacia hidrográfica - lagoa, e os efeitos na hidrodinâmica do lago, utilizando como suporte o acoplamento da modelagem hidrológica - hidrodinâmica, e o uso de técnicas de sensoriamento remoto para o monitoramento de parâmetros de qualidade da água (*e.g.*, clorofila-*a*, temperatura da superfície d'água e níveis da água). A área de estudo é a bacia hidrográfica da Lagoa Mirim, localizada no sul do Brasil, possuindo uma área total de 58.000 km^2 (56% no Uruguai e o restante no Brasil). Foram propostos e testados modelos empíricos para estimativa de clorofila-*a* em um lago raso subtropical, baseados em imagens do sensor MODIS e técnicas estatísticas. Além disso, foi desenvolvido e avaliado o acoplamento da modelagem hidrológica-hidrodinâmica de grande escala e o sensoriamento remoto. O modelo hidrológico distribuído de grande escala MGB-IPH acoplado com o modelo hidrodinâmico IPH-ECO foi utilizado para simular a bacia hidrográfica e os principais componentes hidrodinâmicos da Lagoa Mirim. O modelo mostrou bom desempenho quando comparado com observações de vazões, além de dados provenientes de sensoriamento remoto, através de altimetria espacial.

As simulações mostraram importantes aspectos sobre a estrutura de fluxo, campos de velocidade e níveis d'água na lagoa, assim como a influência de grandes rios, forçantes externas como o vento (intensidade e direção) e o impacto do estressor antrópico (retiradas para irrigação) no sistema. As simulações permitiram avaliar aspectos relacionados com as variações espaciais e temporais (diurna, mensal, sazonal e inter-anual) da temperatura da superfície da água, a dinâmica dos fluxos de calor (sensível e latente) e os efeitos de eventos meteorológicos de pequena escala como frentes frias, os quais têm um impacto significativo sobre a temperatura superficial da água e os fluxos de calor na lagoa. Quanto aos modelos empíricos para estimativa de clorofila-*a* a partir do MODIS, os resultados mostram que um simples e eficiente modelo desenvolvido a partir de análise de regressão múltipla, apresentou ligeiras vantagens sobre os modelos de redes neurais artificiais, modelos multiplicativos não paramétricos e modelos empíricos (*e.g.*, Appel, Kahru, FAI e O14a) usualmente utilizados na estimativa de Chl-*a* em ambientes aquáticos. Resultados também indicam que é inapropriado generalizar um único modelo desenvolvido a partir do conjunto total de dados, para estimar concentrações de Chl-*a* na lagoa, o que corrobora a heterogeneidade espacial na distribuição de Chl-*a* e as diferenças entre regiões (litoral e pelágica). A modelagem hidrológica-hidrodinâmica de grande escala apoiada por informação de sensoriamento remoto, mostrou ser uma abordagem promissora para o entendimento da estrutura e funcionamento de lagoas rasas de grande porte e longo prazo, úteis para a gestão integrada dos recursos hídricos.

Palavras-chave: Modelagem hidrológica - hidrodinâmica, processos hidrológicos, sensoriamento remoto, clorofila-*a*, temperatura superficial d'água, fluxos de calor.

Abstract

Integrating watershed-lake from large scale hydrological-hydrodynamic modeling and remote sensing

Author: Andrés Mauricio Munar Samboní
Advisors: David da Motta-Marques, Juan Martin Bravo e C. Ruberto Fragoso Jr

The last decade, the water resource management is being complex due to the rapid socioeconomic development and environmental changes in river basins. Computations models are important support tools in water resource management and make decision providing important information and allowing a better comprehension of the physical, chemical and biologic processes, which occur in different temporal/spatial scales. In this thesis, the objective was to understand the hydrological functioning of the integrated basin- lake system and its effects on hydrodynamics, using hydrodynamic - hydrodynamic modeling and water quality monitoring (*e.g.,* chlorophyll-*a*, water surface temperature and water levels) from remote sensing techniques. The study area is the Lake Mirim basin, located between Brazil and Uruguay (basin total area 58.000 km^2). Empirical models were proposed and tested to chlorophyll-*a* estimation in a shallow subtropical lake, based on MODIS imagery and statistics techniques. In addition, we developed and assessed the coupling of large scale hydrological/hydrodynamic modeling and remote sensing techniques. The large-scale distributed hydrological model MGB-IPH coupled with the hydrodynamic model IPH-ECO were used to simulate the river basin and the hydrodynamic components of the Lake Mirim. The coupled model showed good performance when compared to *in-situ* measurements and satellite altimetry data. The simulations showed important aspects relate to flow structure, velocity fields and lake water levels, as well as the influence of large rivers, external forcing as such the wind (intensity and direction), and the impact of anthropogenic stressors (irrigation withdrawals) in the system. The simulations allowed assessing the spatial and temporal variations (diurnal, monthly, seasonal and

inter-annual) in the water surface temperature, heat fluxes dynamics (sensible and latent) and the effects of short time-scale events, as such cold fronts passages over the lake, which cause strong impacts on the water surface temperature and heat fluxes in the lake. Regarding the empirical models developed to chlorophyll-*a* estimation from MODIS imagery, the results showed that a simple and efficient model developed from multiple regression analysis, performed best in comparison with artificial neural network models, non-parametric multiplicative models, and empirical models (*e.g.*, Appel, Kahru, FAI and O14a) common used in the Chl-*a* estimation in aquatics environments. Results also indicated that is inappropriate to generalize a single model developed from the total datasets to estimates Chl-*a* in the lake, which corroborates the spatial heterogeneity (Chl-*a* distribution) and the differences among regions (littoral and pelagic). The synergy between large-scale hydrological-hydrodynamic modeling, *in situ* measurements and remote sensing techniques provided a promising approach to improve the comprehension of the structure and ecosystem functioning of large shallow lakes in long-term time scale, useful to water resources management.

Keywords: Hydrological/hydrodynamic modeling, Hydrological processes, Clorofila-*a*, Water surface temperature, Heat fluxes, Remote Sensing techniques.

Lista de siglas

ALM - Agência da Lagoa Mirim

ANA - Agência Nacional de Águas

AVHRR - Advanced Very High Resolution Radiometer

ASTER - Advanced Spaceborne Thermal Emission and Reflection Radiometer

CAPES - Coordenação de Aperfeiçoamento de Pessoal de Nível Superior

CNPq - Conselho Nacional de Desenvolvimento Cientifico e Tecnológico

CPTEC - Centro de Previsão do Tempo e Estudos Climáticos

DEM - Digital Elevation Model

ESA- European Space Agency

ENVISAT- Environmental Satellite

GLEON - Global Lake Ecological Observatory Network

ICESat - Ice, Cloud, and Land Elevation Satellite

INIA - Instituto Nacional de Investigación Agropecuaria

INMET - Instituto Nacional de Meteorologia

INPE - Instituto de Pesquisas Espaciais

INUMET - Instituto Uruguayo de Meteorología

IPH - Instituto de Pesquisas Hidráulicas

IPH - ECO - Modelo Hidrodinâmico para ecossistemas aquáticos

IRGA - Instituto Rio Grandense do Arroz

MERIS - Medium Resolution Imaging Spectrometer

MGAP - Ministerio de Ganaderia, Agricultura y Pesca

MODIS - Moderate- Resolution Imaging Spectroradiometer

MC - Muskingum Cunge model

MGB-IPH - Modelo Hidrológico de Grandes Bacias

NASA - National Aeronautics and Space Administration

OLCI - Ocean and Land Colour Instrument

SEMA - Secretaria Estadual do Meio Ambiente do Rio Grande do Sul

TRMM - Tropical Rainfall Measurement Mission

UFRGS - Universidade Federal do Rio Grande do Sul

USGS - US Geological Survey

Sumário

Capítulo 1

Introdução

Nos últimos anos, o impacto da mudança climática e as atividades antrópicas sobre os recursos naturais têm causado fortes alterações nos fluxos de matéria e energia. As mudanças referidas ao ciclo hidrológico ameaçam a segurança hídrica causando alterações no comportamento dos padrões de precipitação (aumento da intensidade e da variabilidade) e a disponibilidade hídrica (Stocker et al., 2013). Esses impactos nos ecossistemas aquáticos como lagos e reservatórios, provocam efeitos nas características físicas, incluindo níveis da água, regimes de estratificação e mistura, e na qualidade da água (alterações no ciclagem de nutrientes) (Nickus et al., 2010). Embora exista a necessidade de abordagens multidisciplinares e novas ferramentas de gestão que auxiliem a conservação e o monitoramento desses recursos (Kragt et al., 2013), a complexidade dos processos envolvidos e as características multidisciplinares dos problemas requer abordagens integradas e ferramentas robustas.

Modelos hidrológicos acoplados com modelos hidrodinâmicos constituem uma importante ferramenta para avaliar simultaneamente o sistema bacia-lago, permitindo analisar a resposta do lago diante de diferentes usos, ajudando no entendimento da dinâmica, estrutura, funcionamento e monitoramento desses recursos. A partir dessa abordagem integrada, é possível representar melhor a hidrologia das bacias de contribuição e a resposta do lago nas diferentes variáveis hidrodinâmicas (*e,g.,* níveis da água, campos de velocidade, estrutura de fluxo) e na qualidade da água (Dargahi and Setegn, 2011; Guzman et al., 2015).

Paralelamente às ferramentas de modelagem hidrológica/hidrodinâmica, têm se desenvolvido um grande número de técnicas de sensoriamento remoto para observação de variáveis hidrológicas e monitoramento de parâmetros de qualidade da água, permitindo o monitoramento de grandes áreas remotas (Alsdorf et al., 2007), com uma cobertura espaço-temporal superior as observações *in situ*. Essas técnicas fornecem importantes fontes de dados complementares para calibrar e validar modelos hidrológicos/hidrodinâmicos e de qualidade da água em áreas pouco monitoradas ou regiões com acesso limitado aos dados.

Na primeira parte deste capítulo será abordada a integração entre bacia hidrográfica e lagoa, usando o acoplamento entre modelagem hidrológica de grande escala e modelagem hidrodinâmica/qualidade de água. Na segunda parte será abordada a utilização do sensoriamento remoto no monitoramento de parâmetros de qualidade da água como clorofila-*a* e temperatura da superfície da água em um grande lago raso subtropical.

1.1 Pareamento Bacia Hidrográfica - Lagoa

A avaliação simultânea dos processos envolvidos na geração de escoamento superficial proveniente das bacias hidrográficas e o funcionamento de lagos e reservatórios é complexa, em função de cada processo ocorrer em diferentes escalas espaciais e temporais. Forçantes hidrológicas como as descargas dos rios (Fig. 1) e forçantes externas como o vento (intensidade e direção) (Fig. 2) podem influenciar o comportamento de lagos e reservatórios, provocando alterações na hidrodinâmica (Miranda, 2002).

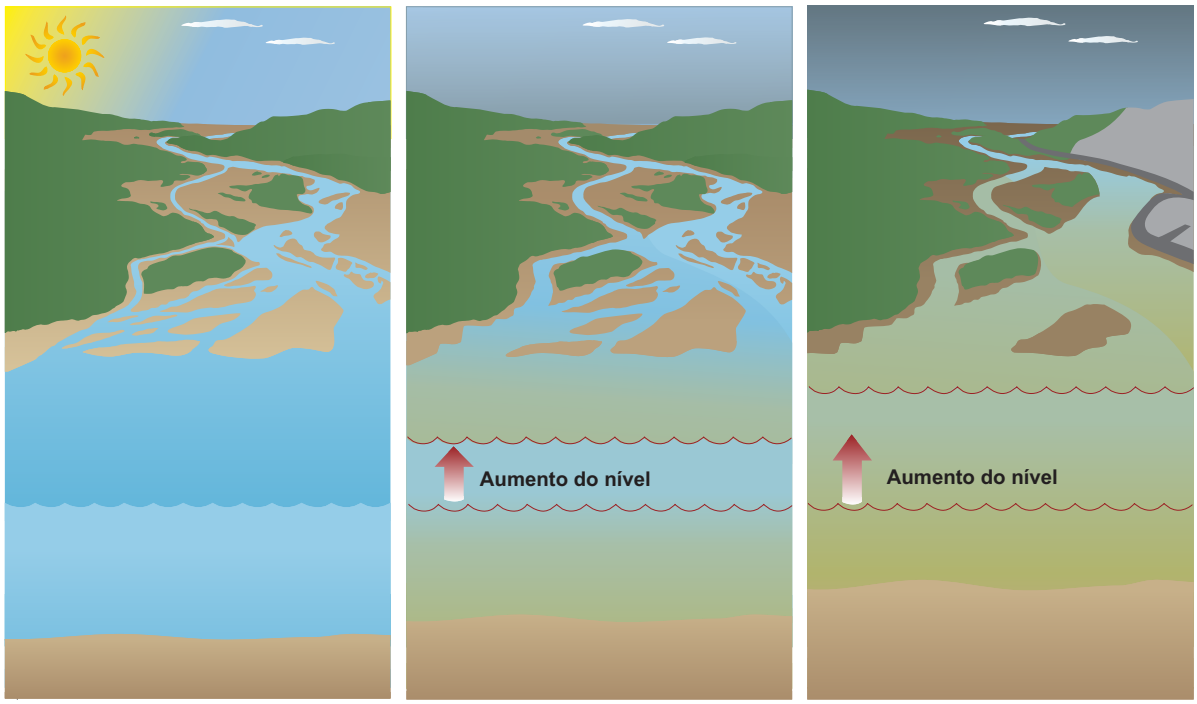

(a) (b) (c)

Figura 1 – Comparação da entrada de um rio em um lago, mostrando um ambiente limpo **(a)**, e um ambiente com entrada sedimentos, nutrientes e toxinas **(b)** que levam a um ambiente insalubre e improdutivo com alta carga de sedimentos e aumento nos níveis d'água **(c)**

A influência da descarga fluvial sobre lagos e reservatórios em grandes escalas de tempo (meses e anos) é um fator importante que regula os níveis d'água, sendo ainda responsável pelo aporte de sedimentos, provocando alterações na produção primária

e na qualidade da água desses ecossistemas (Fig. 1) (Dronkers, 1996; Uncles and Stephens, 1996). As descargas pluviais influenciam nos padrões de circulação e mistura desses ecossistemas e desempenham um papel importante no clima regional e local (Dessie et al., 2015). A influência das descargas fluviais também pode ser observada no controle da circulação residual, provocando padrões espaciais e temporais que refletem nos processos de transporte, estratificação e cisalhamento na coluna d'água (Jay, 1990; Kuo et al., 1990).

Da mesma forma, o vento como principal fonte de energia cinética, controla a troca de processos entre as regiões litorânea e pelágica de ecossistemas lênticos (Fig. 2). Em ambientes rasos e costeiros, o vento influencia nos processos de resfriamento e aquecimento, podendo causar alterações em toda a coluna d'água (Panosso et al., 1998).

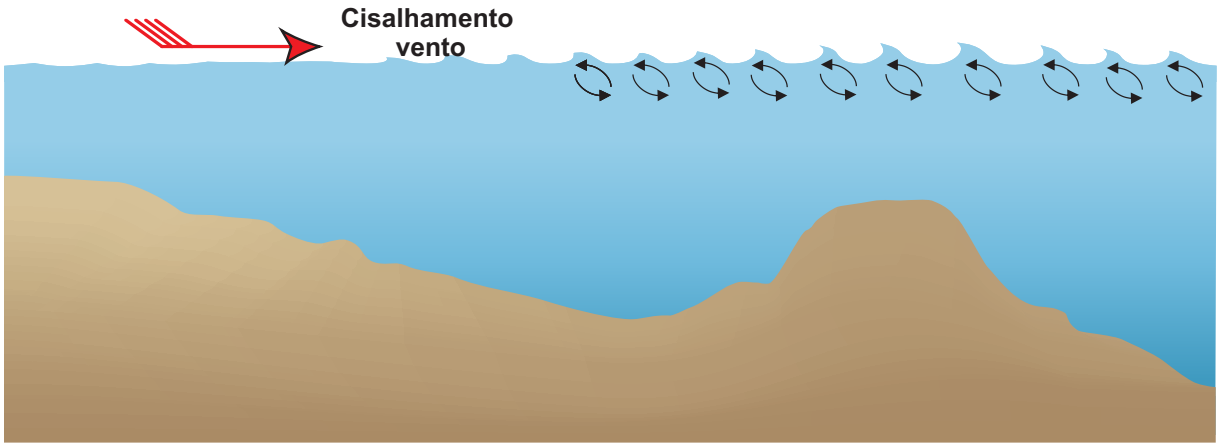

Figura 2 – Efeito do vento na dinâmica e circulação da água de lagos e reservatórios. As setas indicam os movimentos da massa d'água.

O vento age sobre o sistema causando movimentos da massa d'água, tais como as correntes de densidade, circulação e ondas de superfície, ressurgências, correntes turbulentas, ondas internas, entranhamento, entre outros (Hutter et al., 2010). Além disso, durante a ação constante do vento, a superfície do corpo d'água tende a inclinar-se na direção do vento, ocasionando um desnível que depende da intensidade do vento, da profundidade e do comprimento do corpo d'água (Martin and McCutcheon, 1998). Quando o vento diminui sua intensidade, a superfície do corpo d'água volta a seu estado de repouso, gerando a oscilação da superfície d'água.

Neste sentido, o conhecimento quantitativo dos processos hidrológicos da ligação bacia - lagoa e das forçantes hidrológicas e externas torna-se importante para dar suporte a uma melhor compreensão do funcionamento desse ecossistemas.

1.1.1 Modelagem Hidrológica - Hidrodinâmica

Modelos matemáticos são importantes ferramentas de suporte na gestão e qualidade da água de ecossistemas aquáticos permitindo uma melhor compreensão dos processos físicos, químicos e biológicos envolvidos (Ji, 2017). A modelagem hidrológica constitui uma ferramenta indispensável para auxiliar a compreensão dos processos hidrológicos e sua relação com outros processos geofísicos, assim como dar suporte a Sistemas de Previsão Hidrológica visando à redução da vulnerabilidade da população local à eventos extremos. Diversos modelos hidrológicos vêm sendo utilizados para avaliar a resposta das bacia hidrográficas diante de alterações, permitindo estudar as relações entre a quantidade e a qualidade da água escoada em uma bacia em diferentes escalas, e o comportamento da bacia frente a diversos impactos (e.g., mudanças no uso do solo e cobertura vegetal, atividades humanas, mudança climática). Contudo, a maioria desses modelos carecem da capacidade para simular integradamente os processos hidrológicos e a hidrodinâmica/qualidade da água em grandes corpos de água.

Numerosos modelos hidrodinâmicos e de qualidade de água, tais como MIKE21 (Warren and Bach, 1992), GEMSS (ERM, 2006), CE-QUAL-W2 (Cole and Wells, 2006), WASP (Wool et al., 2006) e EPD-RIV1 (Martin et al., 2002) têm sido usados para analisar a hidrodinâmica e os processos de qualidade da água apenas em grandes corpos de água, sem levar em conta o que ocorre na bacia hidrográfica, onde a maioria dos processos são iniciados (EPA, 2000). Embora não exista um único modelo disponível que conte com a capacidade de simular simultaneamente processos hidrológicos - hidrodinâmicos em bacias hidrográficas e grandes corpos de água, existem abordagens que permitem realizar o acoplamento entre modelos hidrológicos e hidrodinâmicos. Uma alternativa é o acoplamento *offline* (Bravo et al., 2011), o qual permite a utilização do escoamento superficial gerado no modelo hidrológico como dado de entrada para o modelo hidrodinâmico. Uma vez realizado o acoplamento é possível avaliar diferentes cenários de mudança da bacia hidrográfica, e simular as respectivas respostas no ecossistema aquático.

A integração de modelos hidrológicos com modelos hidrodinâmicos permite uma melhor compreensão do comportamento integrado bacia - lagoa, servindo de base na melhora da representação do impacto da hidrologia da bacia e os efeitos na lagoa (*i.e.*, padrões hidrodinâmicos, regime de mistura, importância da descarga fluvial no balanco hídrico da lagoa). Esta representação complementa o entendimento dos processos físicos, químicos e biológicos desses ecossistemas, permitindo a possibilidade de simular cenários reais e hipotéticos. No entanto, uma das desvantagens da integração de modelos hidrológicos com modelos hidrodinâmicos, reside na grande quantidade de dados e parâmetros de entrada requeridos, que são limitados na maioria dos casos (Bonnet and Wessen, 2001; Dias et al., 2009), especialmente em países desenvolvidos, nos quais os dados hidrológicos não são de livre acesso (Chipman and Lillesand, 2007).

Neste contexto, os dados provenientes de sensoriamento remoto surgem como uma alternativa para obter informação em locais com escassez de dados ou em regiões não monitoradas (Alsdorf et al., 2007; Calmant et al., 2008).

Recentes estudos tem acoplado modelos hidrológicos de base física com modelos hidrodinâmicos em lagos e reservatórios (Dargahi and Setegn, 2011; Debele et al., 2008; Li et al., 2013; Xu et al., 2007), principalmente para avaliar a complexidade dos processos hidrológicos que ocorrem na bacia e os efeitos no comportamento hidrodinâmico do lago, assim como o efeito das transformações bióticas e abióticas de nutrientes que ocorrem ao longo da água, desde a precipitação até seu armazenamento. Outros estudos têm avaliado o impacto de eventos meteorológicos de pequena escala, como a passagem de sistemas frontais (*e.g.* frentes frias) sobre lagos e reservatórios (Curtarelli et al., 2015, 2014), os quais causam alterações nos processos físicos que ocorrem na coluna da água. No entanto, a maioria desses estudos são limitados devido ao curto período de análise utilizado (*e.g.,* meses) (Dargahi and Setegn, 2011) impossibilitando avaliar diferentes aspectos como dinâmica sazonal nos níveis da água do lago, potenciais efeitos da mudança no uso do solo e cobertura vegetal da bacia e o efeito das descargas pluviais na lagoa. Apesar dos esforços que têm sido realizados para a integração de modelos hidrológicos e hidrodinâmicos em lagos e reservatórios, ainda é requerido o desenvolvimento de novas abordagens de simulação, que inclua a verificação do papel de diferentes processos hidrológicos em grande escala e seu efeito no comportamento hidrodinâmico do lago em longo prazo (*e.g.,* variações sazonais e inter-anuais dos níveis da água, efeito das descargas pluviais). Adicionalmente, essas abordagens permitiriam avaliar impactos de forçantes externas tais como o vento (intensidade e direção) e estressores antropogênicos (retiradas da água para irrigação) no comportamento do lago, assim como o impacto de eventos meteorológicos de pequena escala (*e.g.* frentes frias).

1.2 Sensoriamento remoto da qualidade da água: estimativa de clorofila-*a* e temperatura superficial em lagos

O monitoramento e avaliação da qualidade da água é fundamental para a gestão, manutenção e gerenciamento dos recursos hídricos. Ao mesmo tempo, o monitoramento usando abordagens convencionais tende a ser limitado em termos de cobertura espacial e frequência temporal (*e.g.*, amostragens pontuais em intervalos mensais ou trimestrais). O sensoriamento remoto tem o potencial para prover uma importante fonte complementar de dados em escalas locais e globais (*e.g.*, amostragens em grande escala espacial em intervalos diários). Técnicas de sensoriamento remoto

podem ser usadas no monitoramento de parâmetros de qualidade de água (*e.g.*, sólidos suspensos (turbidez), clorofila-*a* e temperatura). Essas técnicas são baseadas no principio que a água absorve/espalha a radiação incidente proveniente do sol na coluna d'água (Fig. 3), em função da irradiância do sol e da atmosfera recebida.

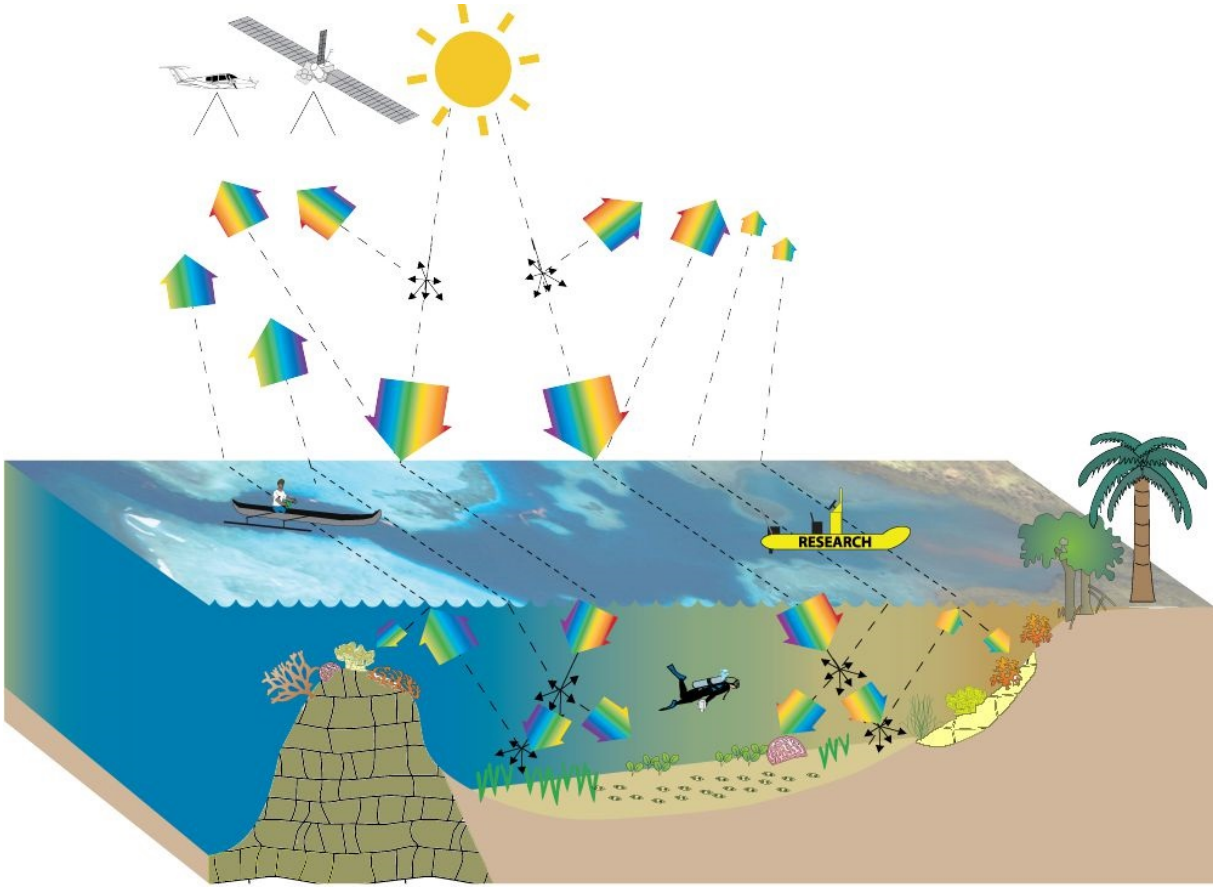

Figura 3 – Interações da luz no monitoramento da qualidade da água através de sensoriamento remoto. As setas coloridas representam a radiação solar, e as interações com a atmosfera, a coluna d'água e o bênton. As mudanças na largura das setas indicam a quantidade de radiação sendo transmitida. Extraído de Longstaff and Nauman (2010)

A radiância total ascendente saindo de um corpo d'água (L_t, eq. 1) depende da radiância de espalhamento atmosférico (L_p), da radiância da superfície da água (L_s), da radiância volumétrica (L_v) e da radiância do fundo do corpo da água (L_b) (Jensen, 2009).

$$L_T = L_p + L_s + L_v + L_b \tag{1}$$

Por outro lado, a radiância volumétrica (L_v, eq. 2) , é uma função da água em estado puro ($W_{c(\lambda)}$), dos sedimentos em suspensão ($S_{M(\lambda)}$), da clorofila-*a* ($Chl_{c(\lambda)}$) e da matéria orgânica dissolvida ($DOM_{c(\lambda)}$).

$$L_v(\lambda) = f(W_{c(\lambda)}, S_{M(\lambda)}, Chl_{c(\lambda)}, DOM_{c(\lambda)}) \tag{2}$$

Um importante parâmetro utilizado no monitoramento da qualidade da água é a clorofila-*a* (Chl-*a*), pois além de ser um indicador de biomassa fitoplanctônica é o compontente opticamente ativo mais útil na avaliação do estado trófico em ecossistemas aquáticos (Carlson, 1977; Huot et al., 2007; Schalles, 2006). Porém, a estimativa de Chl-*a* através de técnicas de sensoriamento remoto é complexa, uma vez que a reflectância da Chl-*a* tem diferentes comportamentos em função da concentração de partículas em suspensão (Fig. 4), atingindo o pico máximo de reflectância entre 690-700 nm (Jensen, 2009).

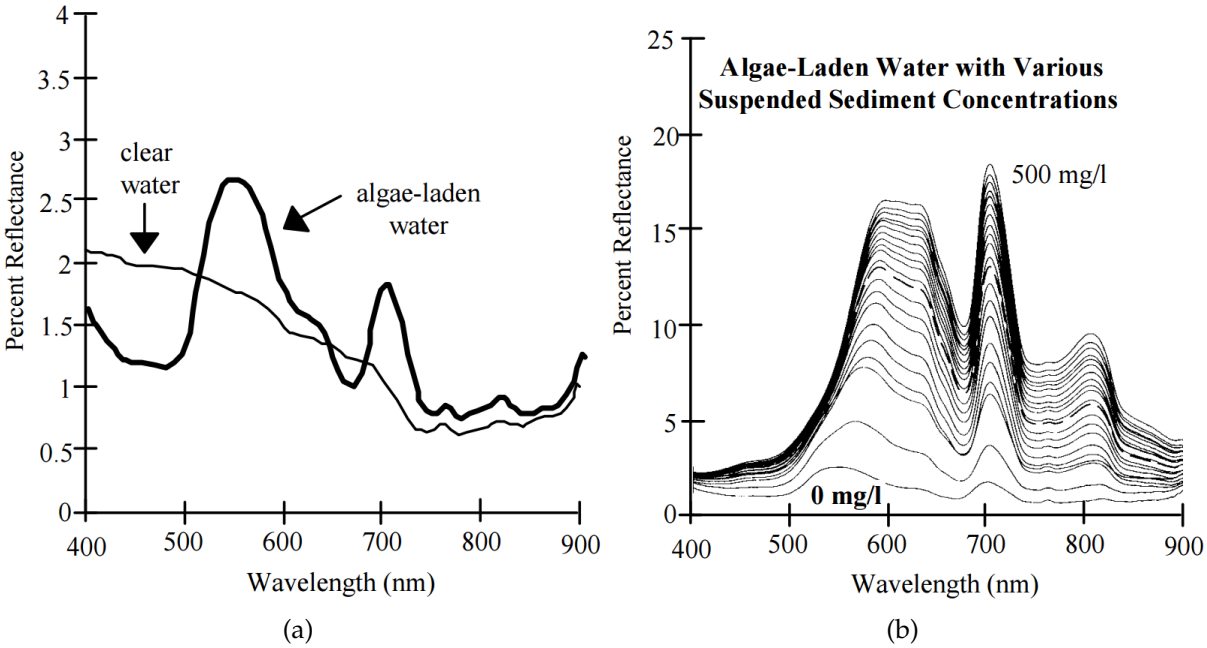

Figura 4 – **(a)** Percentagem de reflectância de água clara e de água com algas com base em medidas *in situ* realizadas com um espectroradiômetro. **(b)** Percentagem de reflectância de água com algas e com várias concentrações de sedimentos em suspensão variando de 0-500mg/L (Jensen, 2009)

Tradicionalmente, métodos convencionais de monitoramento de clorofila-*a* e temperatura d'água envolvem medições *in-situ* e análise de laboratório, gerando informações limitadas em termos de variabilidade e cobertura espaço-temporal, necessitando de tempo e gerando custos elevados. Nesse contexto, o uso do sensoriamento remoto surge como opção para avaliar padrões espaciais e temporais, normalmente não obtidos usando métodos convencionais (Olmanson et al., 2011), constituindo-se uma ferramenta valiosa para o monitoramento em grande escala.

Diversas técnicas de sensoriamento remoto tem sido amplamente utilizadas no monitoramento de clorofila-*a* em lagos e reservatórios, particularmente utilizando imagens do satélite Landsat (Allan et al., 2015; Tebbs et al., 2013) e Hyperion (Giardino et al., 2007). Recentemente, novos sensores, tais como o MERIS (*Medium Resolution Imaging Spectrometer*) e o MODIS (*Moderate- Resolution Imaging Spectroradiometer*), tem sido utilizados satisfatoriamente no monitoramento da concentração de clorofila-*a*, por

possuírem boa resolução espectral e temporal, com bandas específicas para predição de clorofila-*a*. O MERIS é mais voltado para a estimativa da clorofila-*a* principalmente em águas oceânicas e costeiras, mas tem sido aplicado com sucesso em lagos (e.g. Olmanson et al., 2011; Ruiz-Verdú et al., 2008; Wynne et al., 2013). Embora o sensor tenha saído de operação, espera-se sua continuidade em futuras missões (*e.g.*, Sentinel-3 - OLCI (*Ocean and Land Colour Instrument*) da ESA (*European Space Agency*). Entretanto, o MERIS possui como principal desvantagem o fato de que nem todos os dados são disponibilizados gratuitamente.

O sensor MODIS, a bordo dos satélites da NASA: Terra e Aqua, vem sendo utilizado satisfatoriamente na estimativa de Chl-*a* em diversos lagos (e.g. Bergamino et al., 2010; Chavula et al., 2009; Chen and Quan, 2013). O sensor se destaca por produzir imagens com alta resolução temporal (diárias) e de acesso gratuito, com informações adequadas à predição da concentração de clorofila-*a*. O satélite Terra está programado para passar de norte a sul cruzando o Equador às 10:30h em sua órbita descendente, enquanto que, o satélite Aqua passa de sul a norte cruzando o Equador às 13:30h (Fig. 5). O MODIS produz informações em 36 bandas espectrais entre 0.405 μm e 14.385 μm, incluindo 7 bandas espectrais desenhadas para a cobertura do solo, 7 bandas para a cor do oceano, e outras 22 bandas espectrais para a atmosfera.

(a) (b)

Figura 5 – **(a)** Sensores MODIS a bordo dos satélites Terra e Aqua (`http://climate.nasa.gov/nasa_role/`). **(b)** Sistema de escaneio do sensor MODIS-Aqua (`http://sos.noaa.gov/images/atmosphere/`)

Nos últimos anos, vem crescendo o uso de diferentes bandas espectrais do sensor MODIS para estimar Chl-*a* em lagos e reservatórios, sendo possível observar diferentes modelos empíricos utilizados para este fim (El-Alem et al., 2012; Huang et al., 2014; Wang et al., 2011). Contudo, os parâmetros de cada modelo empírico são ajustados

usando dados *in-situ* de locais específicos, podendo variar os constituintes bio-óticos presentes no corpo hídrico, limitando seu uso em outros locais.

A avaliação da temperatura da água, assim como a Clorofila-*a*, é essencial para o entendimento da dinâmica dos ecossistemas aquáticos, uma vez que é um parâmetro que condiciona as funções dos organismos, a manutenção ecológica, e que pode controlar o clima regional (Austin and Colman, 2007; Burnett et al., 2003; Horne and Glodman, 1994).

Nas últimas décadas, o sensoriamento remoto, vem sendo usado como uma alternativa para o monitoramento da temperatura superficial d'água, apresentando um grande potencial para complementar o monitoramento convencional de lagos e reservatórios (Bukata, 2013). Diversas técnicas de sensoriamento remoto tem sido utilizadas na estimativa da temperatura da superfície d'água, usando imagens AVHRR (*Advanced Very High Resolution Radiometer*) (Wooster et al., 2001), imagens ASTER (*Advanced Spaceborne Thermal Emission and Reflection Radiometer*) e imagens Landsat ETM+ (*Enhanced Thematic Mapper Plus*) (Steissberg et al., 2005). Esses estudos disponibilizaram informações importantes para o desenvolvimento de novas estratégias para o gerenciamento desses ecossistemas, no entanto com algumas limitações nas resoluções espaciais, espectrais, radiométricas e temporais.

Estudos mais recentes têm usado o sensor MODIS na estimativa da temperatura da superfície da água em lagos (Alcântara et al., 2010; Crosman and Horel, 2009; Ke and Song, 2014; Liu et al., 2015; Rolim et al., 2015; Sima et al., 2013; Xiao et al., 2013; Zhang et al., 2014), e seus resultados demostram que a temperatura estimada a partir do MODIS, se ajusta bem com a temperatura observada na superfície.

O sensoriamento remoto usado para estimar parâmetros de qualidade de água (*e.g.*, Clorofila-*a* e temperatura da superfície d'água), pode ser utilizado na calibração e validação de modelos hidrodinâmicos e de qualidade da água integrados. Esta proposta permite investigar os erros dos modelos com dados em alta frequência e boa resolução espacial.

1.3 Objetivos

O objetivo desta tese de doutorado é contribuir para o entendimento do funcionamento hidrológico do sistema integrado da bacia hidrográfica da Lagoa Mirim e os efeitos na hidrodinâmica e na qualidade d'água, utilizando como suporte o acoplamento da modelagem hidrológica - hidrodinâmica em grande escala e o monitoramento de parâmetros de qualidade da água (*e.g.* clorofila-*a* e temperatura da superfície d'água) através de técnicas de sensoriamento remoto. Desta forma, este trabalho buscou avaliar a integração dessa abordagem para a compreensão dos fatores que influenciam o comportamento e hidrodinâmica de uma lagoa subtropical e sua

relação com as contribuições da bacia hidrográfica, em termos de vazão e os processos hidrológicos dominantes.

Mais especificamente, esta pesquisa visa:

- ❏ Analisar os efeitos de forçantes hidrológicas como as descargas dos rios e fatores externos como o vento e as retiradas de água no comportamento das principais variáveis hidrodinâmicas (níveis d'água e campos de velocidade) da Lagoa Mirim.
- ❏ Estudar as variações espaciais e temporais (diurna, mensal, sazonal e inter-anual) da temperatura da superfície d'água e os fluxos de calor (latente e sensível) da Lagoa Mirim, acoplamento modelagem hidrológica - hidrodinâmica de grande escala e técnicas de sensoriamento remoto.
- ❏ Avaliar o efeito de eventos meteorológicos de pequena escala (*e.g.,* passagem de frentes frias) sobre a temperatura da superfície da água e os fluxos de calor latente e calor sensível na Lagoa Mirim.
- ❏ Desenvolver e comparar modelos empíricos multivariados para estimativa de clorofila-*a* em um lago raso subtropical, mediante o uso de técnicas de sensoriamento remoto.

Os objetivos citados estão contidos nas seguintes questões científicas:

- Qual é a influência dos rios afluentes, as retiradas de água e forçantes externas como o vento, no comportamento do sistema integrado Bacia - Lagoa e como eles podem alterar a hidrodinâmica da lagoa? (Capítulo 2)
- A modelagem hidrológica - hidrodinâmica de grande escala poderia representar o comportamento do sistema nas diferentes variáveis hidrológicas (vazões, níveis d'água) se comparado com observações *in-situ* e dados oriundos de sensoriamento remoto? (Capítulo 2)
- Como é o desempenho do modelo hidrológico - hidrodinâmico de grande escala quando simulada a temperatura da superfície d'água versus as estimativas provenientes de sensoriamento remoto? (Capítulo 3)
- Como é a dinâmica da temperatura da superfície d'água e os fluxos de calor (latente e sensível) da Lagoa Mirim e sua variabilidade espacial e temporal (diurna, mensal, sazonal e inter-anual) (Capítulo 3)?
- Será que eventos meteorológicos de pequena escala como a passagem de sistemas frontais (*e.g.* frentes frias) poderiam influenciar a dinâmica da temperatura da água e os fluxos de calor (sensível latente) no sistema? (Capítulo 3)
- É possível desenvolver modelos empíricos para estimar concentrações de clorofila-*a* em um lago raso subtropical através de técnicas de sensoriamento

remoto? Como seria a acurácia desses modelos, quando comparados com modelos comumente utilizados? (Capítulo 4)

1.4 Organização da Tese

Com o propósito de responder aos objetivos da tese, foram delineados capítulos ou manuscritos em forma de artigos. Na Figura 6 se apresenta uma visão geral dos temas abordados em cada capítulo e a relação entre eles.

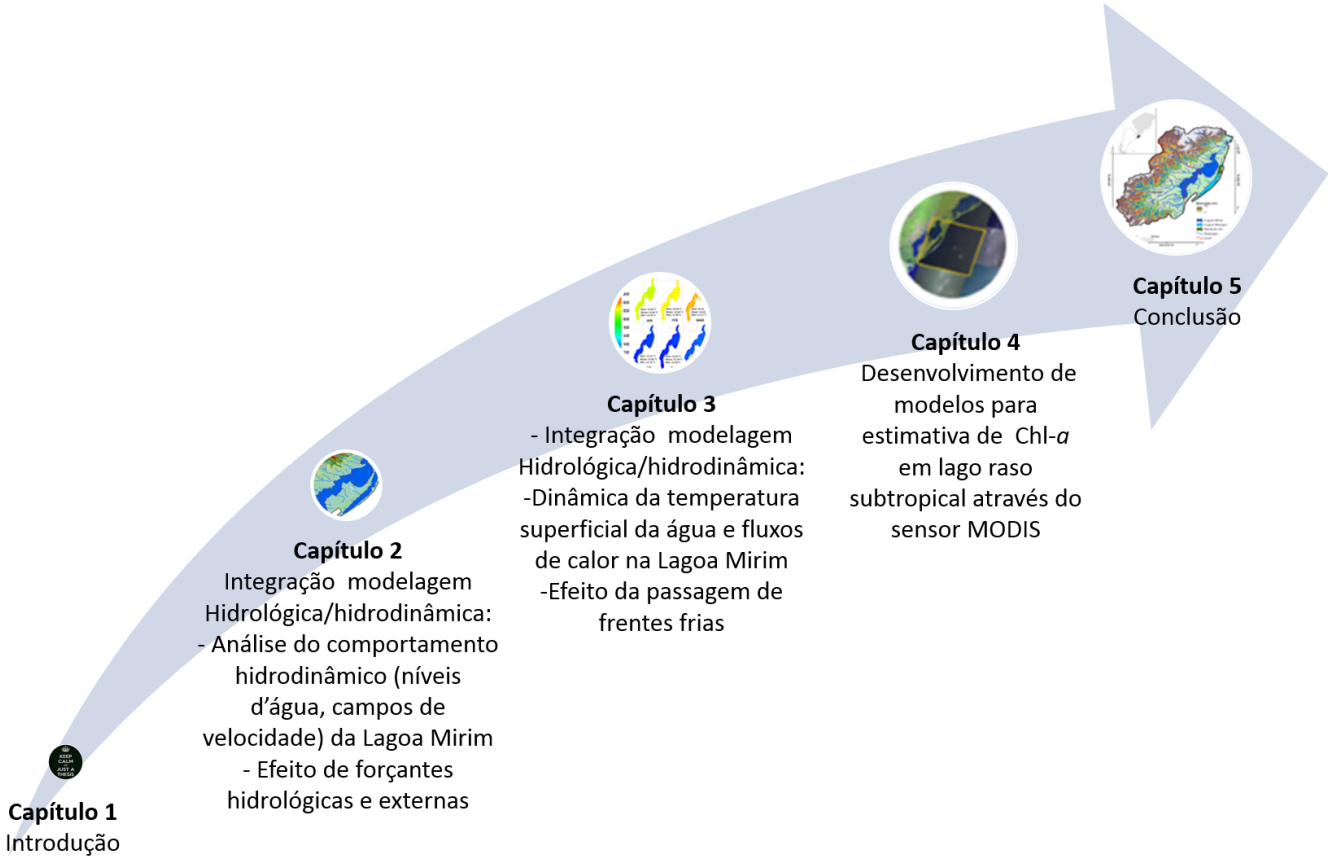

Figura 6 – Visão geral e relação entre temas abordados em cada capítulo da tese.

Baseado na figura anterior, se apresenta a seguir um delineamento de cada capítulo:

Capítulo 2. Pareamento Bacia - Lagoa: Modelagem hidrológica - hidrodinâmica da Lagoa Mirim. Neste capítulo são apresentados os resultados e discussões da integração de um modelo hidrológico de grande escala com um modelo hidrodinâmico. O objetivo deste estudo foi analisar de maneira integrada o comportamento hidrológico do sistema e avaliar os efeitos dos rios afluentes, as retiradas de água e a influência de

forçantes externas como o vento na hidrodinâmica da Lagoa.

Capítulo 3. Dinâmica da temperatura da superfície d'água na Lagoa Mirim integrando modelagem hidrológica - hidrodinâmica e dados MODIS LST. Este capítulo visa estudar a variabilidade espacial e temporal (diurna, mensal, sazonal e inter-anual) da temperatura da superfície d'água e os fluxos de calor, sob distintas condições meteorológicas (*e.g.* passagem de frentes frias) na Lagoa Mirim, acoplando modelagem hidrológica - hidrodinâmica de grande escala e validando com observações *in-situ* e estimativas de sensoriamento remoto.

Capítulo 4. Estimando concentrações de clorofila-*a* em um grande lago raso subtropical através de dados MODIS. Neste capítulo são apresentados os resultados e discussões da aplicação de modelos de regressão linear múltipla (MLR), redes neurais artificiais (ANN), regressão multiplicativa não paramétrica (NPMR) e quatro algoritmos empíricos (Appel, Kahru, FAI e O14a) para estimar concentrações de clorofila-*a* usando distintas combinações de bandas espectrais do sensor MODIS.

Capítulo 5. Conclusão. Neste capítulo é apresentada a conclusão geral da tese, dando resposta às questões científicas específicas propostas nos objetivos do trabalho.

No Apêndice A é feita uma breve descrição do modelo MGB-IPH, seus processos representados e algumas formulações utilizadas. No Apêndice B é avaliado o desempenho de modelo MGB-IPH em uma sub-bacia da Lagoa Mirim (Piratini), utilizando como entrada dados de chuva observada e dados de chuva derivados do produto MERGE, e finalmente no Apêndice C é realizada uma breve descrição do modelo IPH-ECO, seus componentes hidrodinâmico e qualidade da água.

Capítulo 2

Coupling large-scale hydrological and hydrodynamic modeling: Toward a better comprehension of shallow lake-watershed processes

This chapter is based on the following paper submitted to:
Journal of Hydrology

Andrés Mauricio Munar, J. Rafael Cavalcanti, Juan Martin Bravo, Fernando Mainardi Fan, David da Motta-Marques and Carlos Ruberto Fragoso Jr.

Abstract

Changes in hydrological processes and the associated impacts on water resources are widely recognized problems. Coupling hydrological models with hydrodynamic models allows one to understand how catchment features (land use, topography, etc.) impact the local circulation pattern in large water bodies in response to basin forcing factors. However, in large lakes and lagoons, simple approaches using lumped models are limited to representing the high spatial heterogeneity of these ecosystems. Here, we evaluated a complex integrated approach to assess the hydrological responses to external forcing factors such as wind in the hydrodynamics of a large shallow subtropical lake. The case studied is the Lake Mirim basin, where the system was analyzed by coupling a large-scale hydrological model and a hydrodynamic model. Our findings indicated that (i) the integrated model was capable of representing the spatial and temporal variability of lake water-surface levels when compared against in-situ measurements and satellite altimeter data; (ii) the main hydrodynamic processes (water levels and flow structure) are controlled on seasonal scales (months) by the river discharges, and on short time scales (days) by wind influence (intensity and direction); and (iii) the modeling strategy allowed evaluation of anthropogenic stressors on the lake levels. This approach is a first attempt in the development of a physically based management model, allowing simulation of this complex system as a whole, helping to understand the main factors controlling the hydrodynamic processes.

Keywords: Hydrologic processes; Hydrodynamic processes; Satellite altimetry; Lake Mirim; MBG-IPH; IPH-ECO

2.1 Introduction

Lakes and reservoirs are important resources for drinking water, agriculture, recreation, power generation, and flood control (Maltby et al., 2011; Zedler and Kercher, 2005). Many of these waterbodies are threatened by changes in hydrological processes in upland basins, human activities, and climate change, leading to significant variations in both water level and hydrodynamic balance (Carpenter et al., 1992; Jones et al., 2001; Legesse et al., 2004) These variations in water volume play a crucial role in physical processes, environmental impacts, and socio-economic implications, such as shoreline damage from episodes of high water levels (Foulds, 1977; Meadows et al., 1997), and water-quality issues during periods of low water levels (Khan et al., 2015; Wildman et al., 2011). In addition, in lakes and reservoirs it is important to understand the catchment and hydrodynamic processes that will control the aquatic ecosystem dynamics such as phytoplankton, sediment transport, and spatial heterogeneity (e.g.,

Curtarelli et al., 2015; Li et al., 2017; Pinardi et al., 2015; Qi et al., 2016)

The main inputs of water for reservoirs, lagoons and lakes located in the downstream portion of large watersheds are the rivers that discharge into these ecosystems. Only a few studies have explored the mathematical modeling of catchment-lake dynamics, considering the behavior of both the watershed and the lake. Often lake modeling studies use approaches that consider only the lake itself, without modeling the catchment where the hydrological processes occur. The majority of lake modeling studies have focused mainly on hydrodynamics and water-quality dynamics. Examples of such applications in southern Brazil are the studies by Barros et al. (2014); Fernandes et al. (2001, 2002, 2005); Marques et al. (2009) and Seiler et al. (2015), who analyzed the Patos Lagoon using hydrodynamic models. In these studies, the inflows from river discharge to the lake were considered only at specific locations and were limited to observed data, with limited temporal frequency. Since the catchment was not modeled properly (*i.e.,* by using a hydrological model) the basin representation and the capacity to analyze different management scenarios and spatially explicit dynamics (*e.g.,* mixing regime, hydrodynamic patterns, river importance to overall water balance) was limited.

In recent years, coupling hydrological models with hydrodynamic models has been used successfully to study the catchment-waterbody relationship, optimizing management practices by describing the importance of representing hydrological and hydrodynamic processes simultaneously (Guzman et al., 2015; Kim et al., 2012), and allowing assessments of changes in waterbody hydrological regimes (Zhang et al., 2014). Some examples of approaches assessing the influence of external forcing on the main hydrodynamic components (*e.g.,* flow structure, velocity fields, water levels) can be found in recent literature. Dargahi and Setegn (2011) studied the recirculation regions, stratification/mixing process and water-withdrawal effects in Lake Tana (Ethiopia) (basin total area: 15,096 km^2; lake water-surface area: 3000 - 3600 km^2), coupling a three-dimensional hydrodynamic model with a catchment model, using a one-year database. This study was limited due to the short time scale employed to assess the potential effect of land-use changes and river discharge on water levels, which is an advantage of this kind of coupled approach. Li et al. (2013) presented another example of the coupled modeling of lake-catchment dynamics. The authors evaluated the performance of a distributed catchment-hydrology model coupled with a lake hydrodynamic model in Poyang Lake (China) (basin total area: 162,000 km^2; lake water-surface area: 1000 - 3000 km^2) using *in-situ* measurements of lake water level. In this case, the authors did not consider the influence of the external forcing factors such as wind stress (velocity and direction) and human activities (*e.g.,* water withdrawals) on the spatial and temporal variability of lake water levels and hydrodynamic patterns. Despite the common advantage of understanding the

behavior of the integrated catchment-lake system simultaneously on different spatial and temporal scales, the long-term dynamics of water-level variation (*i.e.,* seasonality, inter-annual variations, discharge effect) and the hydrodynamic patterns related to external forces (*e.g.,* wind intensity, river discharge) are not commonly assessed.

This coupling between hydrological and hydrodynamic models is not performed directly, with numerical difficulties arising in this regard. The coupled approach can show numerical instabilities due to the different spatial discretization often used in the catchment, where a coarser computational grid is used, and in the lake, where a more-refined computational grid is often applied (Chávarri et al., 2013; Cunge et al., 1980; Wu, 2007). In addition, the hydrological model might oversimplify the representation of physical processes, due to the large computational and spatial scale required to model large watersheds (Todini, 2007). However, the most common problem encountered in using mathematical models to represent aquatic ecosystems is the availability of datasets that are required to use the models. This can be a limitation, especially in developing countries, where the scarcity of available data and the data analysis/preparation can be an excessively time-consuming task (Patro et al., 2009). Also, in these countries, hydrological data are often not publicly accessible (Chipman and Lillesand, 2007). In this regard, remote-sensing data can be an alternative way to obtain the information for sites where *in-situ* measurements are sparse or difficult to obtain (Alsdorf et al., 2007; Calmant et al., 2008). Satellite altimeter data derived from remote sensors are a cutting-edge tool used for validation of models (Schneider et al., 2017), providing data with unprecedentedly high spatial resolution, from ungauged sites. Several studies have used satellite altimeter data to validate both hydrological and hydrodynamic models. The most commonly used altimetry data are from the Envisat mission (Birkinshaw et al., 2014; Paiva et al., 2013a) and the ICESat satellite (Hall et al., 2011; Jarihani et al., 2015; O'Loughlin et al., 2016). These provide valuable information to calibrate and validate hydrological/hydrodynamic models as complementary sources of data for regions where no gauges are available or the data are not in the public domain.

In this study, we investigated the coupling of two different models to simulate the dynamics of a large lake and its catchment. The hydrological processes were simulated using the MGB-IPH model (Collischonn et al., 2007) and the hydrodynamic module of the IPH-ECO model (Fragoso et al., 2009) to assess the catchment-lake behavior at Lake Mirim, a large subtropical shallow lake that lies on the Brazil-Uruguay border. In addition, we validated the use of satellite altimeter data by comparing against *in-situ* and simulated water-level values. This approach is the first attempt to simulate the Lake Mirim basin as a whole, allowing an analysis of the effects of river discharges, water withdrawals, and the influence of external forcing factors such as wind on the hydrodynamics of this lake. This integration allowed us to assess the main factors

controlling the hydrodynamic processes in this ecosystem, using a spatially explicit approach.

Differently from previous studies, here we proposed a first step toward using the synergy between large-scale hydrological-hydrodynamic modeling, satellite altimetry data, and *in-situ* measurements in a large subtropical shallow lake, using 10 years of data. Our approach goes beyond the conventional integration of these three tools, due to the synchronization of the watershed-lake system on a long-term time-scale, allowing simultaneous evaluation of different periods (wet years, dry years, daily variation, and seasonality) and the responses to the impacts of several stressors on the ecosystem.

2.2 Study Area

The Lake Mirim basin (Fig. 1) is a large river basin shared by Brazil and Uruguay (31°00' and 35°00'S, 052°15' and 055°15'W). A digital elevation model (DEM) of the catchment, derived from SRTM (Farr et al., 2007), shows that the topography varies widely, with a hilly region with elevations reaching 509 m a.s.l. and floodplain areas around Lake Mirim, with elevations near 0 a.s.l. The basin surface area is 58,400 km^2, of which 32,704 km^2 (56%) lies in Uruguay and 25,696 km^2 (53%) in Brazil. The basin has six main sub-basins (Fig. 1); the Jaguarão sub-basin is the largest on the Brazilian side (13.1% of the total area), and the Cebollati sub-basin (29.8%) is the largest on the Uruguayan side. The region has a subtropical climate, with mean annual rainfall ranging from 1,200 mm to 1,450 mm and a mean annual temperature of 16 ºC (Kottek et al., 2006).

Lake Mirim, the main waterbody in the basin, has a surface area of approximately 4000 km^2. It is 190 km along the major axis and 40 km wide on average. The maximum depth is 10 m with an average depth of 4.5 m. The lake volume can reach 17 km^3, depending on the hydrological conditions and output flow. The lake is located in a strategic region for Brazil and Uruguay, due to the political and economic significance of the region. Both countries use water from Lake Mirim for irrigating ricefields, as well as a water supply for the surrounding population. Lake Mirim is connected to the larger Patos Lagoon (lake water surface area: 10,000 km^2) through the São Gonçalo Channel (Fig. 1), which is approximately 76 km long and is operated by a sluice/dam system, preventing the entry of seawater into the lake during the dry season and controlling the lake volume.

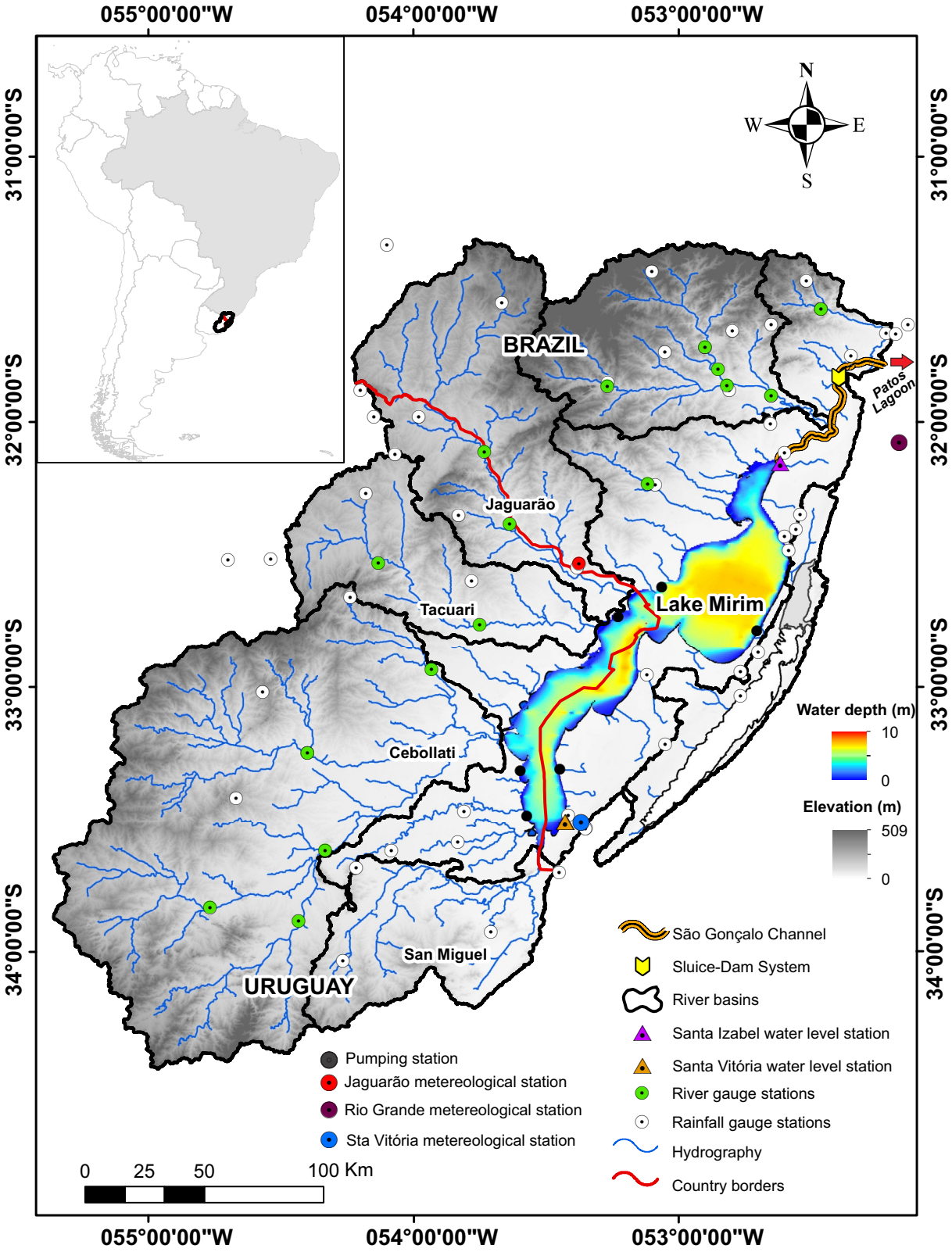

Figure 1 – Lake Mirim basin, showing its main river basins, lake bathymetry, distributed stream gauge stations and water-level gauge stations, country borders, and output flow of the São Gonçalo Channel.

2.3 Data, models and procedures

2.3.1 *In situ* data

Hydrometeorological data for the hydrological model were provided by the *Agência Nacional de Águas* (ANA) and by the *Instituto Nacional de Meteorologia* (INMET), both controlled by the Brazilian authorities and with public-domain data. For the Uruguayan side, meteorological data were provided by the *Instituto Uruguayo de Meteorología* (INUMET), controlled by the Uruguayan authorities and also with public-domain data. The hydrological model was forced using 53 rainfall gauges distributed near the basin boundary, and 17 streamflow gauge stations which were used for flow calibration (Fig. 1). Soil data for the Brazilian side were provided by the *Empresa Brasileira de Pesquisa Agropecuária* (IBGE-EMBRAPA) and the *Ministério do Meio Ambiente* (MMA), both controlled by the Brazilian authorities and with public data. For the Uruguayan side, soil data were obtained from the *Ministerio de Ganadería, Agricultura y Pesca* (MGAP) and the *Ministerio de Vivienda, Ordenamiento Territorial y Medio Ambiente* (MVOTMA), both controlled by the Uruguayan authorities and with public data, using land-cover maps from the Land Cover Classification System, LCCS (FAO, 1998).

The meteorological data used in the hydrodynamic model consisted of hourly air temperature, solar radiation, wind direction and intensity, and daily relative humidity, precipitation and evaporation. The data were obtained from three meteorological stations (Rio Grande, Jaguarão and Santa Vitória) and were provided by INMET. Daily water-level time series were recorded at two gauge stations, located in the northern (Santa Izabel) and southern (Santa Vitória) parts of the lake (Fig. 1), controlled by the Agência da Lagoa Mirim (ALM).

2.3.2 Remote sensing data

The remote-sensing dataset consisted of lake water levels derived from ICESat laser altimeter and ENVISAT satellite altimetry data at six virtual stations along Lake Mirim, obtained from the ground tracks of Envisat (radar) and ICESat (laser) over the lake (Fig. 6). The ICESat accuracy in surface-elevation measurements is around 2 cm, with 70-m footprints spaced every 172 m (Kwok et al., 2004; Zwally et al., 2008). The database used for the 2003-2009 period was obtained from the ICESat platform available on the internet (`http://icesat.gsfc.nasa.gov/icesat/reverb.echo.nasa.gov`). To remove the saturated observations we used the lift saturation index (Hall et al., 2012; O'Loughlin et al., 2016), and to eliminate the series outliers we used the approach proposed by Zhang et al. (2011). Processing and analysis of the ICESat product were performed with a MatLab® routine. The ENVISAT satellite altimetry database for the 2002-2010 period was downloaded from `http://ctoh.legos.obs-mip.fr/products`.

The mean accuracy from the Envisat satellite is about 15 cm (Frappart et al., 2006a,b). We used the Multi-mission Altimetry Processing Software MAPS (Frappart et al., 2015) developed in the *Laboratoire d'Études en Géophysique et Océanographie Spatiales* (LEGOS) for processing and analysis of ENVISAT altimetry data. The statistical analysis for ICESat and ENVISAT data was performed using the median of water-level data estimated from satellite data, compared against the median simulated water-level data.

2.3.3 Mathematical Models

A one-way and off-line coupling between the large-scale hydrological model MGB-IPH) - *Modelo de Grandes Bacias - Instituto de Pesquisas Hidráulicas* (Collischonn et al., 2005, 2007; Collischonn and Tucci, 2001; Fan et al., 2014; Paiva et al., 2013b) and the IPH-ECO model (Fragoso et al., 2009) was adopted. The simulated time-series of river discharges from the hydrological model was used as input for the hydrodynamic model (Fig. 2). The models were run sequentially: first the MGB-IPH model to estimate the incoming flow into the lake, and then the IPH-ECO model, which we used to estimate and calibrate the water levels using the data observed at two stations in Lake Mirim.

2.3.3.1 Hydrological modeling

The MGB-IPH model is a large-scale distributed hydrological model that uses physical and conceptual equations to predict the process of the terrestrial hydrological cycle (Collischonn et al., 2007). In the MGB-IPH model, the basin is divided into small-unit catchments using geoprocessing tools from digital elevation models. Combinations of land use and soil type within each catchment unit are defined following a Hydrological Response Unit (HRU) approach (Kouwen et al., 1993). The MGB-IPH model calculates the evapotranspiration from the Penman-Monteith approach (Shuttleworth, 1993), using five climatology variables: air temperature, atmospheric pressure, wind velocity, vapor pressure and solar radiation. Canopy interception is calculated using the vegetation leaf-area index; the soil water balance and surface runoff are calculated using the approach proposed in the Arno model (Todini, 1996); and the streamflow is estimated through the river network, using the Muskingum-Cunge method. The MGB-IPH model has been successfully used in South America in multiple studies of large basins in recent years (*e.g.,* Collischonn et al., 2005; Fan et al., 2015; Getirana et al., 2010; Nóbrega et al., 2011; Paiva et al., 2013b; Siqueira et al., 2016).

For the MGB-IPH model application, the Lake Mirim basin was divided into 26 sub-basins and 499 small-unit catchments. Each of these sub-basins has its outlet on the lakeshore and is related to the larger rivers in the sub-basin. In the model discretization we used the digital elevation model from SRTM DEM (Farr et al., 2007). Six HRUs were

defined based on available soil-type and land-use maps, and a daily time step was used in the simulations. During the calibration and validation step, the Nash-Sutcliffe efficiency coefficient (Nash and Sutcliffe, 1970) for streamflow (ENS), Nash-Sutcliffe efficiency coefficient for logarithms of streamflow (ENSlog), and relative volume errors (ΔV) were calculated between in situ-observed and model-simulated data, at each available gauging station.

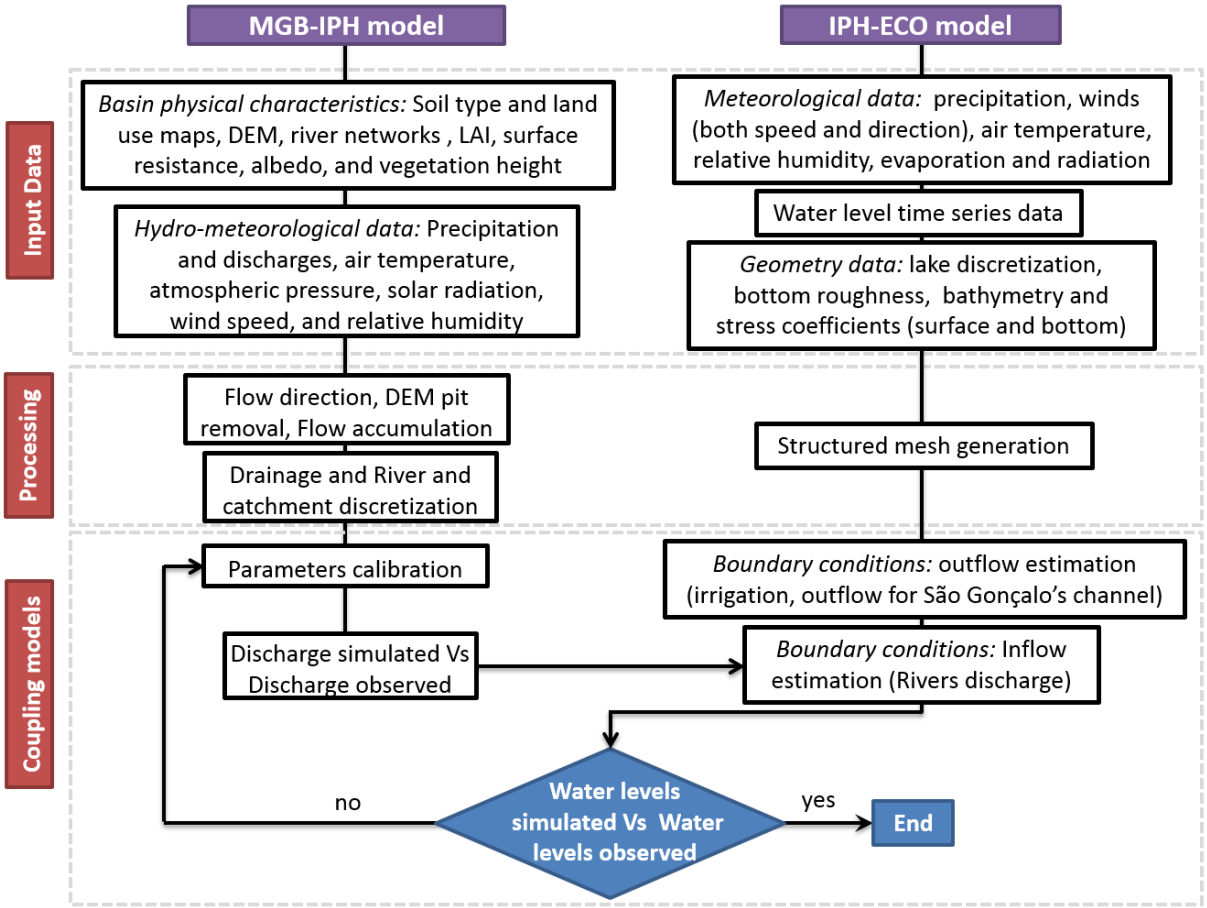

Figure 2 – Conceptual flow chart for coupling large-scale hydrologic and hydrodynamic modeling. The schematic includes input data (hydro - meteorological data), processing and coupling models. The arrows indicate the input-output linkages.

2.3.3.2 Hydrodynamic modelling

The IPH-ECO model (Fragoso et al., 2009) describes the main hydrodynamic, biotic and abiotic components in aquatic environments. It can be used to assess physical, chemical or biological processes separately, or to assess the simultaneous interaction of these processes. The model has a hydrodynamic module that describes the velocity fields and water levels, using a semi-implicit approach based on the TRIM model to solve the Navier-Stokes equation in structured quadrilateral grids (Casulli and Cheng, 1992). The model also uses the *theta* method to improve the accuracy of its numerical

solution (Casulli and Cattani, 1994). The momentum equations are discretized by the use of an Eulerian-Lagrangian approach (Cheng et al., 1993).

Several studies (*e.g.*, Cavalcanti et al., 2016; Fragoso et al., 2011; Pereira et al., 2013) have been developed in Brazil, Denmark and Sweden to assess ecological processes in shallow lakes using the IPH-ECO model. For application to Lake Mirim, the lake was discretized using a 500-m resolution structured quadrilateral grid, resulting in 15,289 computational cells. Only one vertical layer was used, resulting in a two-dimensional vertically integrated model. The implicitness factor θ was set to 0.55 and the horizontal turbulent viscosity to 15 m^2s^{-1}. The bottom roughness was parameterized by using the Chezy coefficient of 60 $m^{1/2}s^{-1}$, and the wetting and drying of computational cells were performed with a drying limit of 0.05 m. The period of simulation was set from 1 January 2000 to 31 December 2010. The simulation was performed using a computational time step of 60 s. The Inflow time series from the hydrological model and a dynamic estimated outflow time-series (explained below) were used as boundary conditions to simulate the Lake Mirim system. To estimate the outflow time-series from Lake Mirim, we included the water withdrawal to ricefields along the lakeshore and the outflow through the São Gonçalo Channel (Fig. 1). To represent water withdrawal to ricefields, we assumed a constant pumping rate (2 L s^{-1} ha^{-1}) during the rice cultivation period (November - February), which was successfully used in a previous application for the same watershed (Fragoso et al., 2011). The water withdrawal to ricefields was calculated from the rice yields in the 2000-2010 period, both on the Brazilian side (IRGA, 2013; Klering et al., 2013) and on the Uruguayan side (MGAP, 2013). The outflows through the São Gonçalo Channel were modeled based on a trapezoidal weir equation. The IPH-ECO model was validated using the time-series data available for daily water level, recorded at the Santa Izabel and Santa Vitória gauge stations. We also validated the IPH-ECO model using six virtual stations derived from the ICESat and ENVISAT missions (Fig. 6). To evaluate the accuracy of the IPH-ECO model, the Nash-Sutcliffe efficiency coefficient (ENS), the coefficient of determination (R^2), BIAS and Root-Mean-Square-Error (RMSE) were calculated between the simulated water level and the *in-situ* and satellite measurement.

2.3.4 Simulation of scenarios

In the Results section, we present the river basin hydrological modeling and the lake hydrodynamic modeling results for the ten-year study period (2000- 2010). We also present the simulated flow structure in the results for Lake Mirim. After the model validation, we conducted tests to evaluate the effects of hydrological and external forcing on the main hydrodynamic components of the lake (*e.g.*, water levels, velocity fields, flow structure). We studied the flow structure in different periods (low and high water), turning off the effects of wind and analyzing the changes in different lake

regions. Next, we evaluated the impacts of irrigation withdrawals on the lake water levels, by running a simulation without withdrawals, using the proposed models.

2.4 Results

2.4.1 River-basin hydrological modeling

The results of the simulated against observed river discharges indicated that the simulated discharges derived from the MGB-IPH model agreed well with the observed discharges (Fig. 3). In more than half of the stream gauges, the ENS was higher than 0.6 and the model accurately represented the mean volume discharge the relative volume errors (ΔV) are lower than 10% for all gauge stations. The comparison between simulated and observed hydrographs at five checkpoints in the Lake Mirim basin (Fig. 4) showed that for some peak flows and seasonal fluctuations from gauge stations located in the upper basin, the hydrological model performed well. However, the smaller peaks were represented with some limitations.

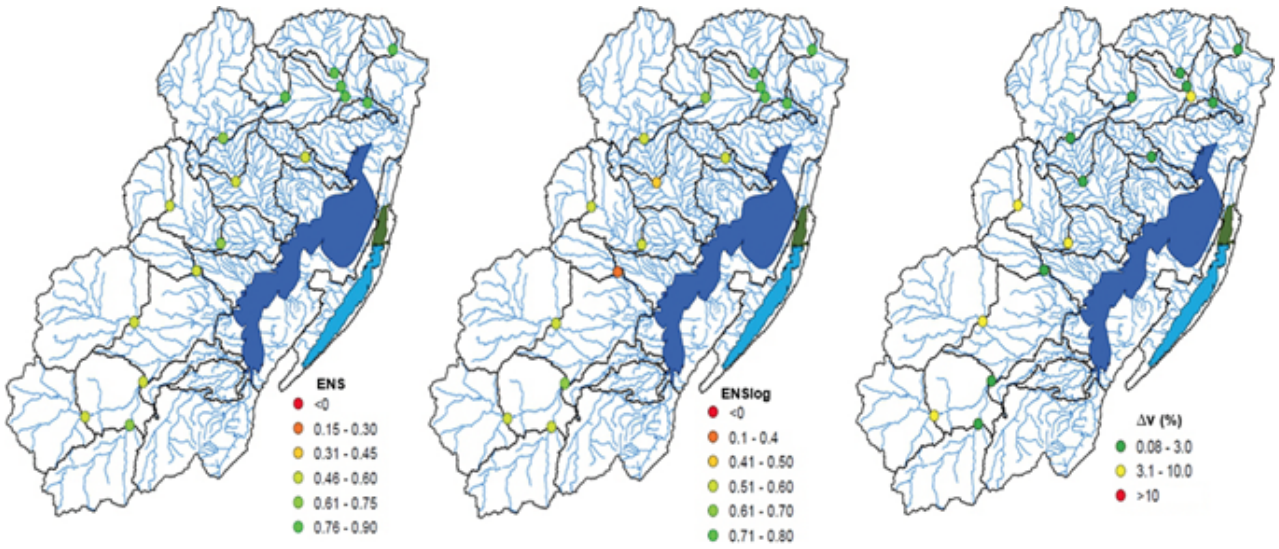

Figure 3 – Performance measurements at different discharge gauging stations during the MGB-IPH model calibration period (from January 2000 to December 2010).

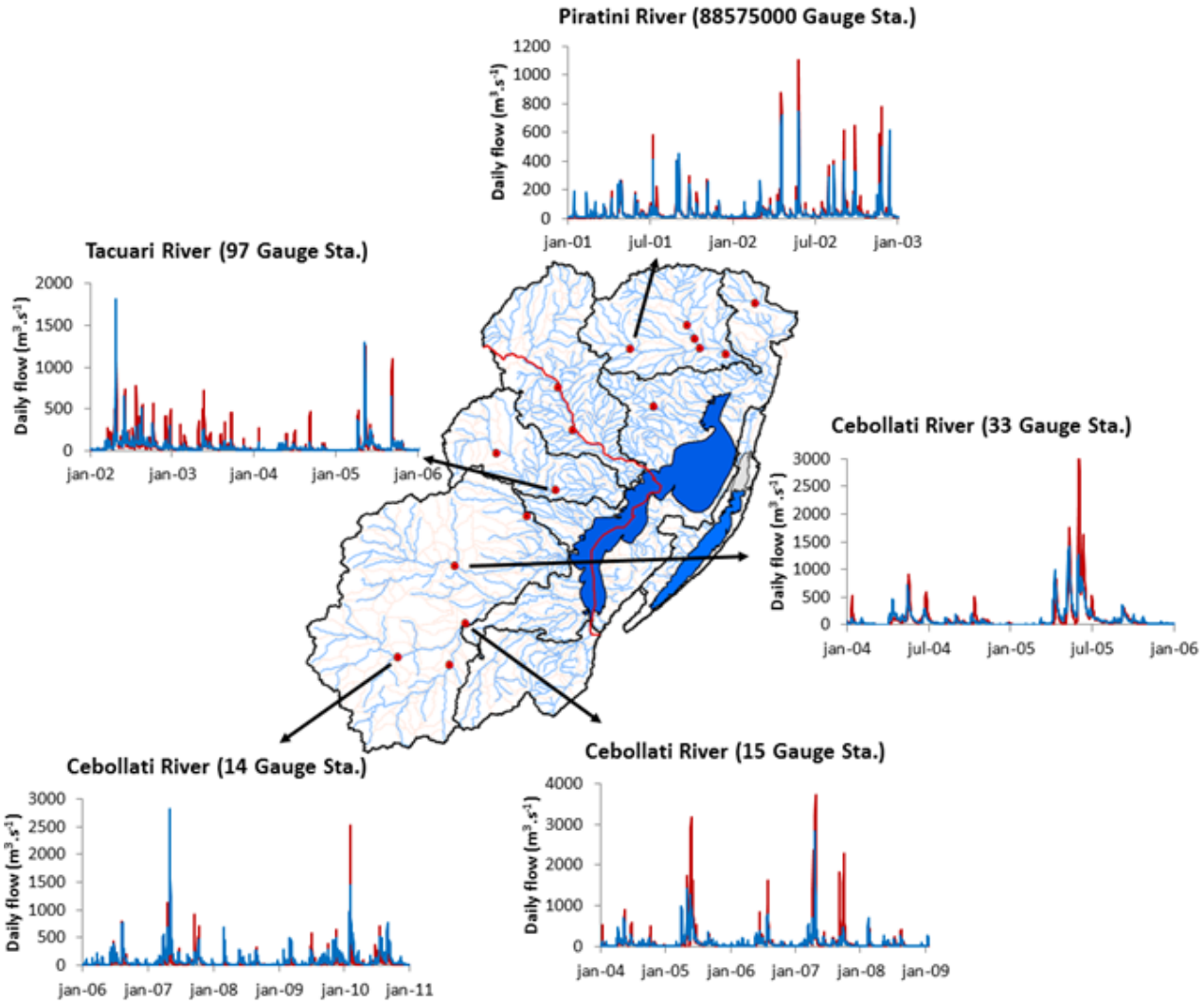

Figure 4 – Comparison of simulated (blue line) and observed (red line) hydrographs at five streamflow gauge stations in the Lake Mirim basin from January 2000 to January 2010

2.4.2 Lake- level model results validated from *in-situ* data

The results for water level showed that the observed daily water surface level was well represented for the 2000-2010 period (Fig. 5). The coupled approach used accurately represented the seasonality and the maximum and minimum periods for the Santa Isabel gauge station (Fig. 5a, ENS = 0.91; R^2 = 0.91; RMSE = 0.321 m; BIAS = -0.32 m) and the Santa Vitória gauge station (Fig. 5b, NS = 0.90; R^2 = 0.90; RMSE = 0.355 m; BIAS = -0.10 m).

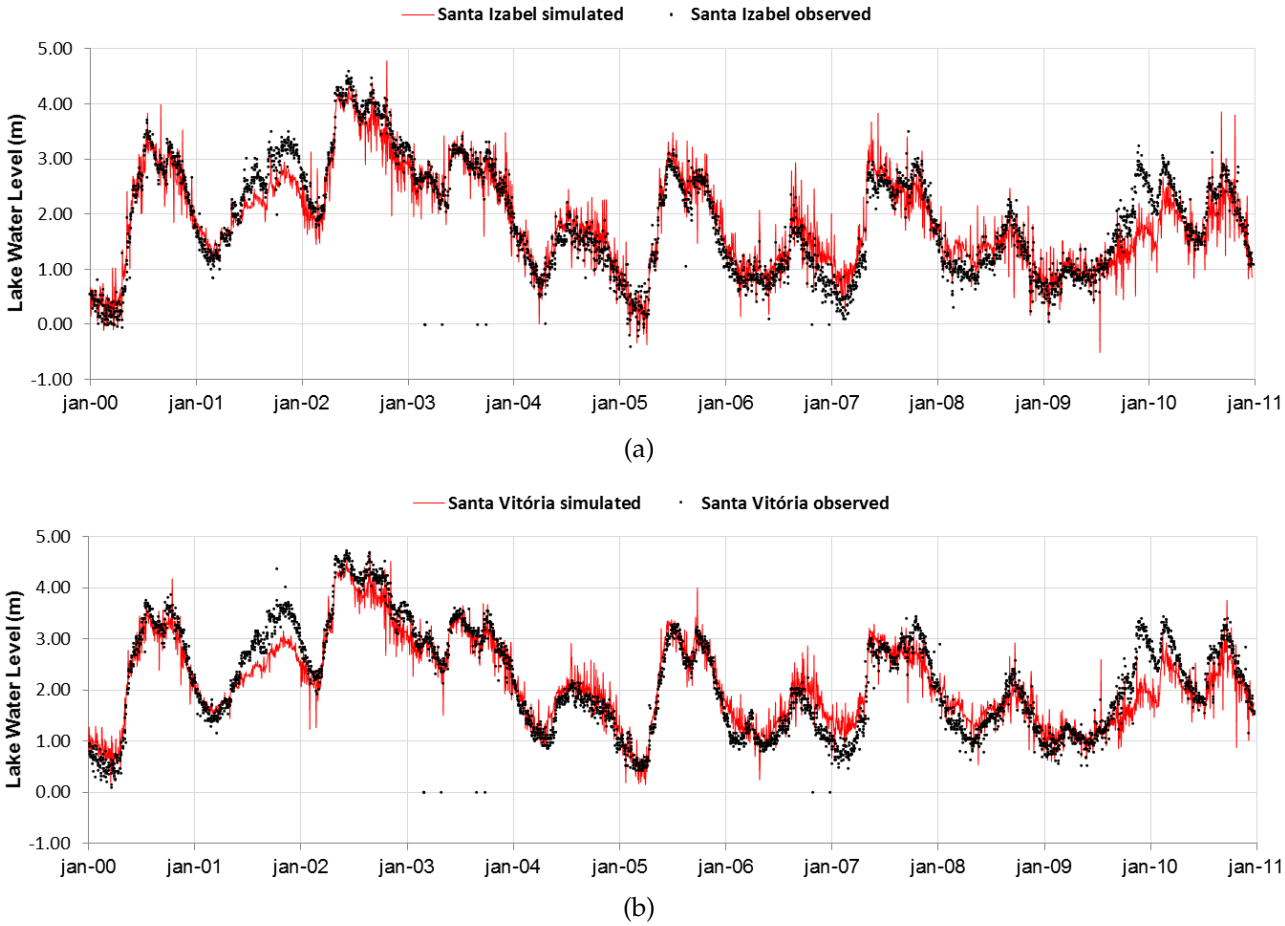

Figure 5 – Hydrodynamic model results vs observed data at the Santa Izabel (a) and Santa Vitória (b) water-level stations for the 2000-2010 period.

2.4.3 Lake water levels validated from satellite altimetry data

Fig. 6 shows the simulated water-level validation at six virtual stations distributed along Lake Mirim. The results showed a good fit between the ICESat altimeter data and the simulated water levels (virtual stations B,C,E,F). The Envisat data provided a poorer fit than the ICESat data (virtual stations A,D), but the general trend of the level variations was well represented.

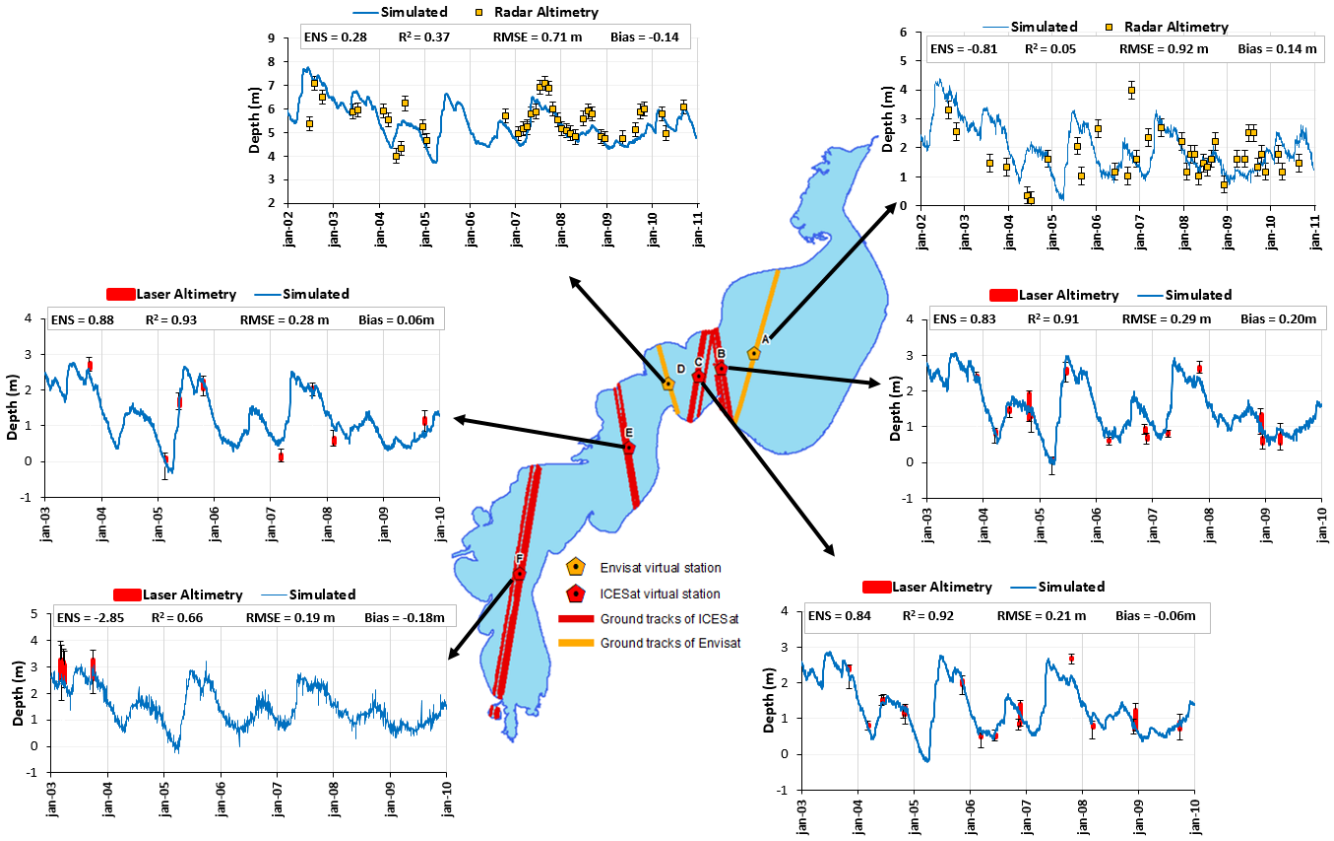

Figure 6 – Water-level model validation at six (A,B,C,D,E,F) virtual stations derived from satellite altimetry data. The blue line in each chart represents the water level simulated from IPH-ECO. Red and yellow box plots indicate the water level derived from laser (ICESat) and radar (Envisat) altimetry respectively. Map inset: ground tracks of Envisat (yellow) and ICESat (red).

2.4.4 Flow structure in Lake Mirim

In view of the difficulty of performing a detailed analysis for all simulations at each time step, only four periods were used to analyze the results: 7 May 2005 (low water-level period, Fig. 7a), 27 May 2005 (rising water-level period, Fig. 7b), 6 July 2005 (high water-level period, Fig. 7c) and 21 December 2005 (falling water-level period, Fig. 7d). The different velocity fields in each period showed a complex flow structure composed of different recirculation areas. The results also showed that the rising water levels (27 May 2005, Fig. 7b) were related to an increase in flow velocities. In the falling water-level period (21 December 2005, Fig. 7d), although the overall velocity intensity was lower, the recirculation areas and flow patterns were similar to the other periods. The maximum flow velocities (about 0.20 m s^{-1}) were observed in deeper regions near the lake center, and the minimum flow velocities were observed in the nearshore areas.

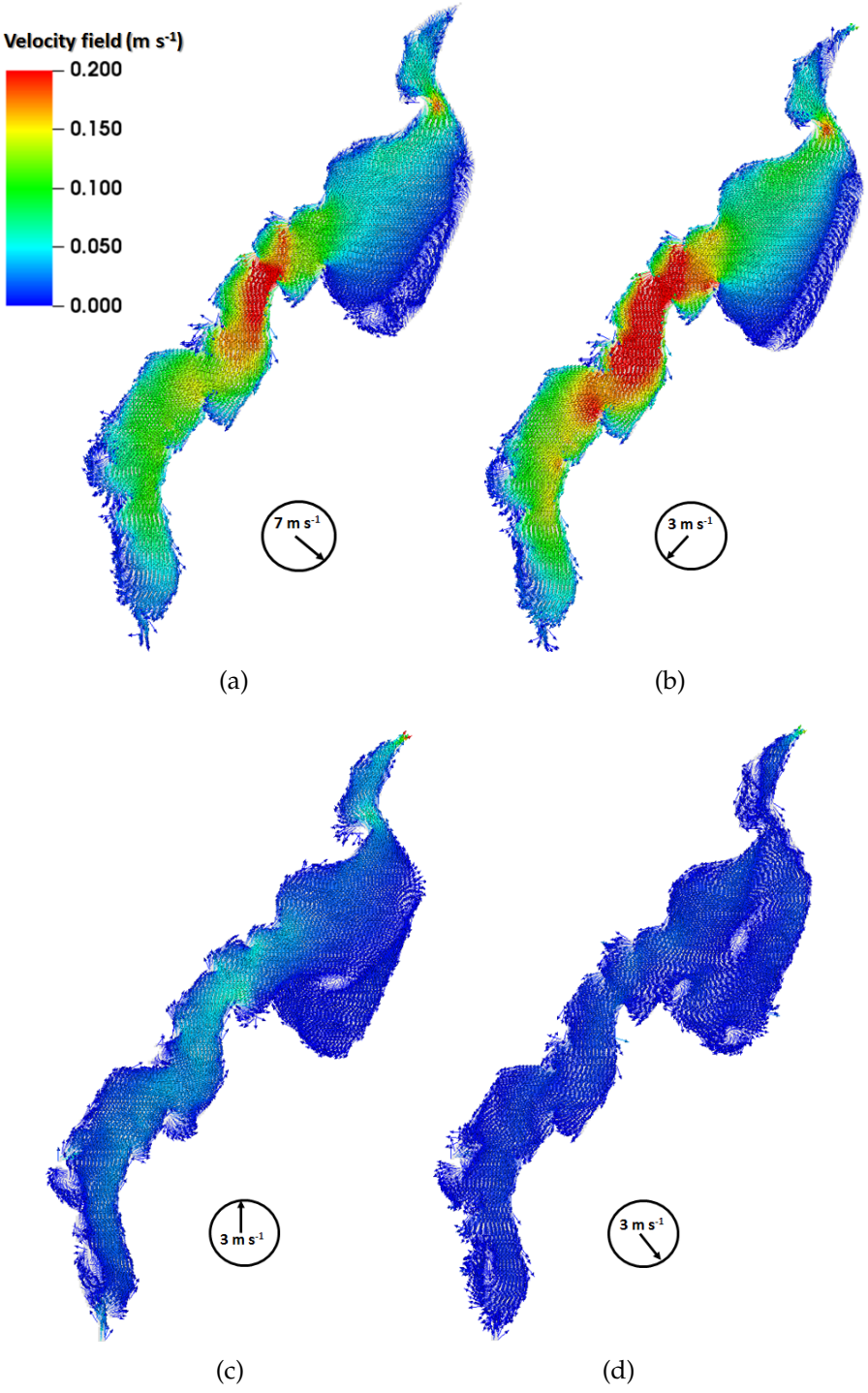

Figure 7 – Velocity fields (m s^{-1}) at the Lake Mirim water surface for (a) 7 April 2005 (low water-level period), (b) 27 May 2005 (rising water-level period), (c) 6 July 2005 (high water-level period), and (d) 21 December 2005 (falling water-level period). The wind sleeve (circle) for each period indicates the instantaneous wind direction and intensity.

2.4.5 Wind action on water levels and velocity fields

Additionally, wind forcing produces wide variations in flow structure and circulation patterns. Fig. 8 shows the velocity fields for a situation without wind, using the same four periods: 7 April 2005 (low water-level period), 27 May 2005 (rising

water-level period), 6 July 2005 (high water-level period) and 21 December 2005 (falling water-level period). For all periods, the wind influences the flow structure, leading to a decrease in surface-flow velocities and circulation patterns.

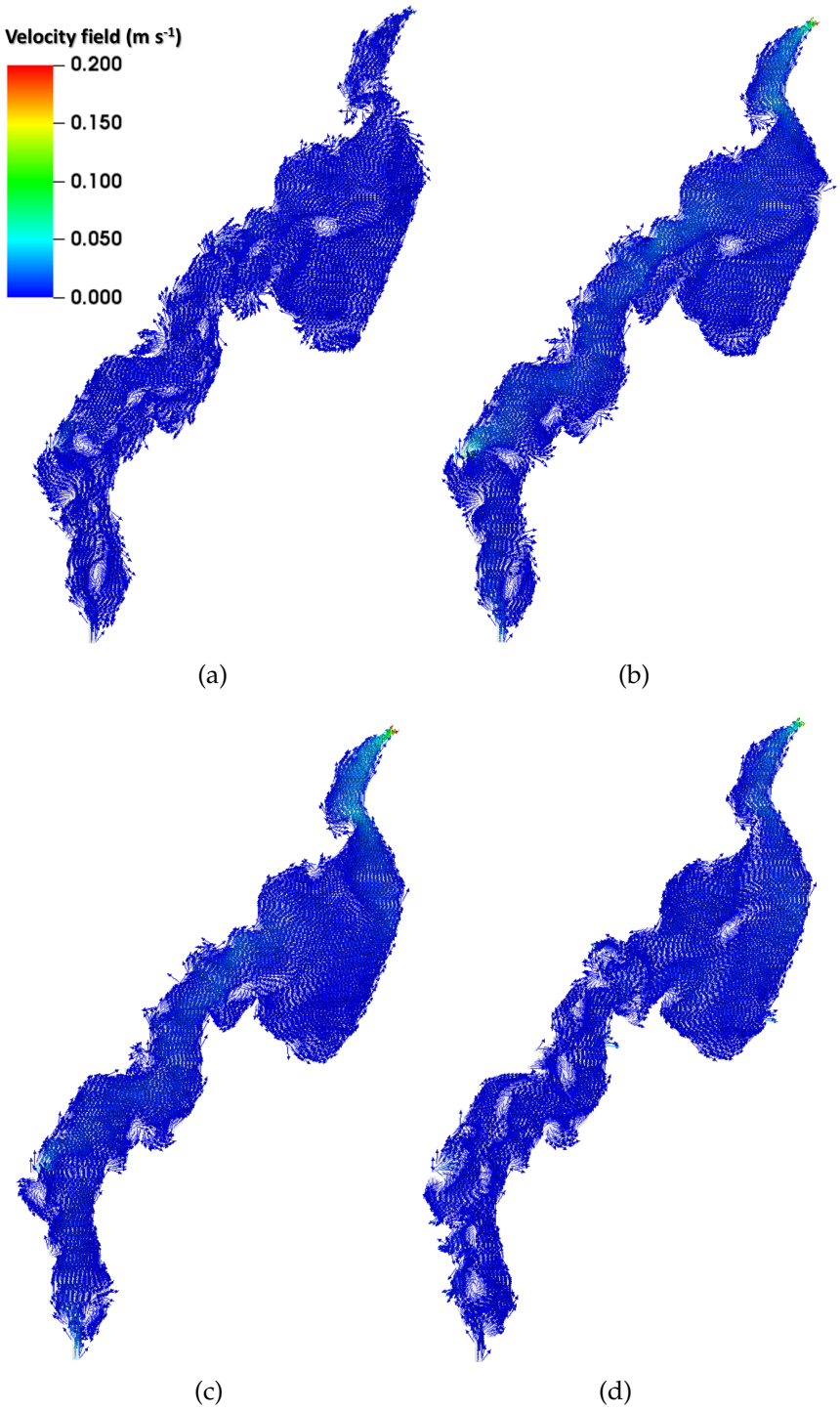

Figure 8 – Velocity fields (m s^{-1}) at the Lake Mirim water surface for a situation without wind for (a) 7 April 2005 (low water-level period), (b) 27 May 2005 (rising water-level period), (c) 6 July 2005 (high water-level period) and (d) 21 December 2005 (falling water-level period).

The results from three representative points located in the northern, central and southern regions of Lake Mirim from January 2000 to December 2010 showed the

influence of wind on the short-term time scale of water-level dynamics (Fig. 9). Daily water levels fluctuate widely when the wind acts on the lake, which was not observed for the situation without wind. The shallow areas were more prone to water-level variations due to wind stress, and fluctuated most at the northern point (1.7 m on 31 October 2010).

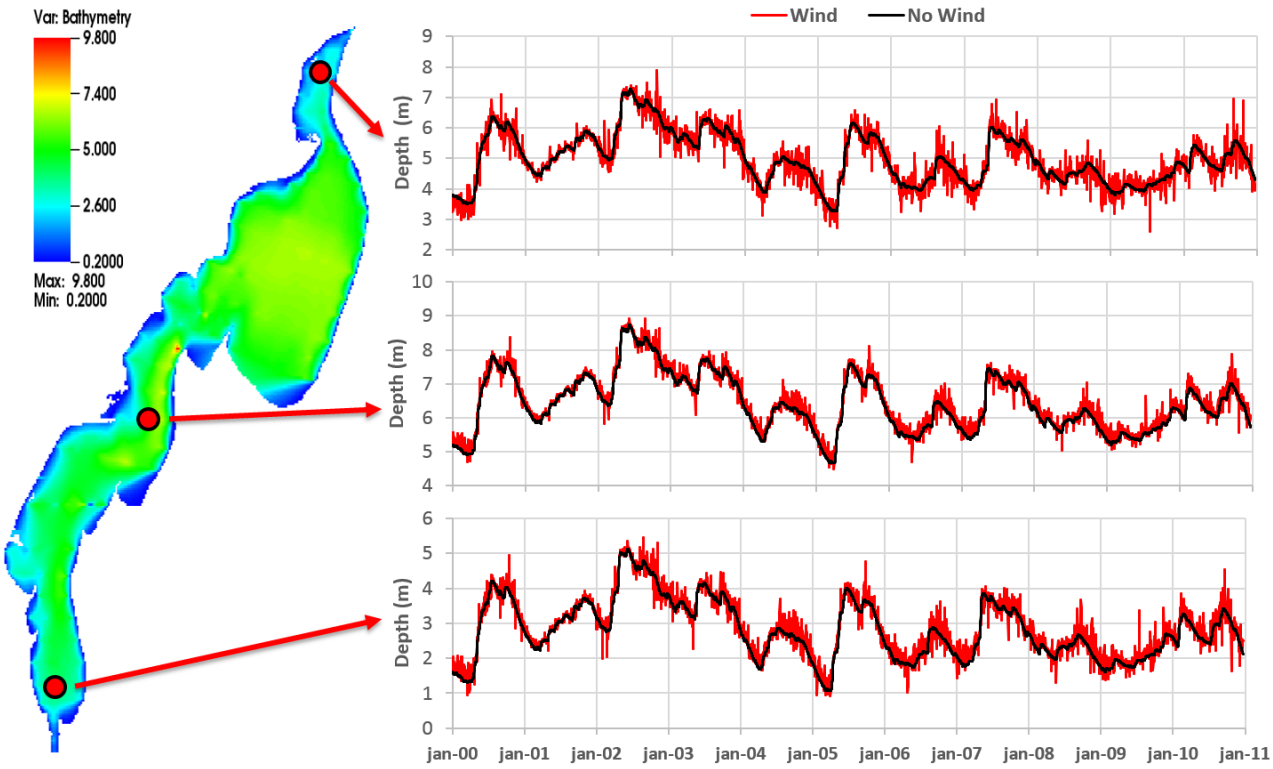

Figure 9 – Wind action (model simulation with and without wind) on surface water levels at the northern, central and southern points of Lake Mirim, for the period analyzed.

2.4.6 Influence of water withdrawals on surface water levels

The impact of reducing the water withdrawals for irrigation on the monthly means and daily water levels is depicted in Fig. 10, where a comparison between the current situation and a non-irrigation situation is shown. The impact of irrigation was stronger during the summer (from November to March, highest variation 0.43 m), whereas almost no variation was observed during spring (from August to October, highest variation 0.09 m). On a yearly basis, the effect of water withdrawal is more variable, with some years being more sensitive to irrigation (*e.g.*, 2001 and 2004-2006) than others (2000, 2002-2003, and 2009-2010).

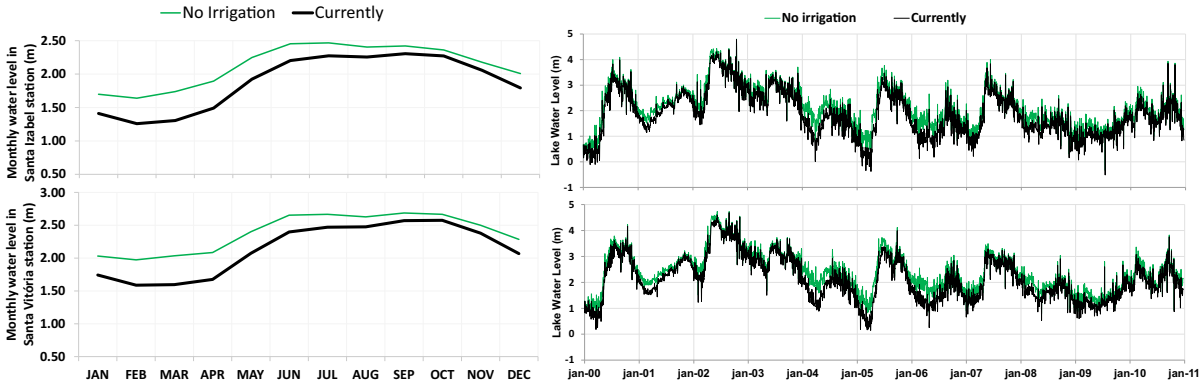

(a) (b)

Figure 10 – Monthly mean (a) and daily (b) surface water levels for irrigation withdrawal at the Santa Izabel (top) and Santa Vitória (bottom) gauge stations.

2.5 Discussion

Examination of the overall performance of the large-scale hydrological model indicated that the MGB-IPH model was able to reproduce observed hydrographs at different spatial scales, and showed better accuracy on the Brazilian side than on the Uruguayan side of the Lake Mirim watershed. This pattern may be related to the smaller number of rain gauges on the Uruguayan side, where the rainfall in the catchments in Uruguay was estimated primarily by interpolation from relatively distant gauges. This was especially important for some higher peak flows in the years 2005 and 2008 in the Cebollati River, which were overestimated by the model. Also, the coarser resolution of the soil-type and soil-use datasets may have made the HRU delineation less reliable, limiting the model calibration. Similar limitations related to input data in applications for South American basins were found by Fan et al. (2014, 2015); Paiva et al. (2013b). Further applications to improve the river-basin hydrological modeling results should include testing with more-detailed rainfall data (*e.g.*, radar or more gauge stations), and to obtain more-detailed spatial data within Uruguay.

The coupling between the large-scale hydrological model (MGB-IPH) and the IPH-ECO hydrodynamic module compared to *in-situ* measurements and satellite altimeter data successfully represented the surface-water levels in Lake Mirim, even for maximum-level (2002) and minimum-level (2005) periods, wet years, dry years, and the seasonal dynamics of the water levels. Although hydrodynamic modeling studies in Lake Mirim were not performed previously, and no field data were available to assess the flow velocity, our results indicated that the coupled models represent reasonably well the expected velocity fields and flow-structure patterns. From, this approach, it was possible to represent the high spatial and temporal heterogeneity in hydrodynamic features, which is difficult to explore with an approach based on lumped

models that employ simplified representations of hydrodynamic processes, obtaining non-representative results in most cases (Kim et al., 2012; Wu, 2007).

The results for the coupled models showed slightly better accuracy in daily water-level estimation at the Santa Isabel gauge station than at the Santa Vitória gauge station. This can be explained by the strong influence of large river discharges (Cebollati River) in the southern lake region, which raise the water level at the Santa Vitória gauge station, as previously observed by Oliveira et al. (2015).

The results for validation of lake water levels from the satellite altimetry data indicated that the model fit better with ICESat-derived levels than with those derived from Envisat satellite data, even though the time-series obtained from Envisat contains more altimetry data (2002-2012 period of operation). The accuracy of our data was consistent with the accuracies found in previous studies (Brenner et al., 2007; Hall et al., 2012; Zhang et al., 2011), which showed that the water-level data from the ICESat instrument had higher precision and vertical accuracy than the Envisat radar data, besides the long repeat cycle (91 days), errors in the saturation, and atmospheric forward scattering (O'Loughlin et al., 2016; Urban et al., 2008). Further altimetry missions using the ICESat-2 and CryoSat-2 satellites could be used to improve accuracy in water-level measurements for Lake Mirim.

Simulation results showed that the velocity fields, circulation patterns and flow recirculation in some lake regions were dominated by the large river discharges and external forcing factors, such as the wind (both speed and direction), which is similar to observations in large lakes within large river basins, such as Lake Tana in Ethiopia (Dargahi and Setegn, 2011) and Poyang Lake in China (Li et al., 2013). Despite the lack of previous studies and field data available to validate our results, they give interesting hints related to the lake hydrodynamics (*e.g.*, circulation patterns), as observed in other studies (Huang et al., 2014; Laval et al., 2003; Lindim et al., 2011). For Lake Mirim, because of its large surface area (4000 km^2) and shallow waters (mean depth = 4.5 m), the wind directly influences the dynamic behavior of the water-level variation, as found in similar environments such as Patos Lagoon (Fernandes et al., 2002, 2005) and Lake Mangueira (Fragoso et al., 2011). Wind stress produces seiches that can result in wide variations in the lake water level (up to 3 m between the south and north ends). Southerly winds push the water northward, raising the water levels at the Santa Izabel gauge station; while winds from the north raise the water levels in the southern lake regions.

The larger volume of water withdrawal (Qmax = 420 $m^3\ s^{-1}$ in the 2003-2004 period) due to increasing demand for ricefield irrigation (area to be irrigated > 327 000 ha) (IRGA, 2013; Klering et al., 2013; MGAP, 2013) is another key driving factor, lowering the water levels in Lake Mirim (highest variation 0.43 m). Although drawdown of irrigation water is a common problem in other large lakes (Dargahi and Setegn, 2011;

Desgranges et al., 2006; Leira and Cantonati, 2008), this can be a matter of concern for water-resources management in the Lake Mirim basin, also affecting the physical, chemical, and biological processes in the lake, as in other environments (Ambrosetti et al., 2003; Liu et al., 2015; Tatsumi and Yamashiki, 2015).

Uncertainties still exist with the coupled hydrologic-hydrodynamic modeling, related to: (1) water withdrawals for irrigation of ricefields, which depends on the potential area for the rice crop; (2) the complex variation of the boundary conditions such as the inflows into the Lake Mirim estimated from the hydrological model, and possible inconsistencies in some input data such as precipitation, because of the scarcity of data for the region. These data are the most sensitive variable that causes significant errors in all output variables (*e.g.,* flow discharge and water levels) (Mul et al., 2009; Sharma et al., 2012); (3) the sensitivity of the model parameters related to the river and floodplain features, roughness characteristics, and bathymetry data; (4) the lack of data on the sluice system operating rules in the São Gonçalo Channel; and (5) errors in the numerical solution methods (discretization and iteration errors) of the hydrologic - hydrodynamic models (Chávarri et al., 2013; Wu, 2007).

2.6 Conclusion

This study showed the coupling of the large-scale MGB-IPH hydrological model with the IPH-ECO hydrodynamic module in order to represent the river-basin response and the main hydrodynamic processes in Lake Mirim (*e.g.,* velocity fields and water levels). The coupled models allowed us to assess the hydrodynamic behavior of Lake Mirim during the 2000-2010 period. It was possible to reproduce the lake responses to the watershed, the main external forcing factors such as wind, the spatial and temporal variability of the water levels, and the complex flow structure.

This was the first study coupling a large-scale basin with a large subtropical shallow waterbody, using a ten-year time scale, and validating the results from *in-situ* measurements and satellite altimetry data. Our approach goes beyond the previously reported couplings, allowing us to assess different hydrological conditions in the basin and the lake behavior and the response to the impact of anthropogenic stressors (*e.g.,* irrigation withdrawals), over the long term.

Our results also showed that the main hydrodynamic processes (*e.g.,* water levels, velocity fields, and flow structure) in Lake Mirim are controlled at the seasonal scale (months) by the river discharges from the main tributaries and water withdrawals for irrigation, and at smaller scales (days) by wind (intensity and direction). The simulated water levels showed that irrigation withdrawals significantly influence the water levels.

The proposed approach, integrating distributed hydrological modeling and hydrodynamic modeling, is a first attempt to simulate the Lake Mirim basin as a whole,

improving understanding of the main driving factors that influence the responses of the lake to hydrological processes in the lake-watershed system. The overall methodology proposed here can be used as a tool in future studies involving climate-change scenarios, land use, water quality, sediment transport, and watershed management.

Acknowledgements: We are grateful to the Coordenação de Aperfeiçoamento de Pessoal de Nível Superior (CAPES: `www.capes.gov.br`) and to the Conselho Nacional de Desenvolvimento Cientifico e Tecnológico (CNPq:`www.cnpq.br`) of Brazil for doctoral scholarships awarded to A. M. Munar and J. R. Cavalcanti. The study is part of the research project "*Impacto das mudanças climáticas em ambientes fluviais e lacustres do Rio Grande do Sul*", funded by CNPq. We are also grateful to the Global Lake Ecological Observatory Network (GLEON: `www.gleon.org`) for providing a venue and resources for lake science discussions. The English version of the manuscript was revised by Dr. Janet W. Reid (Trumansburg, NY, U.S.A.).

Referências

Alsdorf, D. E., Rodriguez, E., and Lettenmaier, D. P. (2007). Measuring surface water from space. *Reviews of Geophysics*, 45(2).

Ambrosetti, W., Barbanti, L., and Nicoletta, S. (2003). Residence time and physical processes in lakes. *Journal of Limnology*, 62(1s):1–15.

Barros, G. P., Marques, W. C., and de Paula Kirinus, E. (2014). Influence of the freshwater discharge on the hydrodynamics of Patos Lagoon, Brazil. *International Journal of Geosciences*, 5(09):925.

Birkinshaw, S., Moore, P., Kilsby, C., O'donnell, G., Hardy, A., and Berry, P. (2014). Daily discharge estimation at ungauged river sites using remote sensing. *Hydrological Processes*, 28(3):1043–1054.

Brenner, A. C., DiMarzio, J. P., and Zwally, H. J. (2007). Precision and accuracy of satellite radar and laser altimeter data over the continental ice sheets. *IEEE Transactions on Geoscience and Remote Sensing*, 45(2):321–331.

Calmant, S., Seyler, F., and Cretaux, J. F. (2008). Monitoring continental surface waters by satellite altimetry. *Surveys in geophysics*, 29(4):247–269.

Carpenter, S. R., Fisher, S. G., Grimm, N. B., and Kitchell, J. F. (1992). Global change and freshwater ecosystems. *Annual Review of Ecology and Systematics*, 23:119–139.

Casulli, V. and Cattani, E. (1994). Stability, accuracy and efficiency of a semi-implicit method for three-dimensional shallow water flow. *Computers & Mathematics with Applications*, 27(4):99–112.

Casulli, V. and Cheng, R. T. (1992). Semi-implicit finite difference methods for three-dimensional shallow water flow. *International Journal for numerical methods in fluids*, 15(6):629–648.

Cavalcanti, J. R., da Motta-Marques, D., and Fragoso, C. R. (2016). Process-based modeling of shallow lake metabolism: Spatio-temporal variability and relative importance of individual processes. *Ecological Modelling*, 323:28–40.

Chávarri, E., Crave, A., Bonnet, M.-P., Mejía, A., Da Silva, J. S., and Guyot, J. L. (2013). Hydrodynamic modelling of the Amazon River: Factors of uncertainty. *Journal of South American Earth Sciences*, 44:94–103.

Cheng, R. T., Casulli, V., and Gartner, J. W. (1993). Tidal, residual, intertidal mudflat (TRIM) model and its applications to San Francisco Bay, California. *Estuarine, Coastal and Shelf Science*, 36(3):235–280.

Chipman, J. and Lillesand, T. (2007). Satellite-based assessment of the dynamics of new lakes in southern Egypt. *International Journal of Remote Sensing*, 28(19):4365–4379.

Collischonn, B., Collischonn, W., Silva, B. C., and Tucci, C. E. (2005). Simulação hidrológica da bacia do rio São Francisco usando precipitação estimada pelo satélite TRMM: resultados preliminares. *Anais do XVI Simpósio Brasileiro de Recursos Hídricos, ABRH, João Pessoa (PB)*.

Collischonn, W., Allasia, D., Da Silva, B. C., and Tucci, C. E. (2007). The MGB-IPH model for large-scale rainfall-runoff modelling. *Hydrological Sciences Journal*, 52(5):878–895.

Collischonn, W. and Tucci, C. (2001). Hydrological simulation of large drainage basins. *Brazilian J. Water Resour*, 6(1):15–35.

Cunge, J. A., Holly, F. M., and Verwey, A. (1980). Practical aspects of computational river hydraulics.

Curtarelli, M., Ogashawara, I., Alcântara, E., and Stech, J. (2015). Coupling remote sensing bio-optical and three-dimensional hydrodynamic modeling to study the phytoplankton dynamics in a tropical hydroelectric reservoir. *Remote Sensing of Environment*, 157:185–198.

Dargahi, B. and Setegn, S. G. (2011). Combined 3D hydrodynamic and watershed modelling of Lake Tana, Ethiopia. *Journal of Hydrology*, 398(1):44–64.

Desgranges, J.-L., Ingram, J., Drolet, B., Morin, J., Savage, C., and Borcard, D. (2006). Modelling wetland bird response to water level changes in the Lake Ontario–St. Lawrence River hydrosystem. *Environmental Monitoring and Assessment*, 113(1-3):329–365.

Fan, F. M., Collischonn, W., Meller, A., and Botelho, L. C. M. (2014). Ensemble streamflow forecasting experiments in a tropical basin: The São Francisco river case study. *Journal of Hydrology*, 519:2906–2919.

Fan, F. M., Schwanenberg, D., Collischonn, W., and Weerts, A. (2015). Verification of inflow into hydropower reservoirs using ensemble forecasts of the TIGGE database for large scale basins in Brazil. *Journal of Hydrology: Regional Studies*, 4:196–227.

FAO (1998). *Food and Agriculture Organization of the United Nations. Soil map of the world: Revised legend, Rome*.

Farr, T. G., Rosen, P. A., Caro, E., Crippen, R., Duren, R., Hensley, S., Kobrick, M., Paller, M., Rodriguez, E., Roth, L., et al. (2007). The shuttle radar topography mission. *Reviews of geophysics*, 45(2).

Fernandes, E. H., Dyer, K. R., and Niencheski, L. F. H. (2001). Calibration and validation of the TELEMAC-2D model to the Patos Lagoon (Brazil). *Journal of Coastal Research*, pages 470–488.

Fernandes, E. H. L., Dyer, K. R., Moller, O., and Niencheski, L. F. H. (2002). The Patos lagoon hydrodynamics during an El Nino event (1998). *Continental Shelf Research*, 22(11):1699–1713.

Fernandes, E. H. L., Dyer, K. R., and Moller, O. O. (2005). Spatial gradients in the flow of southern Patos Lagoon. *Journal of Coastal Research*, pages 759–769.

Foulds, D. (1977). Lake levels and shore damages. *Canadian Water Resources Journal*, 2(1):43–54.

Fragoso, C. R., Marques, D. M. M., Ferreira, T. F., Janse, J. H., and van Nes, E. H. (2011). Potential effects of climate change and eutrophication on a large subtropical shallow lake. *Environmental Modelling & Software*, 26(11):1337–1348.

Fragoso, C. R., van Nes, E. H., Janse, J. H., and da Motta Marques, D. (2009). IPH-TRIM3D-PCLake: A three-dimensional complex dynamic model for subtropical aquatic ecosystems. *Environmental Modelling & Software*, 24(11):1347–1348.

Frappart, F., Calmant, S., Cauhopé, M., Seyler, F., and Cazenave, A. (2006a). Preliminary results of ENVISAT RA-2-derived water levels validation over the Amazon basin. *Remote sensing of Environment*, 100(2):252–264.

Frappart, F., Minh, K. D., L'Hermitte, J., Cazenave, A., Ramillien, G., Le Toan, T., and Mognard-Campbell, N. (2006b). Water volume change in the lower Mekong from satellite altimetry and imagery data. *Geophysical Journal International*, 167(2):570–584.

Frappart, F., Papa, F., Marieu, V., Malbeteau, Y., Jordy, F., Calmant, S., Durand, F., and Bala, S. (2015). Preliminary assessment of SARAL/AltiKa observations over the Ganges-Brahmaputra and Irrawaddy Rivers. *Marine Geodesy*, 38(sup1):568–580.

Getirana, A., Bonnet, M.-P., Rotunno Filho, O., Collischonn, W., Guyot, J.-L., Seyler, F., and Mansur, W. (2010). Hydrological modelling and water balance of the Negro River basin: evaluation based on in situ and spatial altimetry data. *Hydrological processes*, 24(22):3219–3236.

Guzman, J. A., Moriasi, D., Gowda, P., Steiner, J., Starks, P., Arnold, J. G., and Srinivasan, R. (2015). A model integration framework for linking SWAT and MODFLOW. *Environmental Modelling & Software*, 73:103–116.

Hall, A. C., Schumann, G. J.-P., Bamber, J. L., and Bates, P. D. (2011). Tracking water level changes of the Amazon Basin with space-borne remote sensing and integration with large scale hydrodynamic modelling: A review. *Physics and Chemistry of the Earth, Parts A/B/C*, 36(7):223–231.

Hall, A. C., Schumann, G. J.-P., Bamber, J. L., Bates, P. D., and Trigg, M. A. (2012). Geodetic corrections to Amazon River water level gauges using ICESat altimetry. *Water Resources Research*, 48(6).

Huang, J., Gao, J., Hörmann, G., and Fohrer, N. (2014). Modeling the effects of environmental variables on short-term spatial changes in phytoplankton biomass in a large shallow lake, Lake Taihu. *Environmental Earth Sciences*, 72(9):3609.

IRGA (2013). *Instituto Rio Grandense do Arroz*.

Jarihani, A. A., Callow, J. N., McVicar, T. R., Van Niel, T. G., and Larsen, J. R. (2015). Satellite-derived Digital Elevation Model (DEM) selection, preparation and correction for hydrodynamic modelling in large, low-gradient and data-sparse catchments. *Journal of Hydrology*, 524:489–506.

Jones, R., McMahon, T., and Bowler, J. (2001). Modelling historical lake levels and recent climate change at three closed lakes, Western Victoria, Australia (c. 1840–1990). *Journal of Hydrology*, 246(1):159–180.

Khan, S. J., Deere, D., Leusch, F. D., Humpage, A., Jenkins, M., and Cunliffe, D. (2015). Extreme weather events: Should drinking water quality management systems adapt to changing risk profiles? *Water research*, 85:124–136.

Kim, J., Warnock, A., Ivanov, V. Y., and Katopodes, N. D. (2012). Coupled modeling of hydrologic and hydrodynamic processes including overland and channel flow. *Advances in Water Resources*, 37:104–126.

Klering, E. V., Fontana, D. C., Alves, R., Rocha, J., and Berlato, M. A. (2013). Estimativa de área cultivada com arroz irrigado para o estado do Rio Grande do Sul a partir de imagens MODIS. *Ciência e Natura*, 35(2):126.

Kottek, M., Grieser, J., Beck, C., Rudolf, B., and Rubel, F. (2006). World map of the köppen-geiger climate classification updated. *Meteorologische Zeitschrift*, 15(3):259–263.

Kouwen, N., Soulis, E., Pietroniro, A., Donald, J., and Harrington, R. (1993). Grouped response units for distributed hydrologic modeling. *Journal of Water Resources Planning and Management*, 119(3):289–305.

Kwok, R., Zwally, H. J., and Yi, D. (2004). ICESat observations of Arctic sea ice: A first look. *Geophysical Research Letters*, 31(16).

Laval, B., Imberger, J., Hodges, B. R., and Stocker, R. (2003). Modeling circulation in lakes: Spatial and temporal variations. *Limnology and Oceanography*, 48(3):983–994.

Legesse, D., Vallet-Coulomb, C., and Gasse, F. (2004). Analysis of the hydrological response of a tropical terminal lake, Lake Abiyata (Main Ethiopian Rift Valley) to changes in climate and human activities. *Hydrological processes*, 18(3):487–504.

Leira, M. and Cantonati, M. (2008). Effects of water-level fluctuations on lakes: an annotated bibliography. *Hydrobiologia*, 613(1):171–184.

Li, Y., Zhang, Q., Werner, A. D., Yao, J., and Ye, X. (2017). The influence of river-to-lake backflow on the hydrodynamics of a large floodplain lake system (Poyang Lake, China). *Hydrological Processes*, 31(1):117–132.

Li, Y., Zhang, Q., Yao, J., Werner, A. D., and Li, X. (2013). Hydrodynamic and hydrological modeling of the Poyang Lake catchment system in China. *Journal of Hydrologic Engineering*, 19(3):607–616.

Lindim, C., Pinho, J., and Vieira, J. (2011). Analysis of spatial and temporal patterns in a large reservoir using water quality and hydrodynamic modeling. *Ecological Modelling*, 222(14):2485–2494.

Liu, X., Qian, K., and Chen, Y. (2015). Effects of water level fluctuations on phytoplankton in a Changjiang River floodplain lake (Poyang Lake): implications for dam operations. *Journal of Great Lakes Research*, 41(3):770–779.

Maltby, E., Ormerod, S., Acreman, M., Dunbar, M., Jenkins, A., Maberly, S., Newman, J., Blackwell, M., and Ward, R. (2011). Freshwaters: openwaters, wetlands and floodplains [chapter 9].

Marques, W. C., Fernandes, E., Monteiro, I. O., and Möller, O. (2009). Numerical modeling of the Patos Lagoon coastal plume, Brazil. *Continental Shelf Research*, 29(3):556–571.

Meadows, G. A., Meadows, L. A., Wood, W. L., Hubertz, J., and Perlin, M. (1997). The relationship between great lakes water levels, wave energies, and shoreline damage. *Bulletin of the American Meteorological Society*, 78(4):675–682.

MGAP (2013). *Ministerio de Ganaderia, Agricultura y Pesca, Uruguay*.

Mul, M., Savenije, H., and Uhlenbrook, S. (2009). Spatial rainfall variability and runoff response during an extreme event in a semi-arid catchment in the South Pare Mountains, Tanzania. *Hydrology and Earth System Sciences*, 13(9):1659.

Nash, J. E. and Sutcliffe, J. V. (1970). River flow forecasting through conceptual models part IâA discussion of principles. *Journal of hydrology*, 10(3):282–290.

Nóbrega, M., Collischonn, W., Tucci, C., and Paz, A. (2011). Uncertainty in climate change impacts on water resources in the Rio Grande Basin, Brazil. *Hydrology and Earth System Sciences*, 15(2):585.

Oliveira, H. A. d., Fernandes, E. H. L., Möller Junior, O. O., and Collares, G. L. (2015). Processos Hidrológicos e Hidrodinâmicos da Lagoa Mirim.

O'Loughlin, F. E., Neal, J., Yamazaki, D., and Bates, P. D. (2016). ICESat-derived inland water surface spot heights. *Water Resources Research*.

Paiva, R., Collischonn, W., Bonnet, M.-P., De Goncalves, L., Calmant, S., Getirana, A., and Da Silva, J. S. (2013a). Assimilating in situ and radar altimetry data into a large-scale hydrologic-hydrodynamic model for streamflow forecast in the Amazon. *Hydrology and Earth System Sciences*, 17(7):2929–2946.

Paiva, R. C. D., Buarque, D. C., Collischonn, W., Bonnet, M.-P., Frappart, F., Calmant, S., and Bulhões Mendes, C. A. (2013b). Large-scale hydrologic and hydrodynamic modeling of the Amazon River basin. *Water Resources Research*, 49(3):1226–1243.

Patro, S., Chatterjee, C., Singh, R., and Raghuwanshi, N. S. (2009). Hydrodynamic modelling of a large flood-prone river system in india with limited data. *Hydrological Processes*, 23(19):2774–2791.

Pereira, F., Fragoso, C. R., Uvo, C., and da Motta-Marques, D. (2013). Pairing multivariate data analysis and ecological modeling in the biomanipulated Lake engelsholm, Denmark. *Journal of Water Management and Research*.

Pinardi, M., Fenocchi, A., Giardino, C., Sibilla, S., Bartoli, M., and Bresciani, M. (2015). Assessing potential algal blooms in a shallow fluvial lake by combining hydrodynamic modelling and remote-sensed images. *Water*, 7(5):1921–1942.

Qi, H., Lu, J., Chen, X., Sauvage, S., and Sanchez-Pérez, J.-M. (2016). Water age prediction and its potential impacts on water quality using a hydrodynamic model for Poyang Lake, China. *Environmental Science and Pollution Research*, 23(13):13327–13341.

Schneider, R., Godiksen, P. N., Villadsen, H., Madsen, H., and Bauer-Gottwein, P. (2017). Application of CryoSat-2 altimetry data for river analysis and modelling. *Hydrology and Earth System Sciences*, 21(2):751.

Seiler, L. M., Fernandes, E. H. L., Martins, F., and Abreu, P. C. (2015). Evaluation of hydrologic influence on water quality variation in a coastal lagoon through numerical modeling. *Ecological Modelling*, 314:44–61.

Sharma, S., Isik, S., Srivastava, P., and Kalin, L. (2012). Deriving spatially distributed precipitation data using the artificial neural network and multilinear regression models. *Journal of Hydrologic Engineering*, 18(2):194–205.

Shuttleworth, W. J. (1993). Evaporation in: Maidment, dr"handbook of hydrology.

Siqueira, V. A., Collischonn, W., Fan, F. M., and Chou, S. C. (2016). Ensemble flood forecasting based on operational forecasts of the regional Eta EPS in the Taquari-Antas basin. *RBRH*, 21(3):587–602.

Tatsumi, K. and Yamashiki, Y. (2015). Effect of irrigation water withdrawals on water and energy balance in the Mekong River Basin using an improved VIC land surface model with fewer calibration parameters. *Agricultural Water Management*, 159:92–106.

Todini, E. (1996). The ARNO rainfall-runoff model. *Journal of Hydrology*, 175(1):339–382.

Todini, E. (2007). Hydrological catchment modelling: past, present and future. *Hydrology and Earth System Sciences*, 11(1):468–482.

Urban, T. J., Schutz, B. E., and Neuenschwander, A. L. (2008). A Survey of ICESat Coastal Altimetry Applications: Continental Coast, Open Ocean Island, and Inland River. *Terrestrial, Atmospheric & Oceanic Sciences*, 19.

Wildman, R. A., Pratson, L. F., DeLeon, M., and Hering, J. G. (2011). Physical, chemical, and mineralogical characteristics of a reservoir sediment delta (Lake Powell, USA) and implications for water quality during low water level. *Journal of environmental quality*, 40(2):575–586.

Wu, W. (2007). *Computational river dynamics*. CRC Press.

Zedler, J. B. and Kercher, S. (2005). Wetland resources: status, trends, ecosystem services, and restorability. *Annu. Rev. Environ. Resour.*, 30:39–74.

Zhang, G., Xie, H., Kang, S., Yi, D., and Ackley, S. F. (2011). Monitoring lake level changes on the Tibetan Plateau using ICESat altimetry data (2003–2009). *Remote Sensing of Environment*, 115(7):1733–1742.

Zhang, Q., Ye, X.-c., Werner, A. D., Li, Y.-l., Yao, J., Li, X.-h., and Xu, C.-y. (2014). An investigation of enhanced recessions in Poyang Lake: comparison of Yangtze River and local catchment impacts. *Journal of Hydrology*, 517:425–434.

Zwally, H. J., Yi, D., Kwok, R., and Zhao, Y. (2008). ICESat measurements of sea ice freeboard and estimates of sea ice thickness in the Weddell Sea. *Journal of Geophysical Research: Oceans*, 113(C2).

Capítulo 3

Surface temperature dynamics and heat fluxes in a large subtropical shallow lake: a synergistic approach combining large-scale hydrologic/hydrodynamic modeling, *in situ* data and MODIS LST

This chapter is based on the following paper to be submitted:
Science of the Total Environment

Abstract

Assessment of large-scale temperature dynamics and heat fluxes in shallow lakes requires comprehensive modelling capabilities to simulate water interactions, the processes that occur and its driving forces. In this study, we investigated the spatial and temporal variations in water surface temperature (WST) and heat fluxes (mainly sensible and latent heat fluxes) for the period comprehended between January 2001 and December 2010 in Lake Mirim, a large (surface area c.a. 4000 km^2) shallow lake located in the broader between Brazil and Uruguay. The aquatic ecosystem was examined using in-situ WST measurements, MODIS land surface temperature (M*D11A1 LST) products and a coupling between a large-scale hydrologic model (MGB-IPH) and a hydrodynamic model (IPH-ECO). The WST values produced by the hydrodynamic model were consistent with measured in-situ data and MODIS derived WST, using both daytime and nighttime time series (R^2 = 0.88; Bias = 1.45 ^{o}C; RMSE = 2.16 ^{o}C; NS = 0.77). Our findings also revealed that cold front passages over Lake Mirim cause strong disturbances in the temperature dynamics and heat fluxes. Coupled large-scale hydrologic and hydrodynamic models will benefit future modeling efforts by providing an effective tool to study the temperature dynamics, heat fluxes, physical and ecological processes in large shallow lakes, and to address the impact of climate change in these ecosystems.

Keywords: Sensible heat flux; Latent heat flux; Cold fronts; Lake Mirim; MBG-IPH; IPH-ECO.

3.1 Introduction

Water Surface Temperature (WST) is an important indicator of climate change which governs most physical, chemical and ecological processes in aquatic ecosystems (Austin and Colman, 2007; Burnett et al., 2003; Piccolroaz et al., 2013; Schneider et al., 2009). The variability of WST within water bodies may occur due to anthropogenic stressors (*e.g.*, hydrological processes in upland basins, pollution discharge) and due to atmospheric conditions (Brown et al., 2006; Webb et al., 2003). Some studies (e.g. O'Reilly et al., 2015; Schneider and Hook, 2010) have shown an increase in the mean WST ranging from 0.01 to 0.1^{o}C in lakes and reservoirs around the globe with a trend to increase in the next years (Schmid et al., 2014). This change in mean water temperature can lead to significant ecosystem changes in biological processes, such as the mineralization of organic carbon and phytoplankton primary productivity (Darchambeau et al., 2014; Gudasz et al., 2015; Kehoe et al., 2015), as well as the interactions and energy fluxes between the atmosphere and the water surface (Alcântara et al., 2010b; Zhang et al., 2014).

The conventional method to evaluate WST relies on *in situ* measurements, which is expensive, time consuming, difficult to apply to large areas, and leads to unreliable results sometimes (Bicudo and Bicudo, 2004). Over the last years, the evaluation of WST in inland waters, such as lakes and reservoirs, using remote sensing techniques has been successfully applied (Bresciani et al., 2011; Crosman and Horel, 2009; Giardino et al., 2015; Sima et al., 2013). Remote sensing tools provide an enormous amount of information, allowing spatial cover on remote sites and large areas (Politi et al., 2012; Rodríguez et al., 2014). Furthermore, it has the advantage of turning the datasets public available in many cases (Trumpickas et al., 2009). Some studies have estimated WST employing different satellites, such as the ASTER mission (Gillespie et al., 1998; Schneider et al., 2009; Steissberg et al., 2005) and Landsat images (Lamaro et al., 2013; Wloczyk et al., 2006). Nevertheless, most of these satellites achieve WST data twice a day every 16 days, leading to some uncertainty for estimates of monthly and annual variations (Murphy et al., 2013; Xu et al., 2013). Recently, WST estimation from MODIS (Moderate Resolution Imaging Spectroradiometer) data, aboard the Terra (EOS AM) and Aqua (EOS PM) satellites, have been successfully applied to several lakes (e.g. Crosman and Horel, 2009; Sima et al., 2013; Zhang et al., 2014), showing good agreement with field data. MODIS satellite is a 36-band instrument which allows daily data collection (in clear-sky conditions) (Wan et al., 2004), providing an opportunity to monitor the overall water surface temperature changes in these ecosystems.

The computational modeling of aquatic ecosystems is an efficient tool to understand the main physical, chemical, and biological processes within these environments (Ji, 2017; Shiflet and Shiflet, 2014). In this context, different models are available such as IPH-ECO (Fragoso et al., 2009), ELCOM (Hodges, 2000), DYRESM-CAEDYM (Hamilton and Schladow, 1997), PCLAKE (Janse, 2005) with the main differences regarding physical processes related to vertical mixing and heat budget computation. While complex three-dimensional models are of interest in deep lakes where stratification plays a key role along the year (Ofir et al., 2017; Recknagel et al., 2014), shallow large lakes are polymitic with intense vertical mixing along the year. For long-term numerical simulations, one can rely on two-dimensional or even one-dimensional models once the models are capable of simulating the free-surface thermodynamics properly (Cavalcanti et al., 2016; Fragoso et al., 2011; Hipsey et al., 2014; Trolle et al., 2011). The majority of computational models resort on four main processes causing changes in water temperature at the free-surface, namely: Net Short-Wave (SW) and Net Long-Wave (LW) Fluxes, Sensible Heat Flux (SE), and Latent Heat Flux (LE). SW is the Solar Radiation energy after accounting the surface albedo reflection. LW is the balance between the Long-Wave radiation emitted by the sun and the Long-Wave radiation reflected by the water surface. SE is the conduction flux between the water surface and the atmosphere, which can be positive or negative. Finally, LE is the heat flux

due to water evaporation/condensation. Each flux can drive surface water temperature variations (Curtarelli et al., 2014; Fink et al., 2014a; McGloin et al., 2014), and due to physical mixing (convective cooling/heating) (MacIntyre and Melack, 1995; MacIntyre et al., 2002) the use of spatial explicit computational models (at least two dimensional) is attractive. In large aquatic ecosystems, the combined assessment of large-scales and horizontal advection on temperature dynamics requires a greater understanding of the capabilities of the model to represent the interactions between physical processes and the heat balance at the water surface.

Recently, the synergy between numerical modeling and remote sensing techniques has been successfully applied in lakes and reservoirs to estimate the short-term scale variations (*i.e.* diurnal, weekly) on WST. This approach allows a better comprehension in coupling between processes and the assessment of different thermal processes under different meteorological conditions (*e.g.,* cold fronts passages). The understanding of the impacts of short-scale meteorological events such as cold fronts in lakes and reservoirs is important due to the effects on the physical, chemical, and biological processes that driven hydrodynamics and water quality in these ecosystems (Alcântara et al., 2010b; Curtarelli et al., 2013, 2014; Gallucci and Netto, 2004; Morais et al., 2010; Tundisi et al., 2004). These events cause changes in the wind (both velocity and direction), temperature, humidity and atmospheric pressure (Lenters et al., 2005; Liu et al., 2011, 2009), cause disturbance in the water quality and ecological dynamics (Tundisi et al., 2010). Nevertheless, in Brazil, few studies combining numerical modeling and remote sensing can be founded in recent literature. Curtarelli et al. (2014) studied the variability in the temperature dynamics, heat budget and thermal structure in the Itumbiara reservoir (Brazil) (water-surface area: 814 km^2). Alcântara et al. (2010b) mapped the water surface temperature (WST) variations and heat flux in the same reservoir from MODIS daytime / nighttime images. Luz et al. (2017) assessed the surface temperature in the Guaíba Lake, from MODIS images. In these studies, there are some limitations due to short-term scale, or the use of remote sensing techniques alone, which tend to limit the behavior of some seasons (winter) due to the number of cloudy imageries, especially under extreme meteorological conditions (*e.g.,* cold fronts passages).

In this study, we assessed the spatial and temporal variability (daily, monthly, seasonal and inter-annual) of water surface temperature and heat fluxes in Lake Mirim for ten years (2001- 2010). This study presents a new approach using *in situ* measurements, MODIS land surface temperature (LST) data, and the coupling between a large-scale distributed hydrological model (MGB-IPH, (Collischonn et al., 2007) with an hydrodynamic/water quality model (IPH-ECO, (Fragoso et al., 2009). This is a first study using the synergy between these three approaches in a large subtropical shallow lake (lake water-surface area: 4000 km^2) in long-term time-scale, allowing to

assess simultaneously different periods (wet years, dry years, and seasonality) and the responses to the impacts of several stressors, such as cold front passages and changes in upland basin, on the ecosystem.

3.2 Study Area

Lake Mirim (Fig. 1), is a large shallow subtropical lake located between Brazil and Uruguay (32°00' and 33°00'S, 052°00' and 054°00'W). The lake surface area is 4000 km^2, 190 km along the major axis and 40 km wide on average. The maximum depth is 10 m with an average depth of 4.5 m. The region has a subtropical climate, with mean annual rainfall ranging from 1,200 mm to 1,450 mm and a mean annual temperature of 16 ºC (Kottek et al., 2006). Lake Mirim is connected to the larger Patos Lagoon (lake water surface area c.a. 10,000 km^2) through the São Gonçalo Channel, which is approximately 76 km long and is controlled by a sluice/dam system, preventing the entry of seawater into the lake during the dry season and controlling the lake volume. The main sub-basins contributing to Lake Mirim are located on the west shore, in which the Cebollati, Jaguarão and Tacuari rivers are the main tributaries. The primary uses of Lake Mirim water if for irrigation of rice crops followed by water supply. The lake is also important for navigation, connecting cities in the southern part of Brazil to cities in the northern part of Uruguay. At east of Lake Mirim is located Lake Mangueira, a large shallow subtropical coastal lake, covering a surface area of c.a. 820 km^2 with a mean depth of 2.6 m and maximum depth of 6.5 m. The lake basin is elongated with 90 km upon its main axis (NE-SW) and 3-10 km wide. The lake has been studied for several years consolidating a concise dataset of physical, chemical, and biological variables (Bohnenberger et al., 2017; Cavalcanti et al., 2016; Fragoso et al., 2008, 2011; Lima et al., 2016)

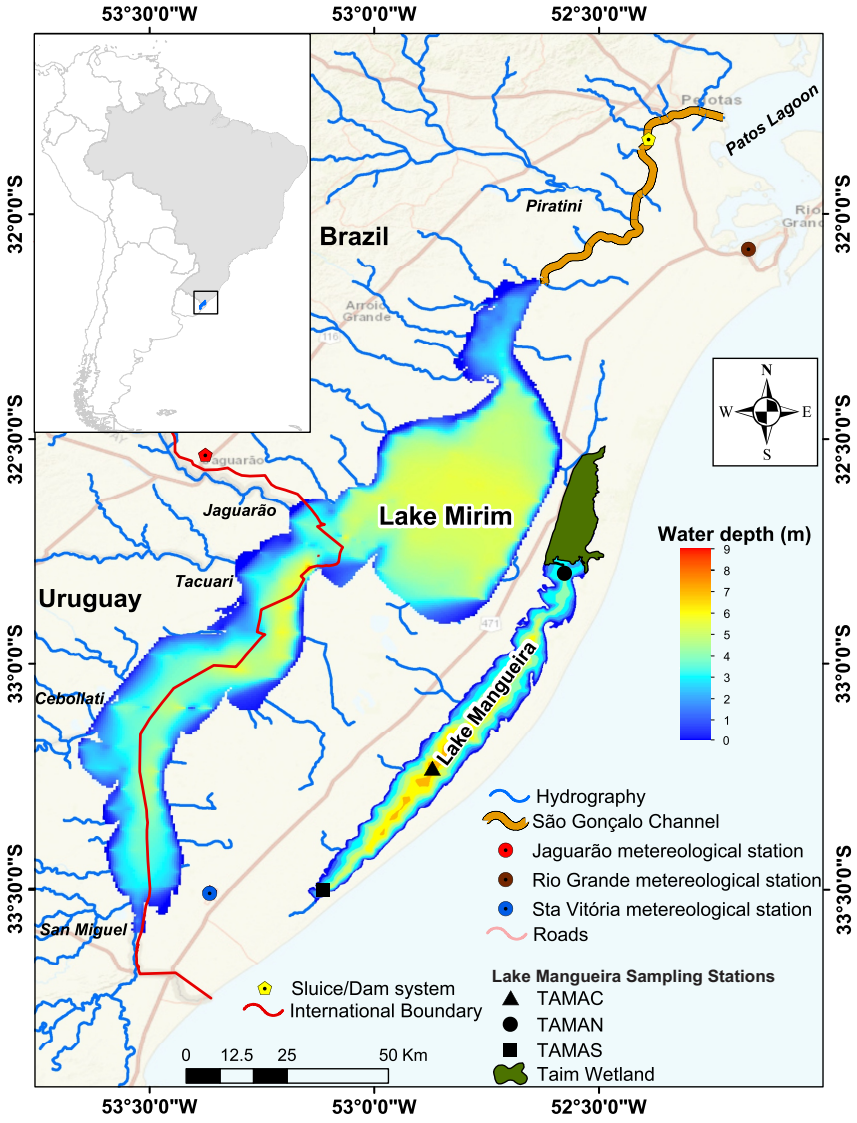

Figure 1 – Lake Mirim and Lake Mangueira location showing its main river basins, lake bathymetry, meteorological stations, country borders, and the São Gonçalo Channel.

3.3 Data and methods

3.3.1 MODIS LST data

MODIS Land Surface Temperature (LST) products were downloaded via the web interface The Land Processes Distributed Interface Active Archive Center (LP DAAC), from The US Geological Survey EROS Data Center available at `http://LPDAAC.usgs.gov`. MODIS/Terra V5 LST/E L3 Global 1 km Grid (MOD11A1 products) with two data per day (daytime e nighttime taken around 10:30 a.m. and 11:30 p.m., respectively), were used. These products were chosen due to consider the imaged area elevation, cloud mask, cloud-contaminated pixels removal and atmospheric correction (Wan, 2008). In addition, the MODIS-derived LST product (MOD11A1) has been successfully validated in other lakes, showing good agreement with the *in situ* measurements, such

as the western TP lakes, Asia (Wang et al., 2007; Zhang et al., 2014), Malawi Lake, Tanzania (Chavula et al., 2009), Qinghai Lake, China (Fei et al., 2013), Taihu Lake, China (Liu et al., 2015), Lakes Jocassee, Keowee, Hartwell, Russell, and Thurmond, USA (Phillips et al., 2016), Great Salt Lake, UT, USA (Grim et al., 2013).

All MODIS cloud-free images available between 2001 and 2010 were downloaded, resulting in a total of 3564 daytime images and 3721 nighttime images. In addition, MODIS quality product was used to assess image quality (Roy et al., 2002). The MODIS Reprojection Tool available at was also used to transforming the sinusoidal projection images (ISIN). The MOD11A1 LST images were processed and analyzed using a MatLab® routine.

3.3.2 *In situ* WST data and MODIS LST Validation

To validate the MODIS LST products we used the approach proposed by Zhang et al. (2014), where the authors examined the WST changes of 52 lakes in the Tibetan Plateu (Asia), validating the MODIS LST product from in situ WST data collected only in one location. The *in situ* measurements of water surface temperature in Lake Mirim were not available, thus the validation of the MODIS LST data used in this study was performed using the concise dataset available for Lake Mangueira, which exhibits similar genesis and hydro-geomorphological characteristics compared to Lake Mirim (Kotzian and Marques, 2004; Schwartzbold and Schafer, 1984). Lake Mangueira WST dataset is a part of an ongoing project and we chose to use the WST field data from January 2001 to December 2010.

3.3.3 Coupled approach: brief description

We employed an off-line coupling (e.g. Bravo et al., 2011) between the large-scale hydrological model MGB-IPH (Collischonn et al., 2005, 2007; Collischonn and Tucci, 2001; Fan et al., 2014; Paiva et al., 2013) and the three-dimensional water quality and hydrodynamic IPH-ECO model (Fragoso et al., 2009). The MGB-IPH model estimated the time-series of river discharges, which are then used as an input for the IPH-ECO model. The latter was able to represent the main hydrodynamic processes in Lake Mirim (*e.g.,* water levels). For more details regarding the coupling of the models, parameterization, calibration and validation of the coupled approach, input data, and boundary conditions the readers are suggested to read Munar et al. (2017)

3.3.3.1 Hydrological modeling

The MGB-IPH model is a large-scale distributed hydrological model. It uses catchment based discretization and combinations of land use and soil type within each catchment unit following a Hydrological Response Unit (HRU) approach (Kouwen

et al., 1993). Simulation methods include energy budget and evapotranspiration from the Penman-Monteith approach (Shuttleworth, 1993), soil water budget using a bucket model, and surface runoff is calculated using the approach proposed in the Arno model (Todini, 1996) based on the variable contributing area concept. The streamflow is estimated through the river network, using the Muskingum-Cunge method. The MGB-IPH model has been used in several Amazonian and South American basins (e.g. Collischonn et al., 2008; Fan et al., 2016, 2015; Getirana et al., 2010; Nóbrega et al., 2011; Pontes et al., 2015; Siqueira et al., 2016). For the Lake Mirim basin, the MGB-IPH parameterization and calibration, hydro-meteorological data used, and simulations were presented in detail in a recent article (Munar et al., 2017).

3.3.3.2 Hydrodynamic modeling and heat budget modelling

The IPH-ECO model (Fragoso et al., 2009) (freely available in: `http://www.ipheco.org`), describes the main physical (water temperature and density, velocity fields, and free-water elevation), biotic and abiotic components in aquatic environments. The model has a hydrodynamic module in which it solves a Reynolds-Averaged Navier-Stokes Equation in structured quadrilateral grids, using a semi-implicit approach based on the TRIM model (Casulli and Cheng, 1992), and its improvements (Casulli and Cattani, 1994). The momentum advection and diffusion are discretized by an Eulerian-Lagrangian approach (Cheng et al., 1993). The water quality module of IPH-ECO is largely based on the PC-Lake model (Janse, 2005), with some modifications for subtropical and tropical regimes. The model was applied successfully in different sites in Brazil, Denmark and Sweden to assess the coupling between physical and ecological processes in shallow environments (e.g. Cavalcanti et al., 2016; Fragoso et al., 2008, 2011; Pereira and Fragoso, 2013).

In order to describe water temperature dynamics coupled with physical processes, IPH-ECO solves an advection-diffusion-reaction type of equation, which integrates the velocity field and water level output from the hydrodynamic module with a heat budget prescribed by Chapra (2008) for lakes. For more details about the computational link between hydrodynamics and water quality variables using IPH-ECO the readers are referred to Cavalcanti et al. (2016). The total Surface Heat Budget in the model is described as a function of short-wave and longwave radiations, sensible heat flux and latent heat flux, as follows:

$$J = J_{sn} + \phi_{al} - \phi_{wl} - \phi_{sf} - \phi_{lf} \tag{1}$$

Where J is the effective surface heat flux balance (W m^{-2}), J_{sn} is the net solar short-wave radiation, ϕ_{al} is the atmospheric longwave radiation, ϕ_{wl} is the water longwave

radiation, ϕ_{sf} is the sensible heat flux and ϕ_{lf} is the latent heat flux. The conversion between energy and temperature is given by the following equation:

$$\Delta T = \frac{J}{\rho C_p H} \tag{2}$$

Where ΔT is the change in water temperature in a given computational cell ($^oC.s^{-1}$), ρ is the water density (kgm^3), C_p is the specific heat capacity of water (4184 $J\ kg^{-1}\ ^oC^{-1}$), and H is the total water depth in the cell (m).

The net short-wave radiation is calculated by accounting for reflection (albedo):

$$J_{sn} = (1 - R_L).J_{sw} \tag{3}$$

where R_L is the Albedo of the specific surface (in this case, set to 0.03) and J_{sw} is the short-wave radiation measure at the surface.

The atmospheric longwave radiation ϕ_{al} is calculated using the following equation:

$$\phi_{al} = \sigma(T_{air} + 273)^4(A + 0.031\sqrt{e_{air}})(1 - R_L) \tag{4}$$

Where σ is the Stefan-Boltzman constant (4.9x10^{-3} J (m^2 d K^4)$^{-1}$ or 11.7x10^{-8} cal (cm^2 d K^4)$^{-1}$, T_{air} is the air temperature (^{o}C), A is a coefficient that varies between 0.5 to 0.7, e_{air} is the air vapor pressure (mmHg). The water longwave radiation ϕ_{wl} is calculated as:

$$\phi_{wl} = \epsilon\sigma(T_s + 273)^4 \tag{5}$$

Where ϵ is the emissivity of radiating body (approximately 0.97) and T_s is the water surface temperature. In the present study, A and ϵ were calibrated (all other parameters were know). The values found for A and ϵ were 0.65 and 0.9 respectively.

The sensible ϕ_{sf} and latent heat flux ϕ_{sf} are estimated as:

$$\phi_{sf} = C_1 f(U_w)(T_s - T_{air}) \tag{6}$$

$$\phi_{lf} = f(U_w)(e_s - e_{air}) \tag{7}$$

Where C_1 is the Bowen's coefficient ($\approx$0.47 mmHg ^{o}C^{-1}), e_s is the saturation vapor pressure at the water surface (mmHg). There is condensation if $e_s < e_{air}$. The term $f(U_w)$

defines the dependence of the transfer of wind velocity over the water surface, and U_w is the wind velocity measured in m s^{-1} at a height of 7m above the water surface. The term $f(U_w)$is described:

$$f(U_w) = 19.0 + 0.95(U_w)^2 \tag{8}$$

3.3.4 Model configuration

Lake Mirim was discretized using a 500-m resolution structured quadrilateral grid, resulting in 15,289 computational cells. The period of simulation was set from 1 January 2001 to 31 December 2010 and the simulation was performed using a computational time step of 60 s. The temporal weight theta was chose as 0.55 and the wet- and drying threshold of computational cells was set to 0.05. The bottom boundary condition was parameterized using a Chezy formulation with Chezy coefficient equal to 60 $m^{1/2}$ s^{-1}.The horizontal eddy viscosity and diffusivity were set to 15 m^2 s^{-1}. A total of 32 inflow series were estimated by the hydrological model with 7 outflow series estimated by rice cultivation area. The meteorological data were collected in three meteorological stations near the lake (see Fig. 1). The parametrization and calibration of the coupled hydrologic-hydrodynamic model, input data, boundary conditions, model validation and more details can be founded in Munar et al. (2017) .

3.3.4.1 Analysis of the results

In order to assess the MODIS LST variability of the water surface temperature against the simulated water temperature variability, we selected seven points ($P_1, P_2, P_3, P_4, P_5, P_6$ and P_7) distributed along the Lake Mirim (Fig. 4a). To evaluate the accuracy of the IPH-ECO model, the coefficient of determination (R^2), Bias, Root-Mean-Square-Error (RMSE), and the Nash-Sutcliffe efficiency coefficient (NS) (Nash and Sutcliffe, 1970) were calculated comparing the median of WST simulated from IPH-ECO versus the median of the MODIS-derived WST (boxplot) at the seven chosen points of the lake. The analysis of the spatial variations (daily, monthly, seasonal, inter annual) of the mean water surface temperature WST was carried out using the VisIt software. The statistical significance of the WST between regions in the Lake Mirim was performed using a MatLab® routine with the Analysis of Variance (ANOVA) confidence level was set to 0.05. In order to assess the significance of spatial differences, we performed a post-hoc analysis using Tukey's HSD (Honestly Significant Difference) test.

Regarding the cold front effects on the water surface dynamics over Lake Mirim, we selected the period of 1 June 2007 to 30 June 2008. This period was chosen

due the occurrence of cold front passages over the lake with the longest duration, according to the CPTEC (*Centro de Previsão de Tempo e Estudos Climáticos*) available at `http://www.cptec.inpe.br/`. During this period, seven important cold fronts passed over the Lake Mirim region. The period of cold action, was represented as $F_1, F_2, F_3, F_4, F_5, F_6$ and F_7. These meteorological events were verified from visual inspection using Geostationary Operational Environmental Satellite (GOES) satellite images.

3.4 Results

3.4.1 Comparison between *in situ* measurements and MODIS LST

The validation of the MOD11A1 products was performed by comparing with three sampling points in the North, Central and South parts of Lake Mangueira (namely: TAMAN, TAMAC and TAMAS) using the 2001 to 2010 period (Fig. 2).The efficiency indices indicated a good agreement between MODIS-derived WST and field measurements ($R^2 \geq 0.80$, Bias ≤ 1.29 °C, RMSE ≤ 2.54 °C and NS ≥ 0.68) with slightly differences in the overall behavior for each spatial location.

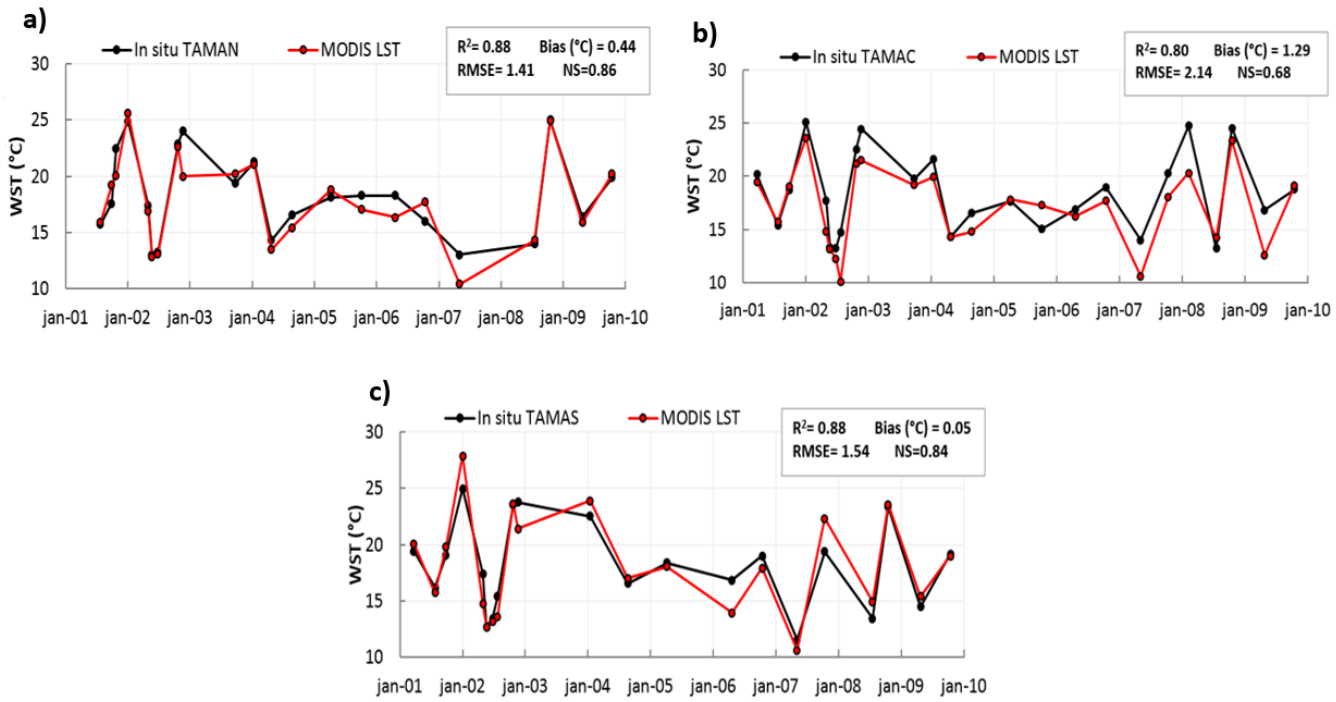

Figure 2 – The water surface temperature at three sampling points in the North (a), Center (b) and South (c) parts of Lake Mangueira (black line) derived from in situ measurements from the 2001 to 2010 period and MODIS LST data (red line) in the same period.

3.4.2 Model simulation

3.4.2.1 Model calibration

The simulated WST using IPHECO agreed with the water surface temperature retrieved from MODIS imagery in Lake Mirim for seven spatially distributed points (Fig. 3). The seven points were chosen randomly along the lake. The simulated water temperature in the seven points was mostly heterogeneous, with the Tukey's HSD test showing significant difference ($p < 0.05$) among regions (Table 1). In general, the adjustment between the model results and the MODIS derived WST showed good efficiency indices ($R^2 = 0.88$; Bias = 1.45 °C; RMSE = 2.16 °C; NS = 0.77 regarding the seven points analyzed.

Table 1 – Tukey's HSD (Honestly significant difference) test for WST simulates in the seven points ($P_1, P_2, P_3, P_4, P_5, P_6$ and P_7) in the Lake Mirim. The statistically significant ($p < 0.05$) differences between the means of the pairwise components analyzed are indicated in bold.

	P_1	P_2	P_3	P_4	P_5	P_6	P_7
P_1	-						
P_2	**0.87**	-					
P_3	**0.89**	0.02	-				
P_4	**0.35**	**-0.52**	**-0.53**	-			
P_5	**0.42**	**-0.45**	**-0.47**	**0.07**	-		
P_6	**0.38**	**-0.48**	**-0.50**	0.03	-0.03	-	
P_7	**0.34**	**-0.52**	**-0.54**	-0.01	**-0.07**	-0.04	-

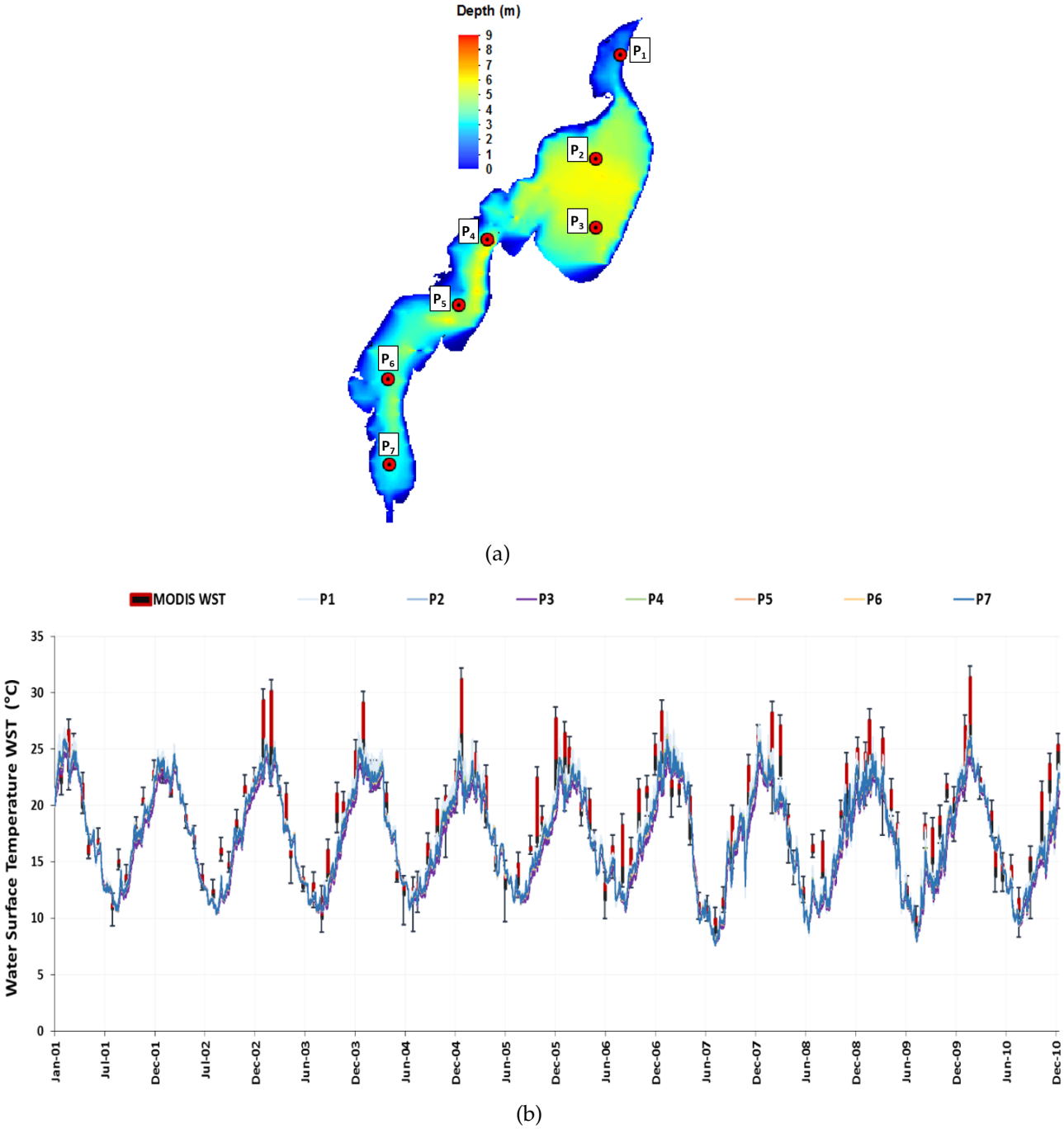

Figure 3 – Location of seven points ($P_1, P_2, P_3, P_4, P_5, P_6$ and P_7) in lake Mirim (a) and IPH ECO model calibration of the WST for 2001-2010 period (b), showing the WST simulated at $P_1, P_2, P_3, P_4, P_5, P_6$ and P_7 points (line plots) and MODIS LST derived (boxplot) values. Each boxplot compiles a monthly median data from MODIS LST for the seven points.

3.4.2.2 Water surface temperature modeling

The simulated WST showed strong monthly variations fluctuating between 23.9ºC (average value in March) and 12.3ºC (average value in August), whereas the annual averages showed a small amplitude in the average values, ranging from 17.9 ºC (average value in 2008) to 20.1ºC (average value in 2010) (Fig. 4). For some

specific years, it is possible to notice shallow regions (*i.e.,* littoral zones) with higher temperatures compare to deep regions (*i.e.,* pelagic zones), showing the heterogeneity in the WST in the Lake Mirim (Fig. 4a). Regarding the monthly mean values, it is possible to notice a strong seasonal variation with an increase of the WST in summer (January to March), and a decreasing in winter (July to September) (Fig. 4b). In addition, during spring (October to December) and autumn (April to June), the WST showed a higher spatial heterogeneity when compared to summer and winter, seasons with higher spatial homogeneity of water surface temperature values.

3.4.2.3 Simulated Heat fluxes

Fig. 5 shows monthly mean values (W.m^{-2}) of the effective surface heat balance, sensible heat flux, and latent heat flux. The model results indicated a marked seasonal dynamics in heat fluxes (Fig. 5a), with the period from December to February the months where the lake gains more heat, especially in shallow areas. From May to August the lake experiences a heat loss with July as the month where heat loss reach highest values in the pelagic area of the lake (-16.4 W.m^{-2}). The maximum monthly heat loss due to sensible heat flux reach the maximum values in January (14.5 W.m^{-2}) and minimum values in July (-12.65 W.m^{-2}) (Fig. 5b). The monthly mean maximum heat loss by latent heat flux (evaporation) is 132.1 W.m^{-2} in January and the lowest heat loss by evaporation in August (12.4 W.m^{-2}) (Fig. 5c). The mean annual heat loss due to evaporation is 68.8 W.m^{-2}. Considering a latent heat of vaporization equal to $2.47x10^{-6}$ $J.Kg^{-1}$, the annual amount of evaporation in the Lake Mirim is E = 878.9 mm.

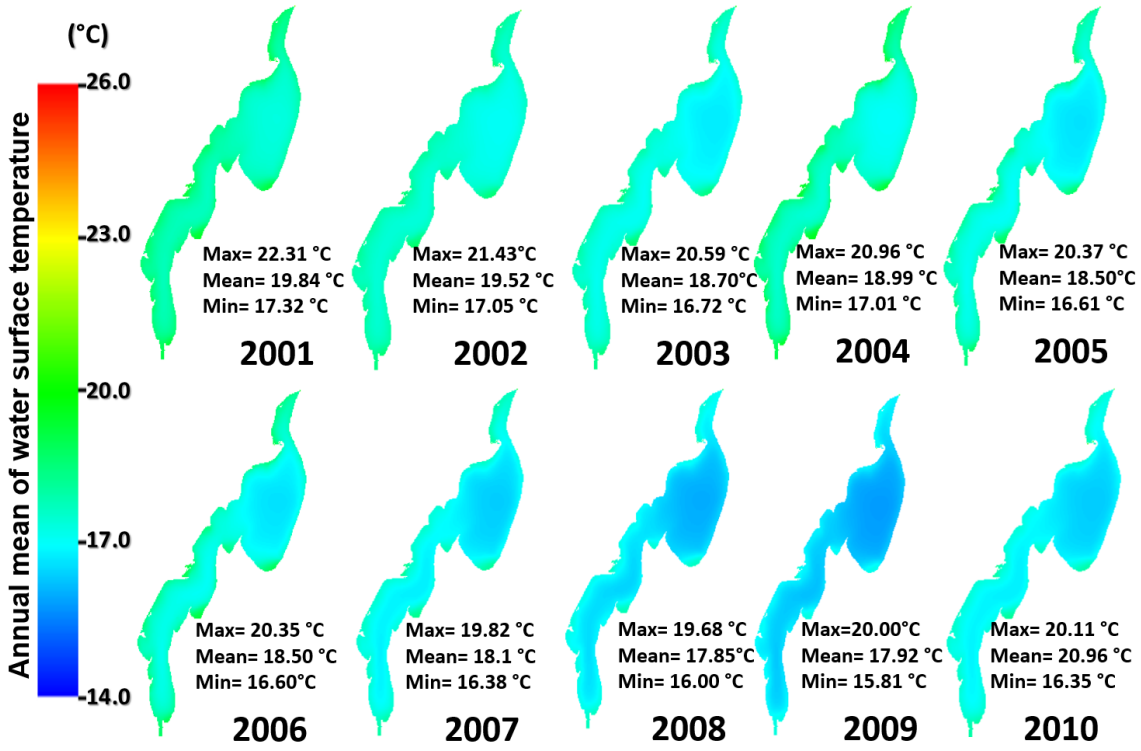

(a)

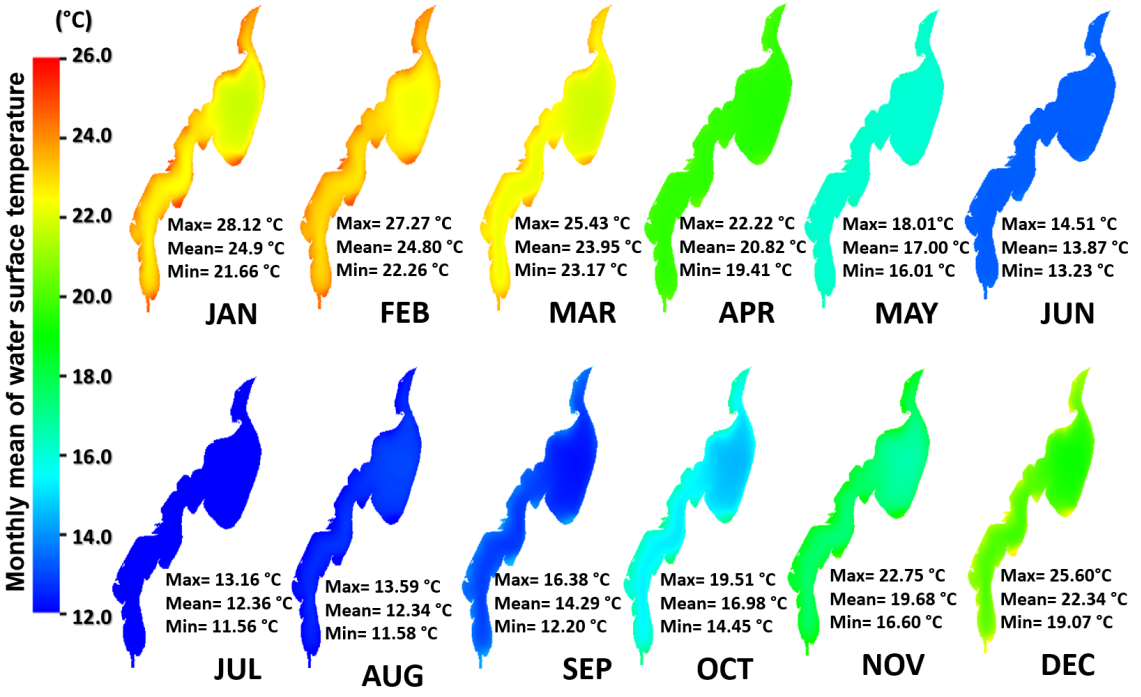

(b)

Figure 4 – Annual (a) and Monthly (b) mean values of water surface temperature for the period comprehended between January 2001 and December 2010. These results are related to IPH-ECO simulations showing maximum, average and minimum values, all units are in centigrade.

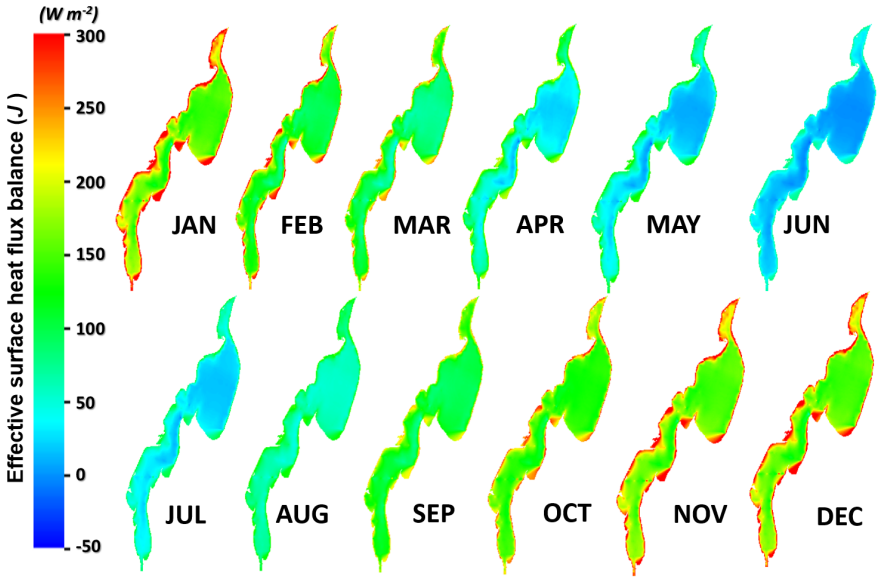

(a)

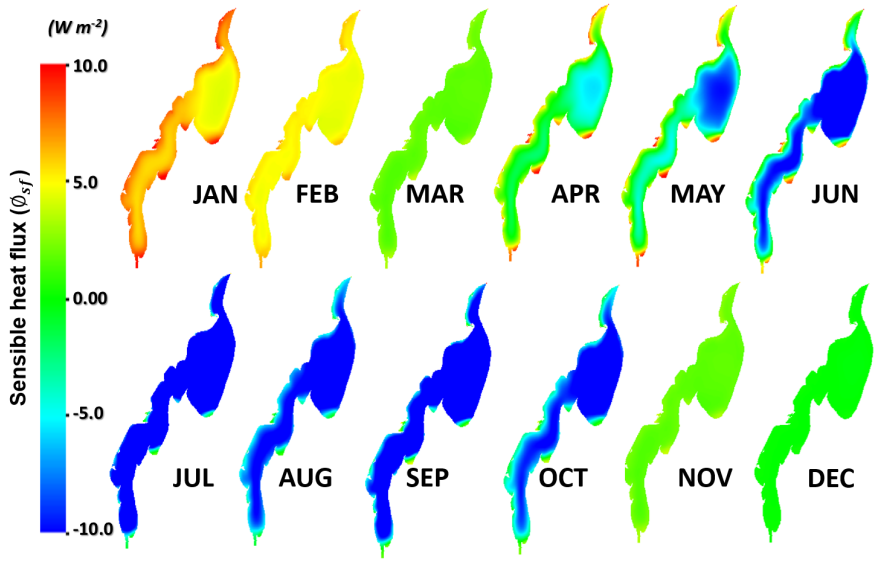

(b)

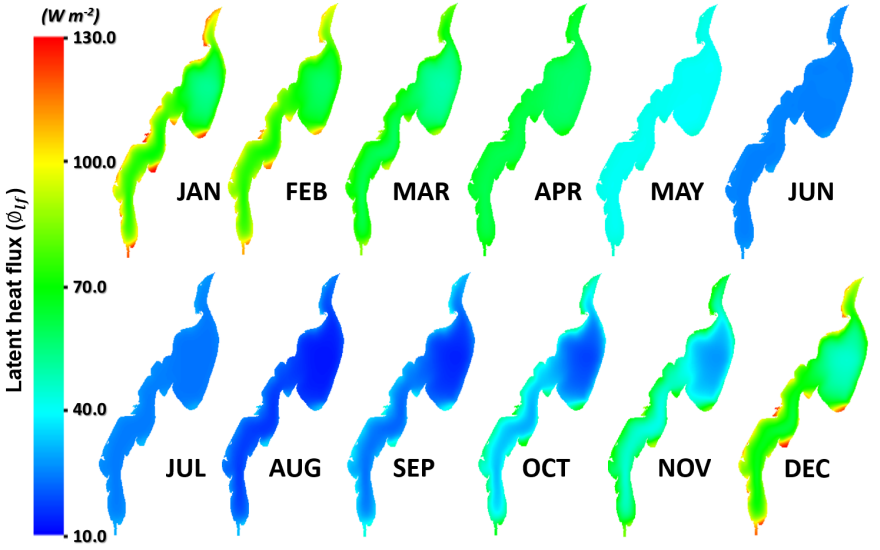

(c)

Figure 5 – Simulated monthly mean values of the effective surface heat balance (a), sensible heat flux (b), and latent heat flux (c) over Lake Mirim. These results are related to IPHECO simulations with units in W.m^{-2}.

3.4.2.4 Effects of cold fronts on the WST, sensible and latent heat fluxes

The analyses of the seven cold fronts (namely: $F_1, F_2, F_3, F_4, F_5, F_6$ and F_7) reported by CPTEC (`http://www.cptec.inpe.br/`) for the period comprehended from June 2007 to June 2008 (period of higher frequency of passages) showed a fast and sharp decreasing in air temperatures (Fig. 6, grey line). For points P1, P4, and P7, representatives of North, Center, and North regions of Lake Mirim, respectively (see Fig. 3a), it is possible to notice a decrease in simulated WST, which agrees with the reported decrease in air temperature (Fig. 6). A detailed analysis of the effects of cold front passages on simulated WST and heat fluxes (namely, sensible and latent heat fluxes) was performed by selecting only the cold fronts F_1 and F_4, which showed higher impact on the system (regarding duration and intensity). These cold front passages reached the Lake Mirim basin in two different seasons: winter (F_1) and spring (F_4) in the southern hemisphere.

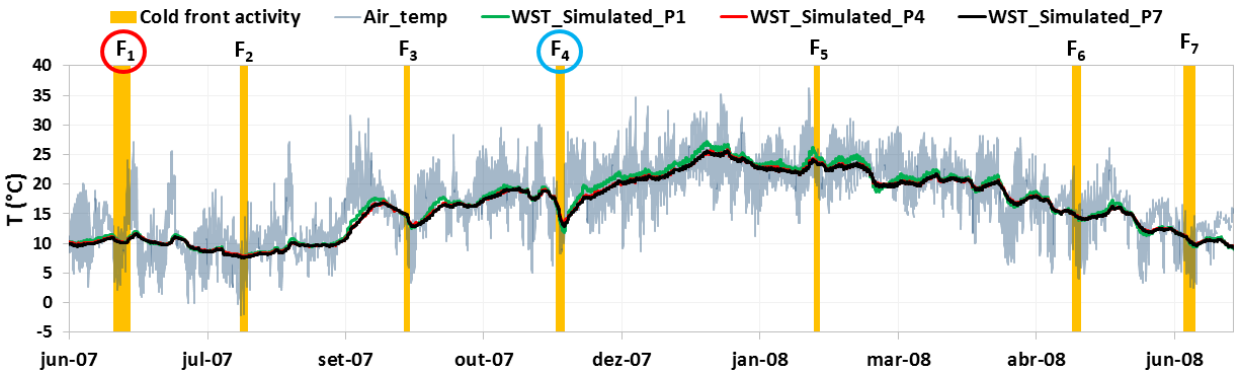

Figure 6 – Cold front activity ($F_1, F_2, F_3, F_4, F_5, F_6$ and F_7) over the Lake Mirim (yellow bar) during the period comprehended from June 2007 to June 2008. A gray line shows air temperature and a green line (P1), a red line (P4), and a black line (P7) shows the simulated WST. The red and blue circles shows the cold front event selected for detailed analysis.

Fig. 7a shows the effect of the F1 cold front event at the three representative points chosen (P1, P4 and P7) in Lake Mirim. On the cold front days (from June, 16 to June, 22), the water surface temperature decreases at the three points reaching a minimum values of 10.0ºC at P7. As expected, the impact was higher on the air temperature reaching a minimum value of 6.7ºC . It is also noticeable that shallow regions tend to be more prone to cold front effects, changing the simulated WST faster than deep regions (Fig. 7b). The effective surface heat flux balance showed positive values (+50 W.m^{-2}) (heat gain) before and after of the cold front passage and negative values (-50 W.m^{-2}) (heat loss) during of the event(Fig. 7c). The sensible heat flux showed a tendency to increase energy after the cold front passage, with values ranging from -20 W.m^{-2} at the beginning of the event to +20 W.m^{-2} at the end of the event (Fig. 7d). The similar behavior is noticed for latent heat flux, with condensation during the cold front passage (-30 W.m^{-2}), and a return to heat loss at the end of the event (+30 W.m^{-2}) (Fig. 7e).

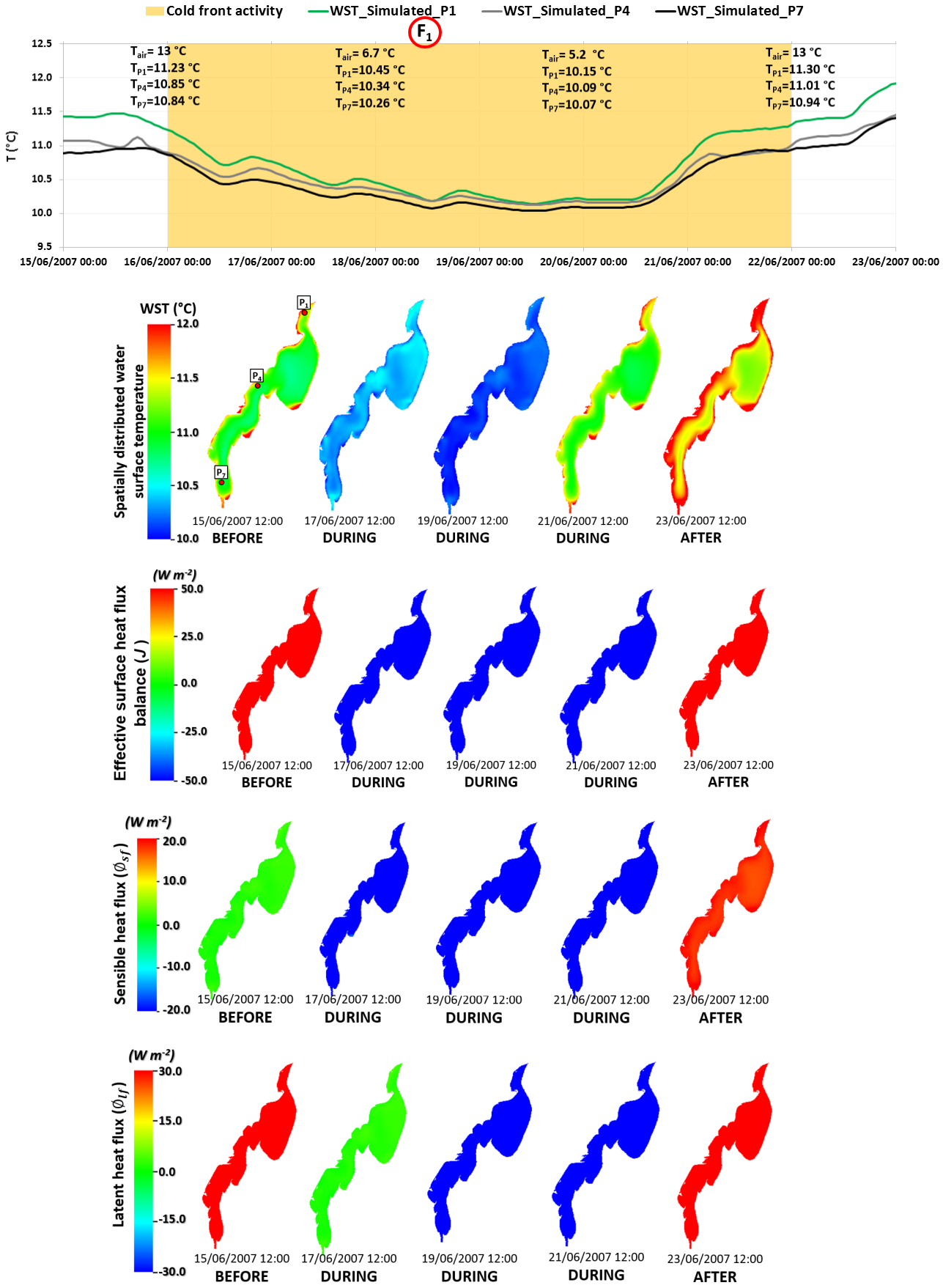

Figure 7 – The effect of the F_1 cold front event on simulated WST, effective surface heat flux balance and heat flux (sensible and latent) in Lake Mirim. (a) Air temperature and simulated WST at P1 (green line), P4 (grey line), and P7 (black line) points, and cold front activity (yellow bar). (b) Spatially distributed simulated WST. (c) Spatial distributed simulated effective surface heat flux balance. (d) Spatial distributed simulated sensible heat flux. (e) Spatial distributed simulated Latent heat flux. The dates of each snapshot is show at the bottom of the maps.

The results regarding the F_4 cold front event showed a higher impact on simulated WST, the effective surface heat flux balance and heat fluxes (latent and sensible) compared to the F_1 event, although the latter had a longer duration (in terms of days). The F_4 event lead to a higher decreasing on the WST of the lake (Fig. 8a), reaching minimum values of 12.1ºC at P1. Spatially distributed WST showed a decreasing, reaching minimum values of 10ºC (16 November 2007) in shallower waters (Fig. 8b). The simulated effective surface heat flux balance noticed heat gain (+200 W.m^{-2}) before and after of the cold front passage and heat loss (-100 W.m^{-2}) during of the event (Fig. 8c). The maximum values of sensible and latent heat flux reached around -23.16 W.m^{-2} and -48.8 W.m^{-2} (17 June 2007) respectively (Fig. 8d and Fig. 8e) during F_4.

3.5 Discussion

3.5.1 Comparison of *in situ* WST and MODIS LST

The validation of the MODIS-derived WST product showed a good fit with *in situ* measurements of water surface temperature at three sampling points (North, Central and South) of Lake Mangueira (Fig. 2), allowing to represent even the maximum (2002) and minimum values (2007) and the seasonal dynamics of the WST. Besides the smaller positive bias showed for the Central point (located in deeper region of the lake), which can be due to the difference in depths between the sample points (Ke and Song, 2014; Kozlov et al., 2014), the accuracy of our results was consistent with the accuracies found previously (e.g. Chavula et al., 2009; Crosman and Horel, 2009; Fei et al., 2013; Liu et al., 2015; Phillips et al., 2016; Sima et al., 2013; Zhang et al., 2014), suggesting the reliability of this approach.

3.5.2 Modelled WST and heat fluxes: spatial and temporal patterns

The IPH-ECO model compared to the validated MODIS - derived water surface temperature (WST) successfully represented the WST in Lake Mirim, in all years of simulation, showing a good for the seven points analyzed ($P_1, P_2, P_3, P_4, P_5, P_6$ and P_7), even for maximum-values (2007) and minimum-level (2009) periods and the seasonal dynamics of WST. As expected, models results indicated that the WST simulated in the seven points (P_2, P_3, P_4, P_5, P_6 and P_7) showed differences statistically significant ($p < 0.05$), indicating a heterogeneity in the WST in the Lake Mirim. This fact can be attributed to the shallow waters (average depth = 4.5m) in the lake, which presents a wide day-to-day variation on water levels. These regions are influenced directly by the solar radiation, leading more fluctuations on the WST that in deep zones, as founded in similar environments (Missaghi and Hondzo, 2010; Soulignac et al., 2017).

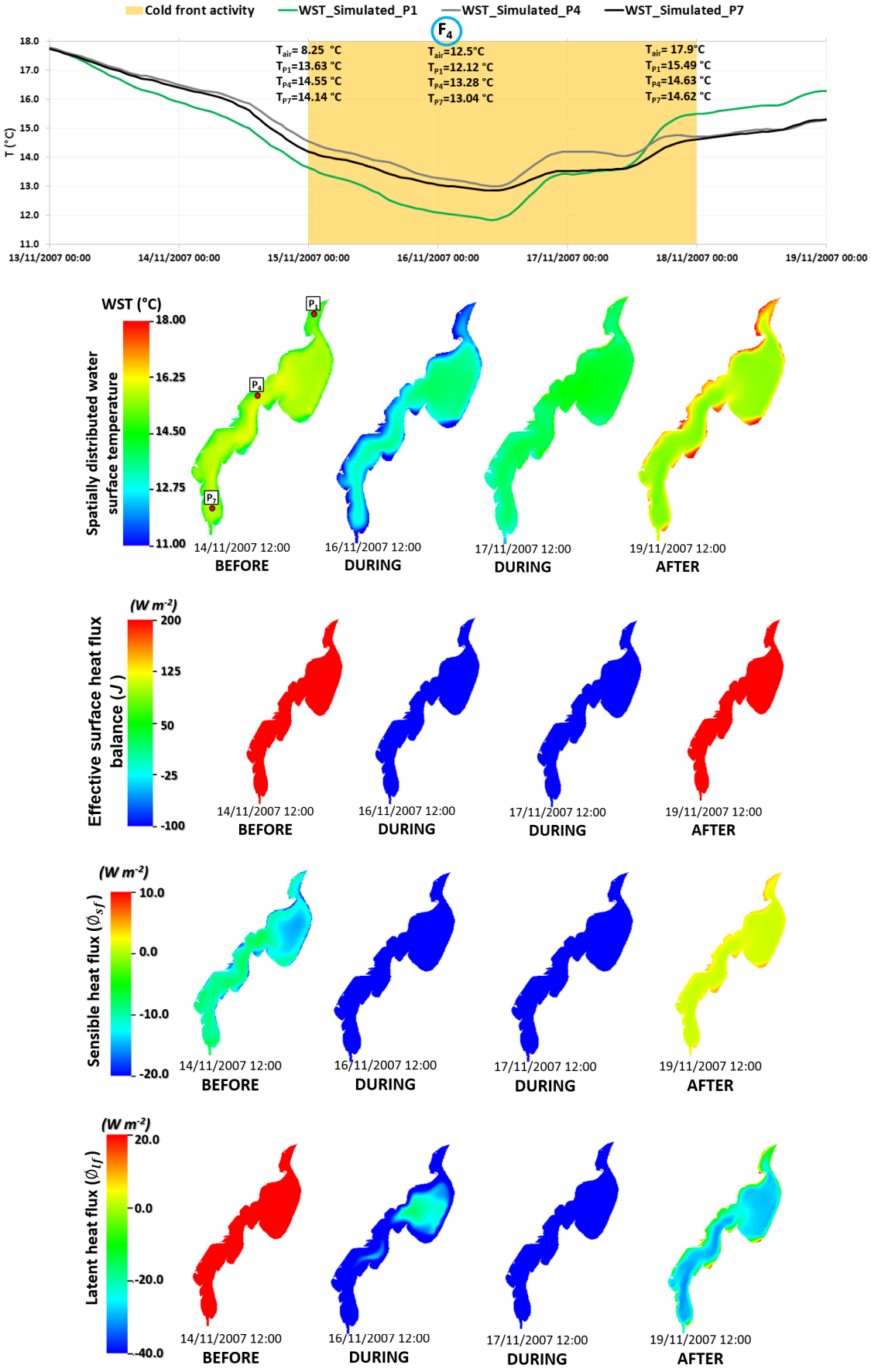

Figure 8 – The effect of the F_4 cold front event on WST, effective surface heat flux balance and sensible and latent heat fluxes in the Lake Mirim, showing its air and water surface temperature simulated at P1 (green line), P4 (grey line) and P7 (black line) points and cold front activity (a), spatially distributed water surface temperature (b) the effective surface heat flux balance (c) sensible heat fluxes (d) and latent heat flux (e), before (14 November 2007) during (16 and 17 November 2007) and after (19 November 2007) F_4 cold front passage.

Regarding annual mean of water surface temperature simulated from IPH-ECO, results allowed distinct thermal zones along to the lake: the shoreline composed by littoral region, which showed the maximum values in WST, and the central region conformed by the pelagic zone, showing the minimum values in WST. The warming began in the shallower waters and coastal regions, while the central part of the lake stayed cool for a long period. This fact is due to the low thermal mass of the shallower regions, which the WST decreases more rapidly that in deep regions (Wells and Sherman, 2001). In these regions, the heat capacity is low and the responses to changes in atmospheric forcing are faster that the deep zones (Liu et al., 2011).

Results for monthly mean of WST revealed a higher spatial homogeneity in winter due to hydrodynamic circulation and the higher winds, which increase the lake mixing during this season. Similar behavior was founded in Lake Mangueira (Cavalcanti et al., 2016; Fragoso et al., 2011), where the WST tend to be more homogeneous in winter.

Results from heat flux simulations indicated a marked seasonal dynamics in the monthly mean of the effective surface heat balance in the Lake Mirim. As expected, the lake gains more heat during summer and loss more heat during winter. This gain began in the shallower regions, while deeper regions tend to be more homogenous for some seasons (spring and fall). In addition, for summer months, the northern region gains more heat that the southern regions. This can be explained by the northwest winds, which warms masses and raise the water levels in the southern lake regions, as found in similar environments such as Patos (Fernandes et al., 2002, 2005) and Lake Mangueira (Fragoso et al., 2011).

Sensible heat flux showed similar behavior with and latent heat flux in the Lake Mirim, where the heat loss reach maximum values in summer (February) and minimum values in winter (July/August). Indeed, most of the time, the lake heat loss and releases energy through sensible and latent heat exchanges with atmosphere. These variations on the heat fluxes were consistent with the reported in others large lakes (Fink et al., 2014a; Liu et al., 2009; Shao et al., 2015) and tropical reservoirs (Alcântara et al., 2010a,b). Additionally, these heat losses (sensible and latent) were due to the air temperature was higher than the WST, and when the vapor pressure of the air was higher than the WST, showing the influence of warmth and moisture in air masses (Shao et al., 2015).

Our results revealed that the heat loss due to latent flux were higher that the sensible flux, indicating that the most part of energy released is due to evaporation and the atmospheric saturation. This fact can be due to the large surface area (4000 Km^2) and the shallow waters (average depth = 4.5m) in the Lake Mirim, influence in a increase of the release energy through heat exchanges with atmosphere, as observed in others shallow lakes (Granger and Hedstrom, 2011; Phillips et al., 2016). Indeed, the latent heat flux has an annual course with a minimum of 12.4 $W.m^{-2}$ in winter and maximum of 132.1 $W.m^{-2}$ in summer. Besides none study in Lake Mirim was performed previously,

and no data were available to assess our results, these values are in the range of values that were found by Fink et al. (2014a), for Lake Constance (European Alps) for the period 1984-2011 (minimum of 15.3 W.m^{-2} in winter and maximum of 76.0 W.m^{-2} in summer). In addition, another key influencing factor that contributes to increase the evaporation in the lake is the external forcings, such as the wind (both speed and direction), which rise the evaporation in shallow waters accelerating the heat fluxes. In these environments, the turbulence prompted by the wind refreshes the air above water and prevents saturation, leading that the surface area over which heat is lost to the atmosphere is increased (Feng and Li, 2010; O'Sullivan and Reynolds, 2008).

3.5.3 Cold front effects

Results from the passages of short-scale meteorological events such as cold fronts over the Lake Mirim, revealed that on the cold front days, the WST showed a decreasing, which influenced on the cooling phase for whole lake, as well as heat loss in the effective surface heat flux balance and an increase in the heat loss due to sensible and latent heat flux to the atmosphere after the cold front passage (Fig. 7 and Fig. 8). Our results were consistent with the founded in previous studies in tropical reservoirs (Curtarelli et al., 2013, 2014) and temperate lakes (Liu et al., 2011, 2009). Curtarelli et al. (2013, 2014) observed also that on the cold front passage days over the Itumbiara reservoir (Brazil), the air temperature and the WST showed a decreasing and there was heat loss noticed in the effective surface heat flux balance. According to these authors, during cold front passages, the heat balance showed a mean value of ?87 W.m^{-2}. These fluxes were similar to the values simulated during the cold front passage (F4) over the Lake Mirim (-100 W.m^{-2}).

The latent and sensible heat loss was higher during the F_4 cold front passage that during F_1. Besides the duration of the F_1 cold front passage was higher that F_4, F_1 reached the Lake Mirim region in June (winter in southern hemisphere), which the air and water surface temperatures were already low. In contrast, F_4 reached the Lake Mirim area in November (spring in southern hemisphere), causing dramatic changes in meteorological conditions (*e.g.*, wind speed, temperature, and humidity) and producing a latent and sensible heat loss higher than F_1.

3.5.4 Model capability and limitations

The coupled model proved to be suitable for representing the WST dynamic, the heat fluxes (latent and sensible) and the effects of cold front passages in the behavior of the Lake Mirim. Results from WST simulations revealed that, for some WST peak, the model performed best, although smaller peak were reproduced with some biases (December 2004 and February 2010). This can be explained by the errors in the

input data (temperature and precipitation), biases associated to the MODIS-derived LST product (MOD11A1) (Phillips et al., 2016), or errors in the numerical solution methods (discretization and iteration errors) of the coupled models (Wu, 2007). Similar limitations also have been founded in other studies (e.g. Fink et al., 2014b; Råman Vinnå et al., 2017). Besides no studies in Lake Mirim have been performed previously, and no *in situ* measurements of the WST to validate our results, the approach proposed using the validated MODIS - derived water surface temperature, represent well the WST dynamic in the lake, describing spatial and temporal (daily, monthly, seasonal and inter-annual) variations, which is difficult to explore from others approaches, such as remote sensing techniques, where the cloud cover and lack of clear-sky images is a limitation for some seasons (winter) (Alcântara et al., 2010b; Crosman and Horel, 2009; Sima et al., 2013).

3.5.5 Potentials implications, future research and perspectives

The approach implemented in this study is a first attempt to assess the WST dynamics and heat fluxes in synoptic scale in a large subtropical shallow lake using a multi-year record. The methodology here proposed could be used as a tool to improve the comprehension of dynamics of systems on anthropic and natural stressors, helping in the supporting for effective water management in these environments. Furthermore, this approach could improve the accuracy of the water allocation decisions, and reduce efforts and costs associated with conventional water quality monitoring in large shallow lakes.

Future research would be addressed to study the potential climatic impacts on water quality of lakes and reservoirs, using the new generation of General Circulation Models in IPCC's Fifth Assessment Report (AR5) CMIP5. In addition, further research should examine the applicability of this approach in studies involving heat flux changes induced by the global warming in large lakes, as started in the recent literature (Fink et al., 2014a,b; Zhong et al., 2016), or studies assessing synoptic disturbances in the variability of heat budget and the air-water interactions in large waterbodies (Feng et al., 2016; Shi et al., 2015).

3.6 Conclusion

This study showed that the synergy between coupling large-scale hydrological/ hydrodynamic model, MODIS - derived water surface temperature (WST) and *in situ* measurements allowed represent the temperature dynamics (daily, monthly, seasonal and inter-annual) and heat fluxes (latent and sensible) in the Lake Mirim, for the period 2001-2010. From this approach was possible to assess the impacts of short-scale

meteorological events, such as cold fronts, in the spatial and temporal variability of the WST and heat exchanges in the lake.

The findings indicated that the main heat losses in the Lake Mirim are due to latent heat flux (*i.e.*, increase in the evaporation rates an atmospheric saturation), where the shallow waters due to the low thermal mass, respond more quickly to the atmospheric forcings (*e.g.,* wind stress, relative humidity, air temperature, shortwave radiation) when compared with deep regions. The cold front activity also influenced the thermal dynamics in the Lake Mirim. Our results suggest that the WST and heat fluxes are strongly dependent of the cold front passages, which increase the heat loss during the events.

In summary, we have shown the first attempt to investigate the behavior of the water surface temperature, latent heat flux and sensible heat flux in a large subtropical shallow lake, integrating distributed hydrological modeling and hydrodynamic modeling with remote sensing techniques. The present study goes beyond the previously reported, being the first long-term and synoptic scale approach in the Lake Mirim, allowing to improve understanding of the main physical process (*e.g.,* heat budget) that occurs in this ecosystem, under different meteorological conditions (cold front passages). The framework here proposed can be used in future studies involving physical/ecological processes, water quality and climate-change scenarios in large shallow lakes.

Acknowledgements: The research was conducted thanks to the support of the *Coordenação de Aperfeiçoamento de Pessoal de Nível Superior* (CAPES:`www.capes.gov.br`) and to the *Conselho Nacional de Desenvolvimento Cientifico e Tecnológico* (CNPq:`www.cnpq.br`) of Brazil. The study is part of the research project "*Impacto das mudanças climáticas em ambientes fluviais e lacustres do Rio Grande do Sul*", funded by CNPq. The authors also acknowledge the *Instituto Brasileiro de Meteorologia* (INMET: `www.inmet.gov.br`) for freely providing the meteorological data used as input to the model. We are also grateful to the Lake Mirim Basin Comitee for providing in situ water elevation recorded for Lake Mirim and to the Global Lake Ecological Observatory Network (GLEON:`www.gleon.org`) for providing a venue and resources for lake science discussions, and also to Dr. Janet W. Reid (Trumansburg, NY, U.S.A.) for revising the English text of the manuscript.

Referências

Alcântara, E., Bonnet, M., Assireu, A., Stech, J., Novo, E., and Lorenzzetti, J. (2010a). On the water thermal response to the passage of cold fronts: initial results for Itumbiara reservoir (Brazil). *Hydrology and Earth System Sciences Discussions*, 7(6):9437–9465.

Alcântara, E. H., Stech, J. L., Lorenzzetti, J. A., Bonnet, M. P., Casamitjana, X., Assireu, A. T., and de Moraes Novo, E. M. L. (2010b). Remote sensing of water surface temperature and heat flux over a tropical hydroelectric reservoir. *Remote Sensing of Environment*, 114(11):2651–2665.

Austin, J. A. and Colman, S. M. (2007). Lake Superior summer water temperatures are increasing more rapidly than regional air temperatures: A positive ice-albedo feedback. *Geophysical Research Letters*, 34(6).

Bicudo, C. and Bicudo, D. (2004). *Sampling in limnology*. Rima, Sção Carlos.

Bohnenberger, J. E., Rodrigues, L. R., da Motta-Marques, D., and Crossetti, L. O. (2017). Environmental dissimilarity over time in a large subtropical shallow lake is differently represented by phytoplankton functional approaches. *Marine and Freshwater Research*, 778(1):105–120.

Bravo, J., Allasia, D., Paz, A., Collischonn, W., and Tucci, C. (2011). Coupled hydrologic-hydraulic modeling of the Upper Paraguay River basin. *Journal of hydrologic engineering*, 17(5):635–646.

Bresciani, M., Giardino, C., and Boschetti, L. (2011). Multi-temporal assessment of bio-physical parameters in lakes Garda and Trasimeno from MODIS and MERIS. *Italian Journal of Remote Sensing/Rivista Italiana di Telerilevamento*, 43(3).

Brown, L. E., Hannah, D. M., and Milner, A. M. (2006). Hydroclimatological influences on water column and streambed thermal dynamics in an alpine river system. *Journal of Hydrology*, 325(1):1–20.

Burnett, A. W., Kirby, M. E., Mullins, H. T., and Patterson, W. P. (2003). Increasing great lake-effect snowfall during the twentieth century: a regional response to global warming? *Journal of Climate*, 16(21):3535–3542.

Casulli, V. and Cattani, E. (1994). Stability, accuracy and efficiency of a semi-implicit method for three-dimensional shallow water flow. *Computers & Mathematics with Applications*, 27(4):99–112.

Casulli, V. and Cheng, R. T. (1992). Semi-implicit finite difference methods for three-dimensional shallow water flow. *International Journal for numerical methods in fluids*, 15(6):629–648.

Cavalcanti, J. R., da Motta-Marques, D., and Fragoso, C. R. (2016). Process-based modeling of shallow lake metabolism: Spatio-temporal variability and relative importance of individual processes. *Ecological Modelling*, 323:28–40.

Chapra, S. C. (2008). *Surface water-quality modeling*. Waveland press.

Chavula, G., Brezonik, P., Thenkabail, P., Johnson, T., and Bauer, M. (2009). Estimating the surface temperature of Lake Malawi using AVHRR and MODIS satellite imagery. *Physics and Chemistry of the Earth, Parts A/B/C*, 34(13):749–754.

Cheng, R. T., Casulli, V., and Gartner, J. W. (1993). Tidal, residual, intertidal mudflat (TRIM) model and its applications to San Francisco Bay, California. *Estuarine, Coastal and Shelf Science*, 36(3):235–280.

Collischonn, B., Collischonn, W., Silva, B. C., and Tucci, C. E. (2005). Simulação hidrológica da bacia do rio São Francisco usando precipitação estimada pelo satélite TRMM: resultados preliminares. *Anais do XVI Simpósio Brasileiro de Recursos Hídricos, ABRH, João Pessoa (PB)*.

Collischonn, B., Collischonn, W., and Tucci, C. E. M. (2008). Daily hydrological modeling in the Amazon basin using TRMM rainfall estimates. *Journal of Hydrology*, 360(1):207–216.

Collischonn, W., Allasia, D., Da Silva, B. C., and Tucci, C. E. (2007). The MGB-IPH model for large-scale rainfall-runoff modelling. *Hydrological Sciences Journal*, 52(5):878–895.

Collischonn, W. and Tucci, C. (2001). Hydrological simulation of large drainage basins. *Brazilian J. Water Resour*, 6(1):15–35.

Crosman, E. T. and Horel, J. D. (2009). MODIS-derived surface temperature of the Great Salt Lake. *Remote Sensing of Environment*, 113(1):73–81.

Curtarelli, M., Alcântara, E., Rennó, C., and Stech, J. (2013). Modeling the effects of cold front passages on the heat fluxes and thermal structure of a tropical hydroelectric reservoir. *Hydrology and Earth System Sciences Discussions*, 10:8467–8502.

Curtarelli, M. P., Alcântara, E., Rennó, C. D., Assireu, A. T., Bonnet, M. P., and Stech, J. L. (2014). Modelling the surface circulation and thermal structure of a tropical reservoir using three-dimensional hydrodynamic lake model and remote-sensing data. *Water and Environment Journal*, 28(4):516–525.

Darchambeau, F., Sarmento, H., and Descy, J.-P. (2014). Primary production in a tropical large lake: The role of phytoplankton composition. *Science of the total environment*, 473:178–188.

Fan, F. M., Collischonn, W., Meller, A., and Botelho, L. C. M. (2014). Ensemble streamflow forecasting experiments in a tropical basin: The São Francisco river case study. *Journal of Hydrology*, 519:2906–2919.

Fan, F. M., Collischonn, W., Quiroz, K., Sorribas, M., Buarque, D., and Siqueira, V. (2016). Flood forecasting on the tocantins river using ensemble rainfall forecasts and real-time satellite rainfall estimates. *Journal of Flood Risk Management*, 9(3):278–288.

Fan, F. M., Schwanenberg, D., Collischonn, W., and Weerts, A. (2015). Verification of inflow into hydropower reservoirs using ensemble forecasts of the TIGGE database for large scale basins in Brazil. *Journal of Hydrology: Regional Studies*, 4:196–227.

Fei, X., Feng, L., Yun, D., Qi, F., Yi, Y., and Hui, C. (2013). Evaluation of spatial-temporal dynamics in surface water temperature of qinghai lake from 2001 to 2010 by using modis data. *Journal of Arid Land*, 5(4):452–464.

Feng, B.-X., Liu, H.-L., Lin, P.-F., and Wang, Q. (2016). Estimation of the surface heat budget over the South China Sea. *Atmospheric and Oceanic Science Letters*, 9(3):191–197.

Feng, Z. and Li, C. (2010). Cold-front-induced flushing of the Louisiana Bays. *Journal of Marine Systems*, 82(4):252–264.

Fernandes, E. H. L., Dyer, K. R., Moller, O., and Niencheski, L. F. H. (2002). The Patos lagoon hydrodynamics during an El Nino event (1998). *Continental Shelf Research*, 22(11):1699–1713.

Fernandes, E. H. L., Dyer, K. R., and Moller, O. O. (2005). Spatial gradients in the flow of southern Patos Lagoon. *Journal of Coastal Research*, pages 759–769.

Fink, G., Schmid, M., Wahl, B., Wolf, T., and Wüest, A. (2014a). Heat flux modifications related to climate-induced warming of large European lakes. *Water Resources Research*, 50(3):2072–2085.

Fink, G., Schmid, M., and Wüest, A. (2014b). Large lakes as sources and sinks of anthropogenic heat: Capacities and limits. *Water Resources Research*, 50(9):7285–7301.

Fragoso, C. R., Marques, D. M. M., Collischonn, W., Tucci, C. E., and van Nes, E. H. (2008). Modelling spatial heterogeneity of phytoplankton in Lake Mangueira, a large shallow subtropical lake in South Brazil. *Ecological Modelling*, 219(1):125–137.

Fragoso, C. R., Marques, D. M. M., Ferreira, T. F., Janse, J. H., and van Nes, E. H. (2011). Potential effects of climate change and eutrophication on a large subtropical shallow lake. *Environmental Modelling & Software*, 26(11):1337–1348.

Fragoso, C. R., van Nes, E. H., Janse, J. H., and da Motta Marques, D. (2009). IPH-TRIM3D-PCLake: A three-dimensional complex dynamic model for subtropical aquatic ecosystems. *Environmental Modelling & Software*, 24(11):1347–1348.

Gallucci, F. and Netto, S. A. (2004). Effects of the passage of cold fronts over a coastal site: an ecosystem approach. *Marine ecology progress series*, 281:79–92.

Getirana, A., Bonnet, M.-P., Rotunno Filho, O., Collischonn, W., Guyot, J.-L., Seyler, F., and Mansur, W. (2010). Hydrological modelling and water balance of the Negro River basin: evaluation based on in situ and spatial altimetry data. *Hydrological processes*, 24(22):3219–3236.

Giardino, C., Bresciani, M., Valentini, E., Gasperini, L., Bolpagni, R., and Brando, V. E. (2015). Airborne hyperspectral data to assess suspended particulate matter and aquatic vegetation in a shallow and turbid lake. *Remote Sensing of Environment*, 157:48–57.

Gillespie, A., Rokugawa, S., Matsunaga, T., Cothern, J. S., Hook, S., and Kahle, A. B. (1998). A temperature and emissivity separation algorithm for Advanced Spaceborne Thermal Emission and Reflection Radiometer (ASTER) images. *Geoscience and Remote Sensing, IEEE Transactions on*, 36(4):1113–1126.

Granger, R. and Hedstrom, N. (2011). Modelling hourly rates of evaporation from small lakes. *Hydrology and Earth System Sciences*, 15(1):267–277.

Grim, J. A., Knievel, J. C., and Crosman, E. T. (2013). Techniques for using MODIS data to remotely sense lake water surface temperatures. *Journal of Atmospheric and Oceanic Technology*, 30(10):2434–2451.

Gudasz, C., Sobek, S., Bastviken, D., Koehler, B., and Tranvik, L. J. (2015). Temperature sensitivity of organic carbon mineralization in contrasting lake sediments. *Journal of Geophysical Research: Biogeosciences*, 120(7):1215–1225.

Hamilton, D. P. and Schladow, S. G. (1997). Prediction of water quality in lakes and reservoirs. Part IâModel description. *Ecological Modelling*, 96(1-3):91–110.

Hipsey, M., Bruce, L., and Hamilton, D. (2014). GLMâGeneral Lake Model: Model overview and user information. *Perth (Australia): University of Western Australia Technical Manual*.

Hodges, B. R. (2000). Numerical Techniques in CWR-ELCOM (code release v. 1). *CWR Manuscript WP*, 1422.

Janse, J. H. (2005). *Model studies on the eutrophication of shallow lakes and ditches*. Wageningen University, Ph.D. thesis.

Ji, Z.-G. (2017). *Hydrodynamics and water quality: modeling rivers, lakes, and estuaries*. John Wiley & Sons.

Ke, L. and Song, C. (2014). Remotely sensed surface temperature variation of an inland saline lake over the central Qinghai–Tibet Plateau. *ISPRS Journal of Photogrammetry and Remote Sensing*, 98:157–167.

Kehoe, M., OâBrien, K., Grinham, A., and Burford, M. (2015). Primary production of lake phytoplankton, dominated by the cyanobacterium Cylindrospermopsis raciborskii, in response to irradiance and temperature. *Inland Waters*, 5(2):93–100.

Kottek, M., Grieser, J., Beck, C., Rudolf, B., and Rubel, F. (2006). World map of the köppen-geiger climate classification updated. *Meteorologische Zeitschrift*, 15(3):259–263.

Kotzian, H. B. and Marques, D. M. (2004). Lagoa mirim e a convenção ramsar: um modelo para ação transfronteiriça na conservação de recursos hídricos. *Revista de Gestão de Água da América Latina*, 1(2):101–111.

Kouwen, N., Soulis, E., Pietroniro, A., Donald, J., and Harrington, R. (1993). Grouped response units for distributed hydrologic modeling. *Journal of Water Resources Planning and Management*, 119(3):289–305.

Kozlov, I., Dailidienė, I., Korosov, A., Klemas, V., and Mingėlaitė, T. (2014). MODIS-based sea surface temperature of the Baltic Sea Curonian Lagoon. *Journal of Marine Systems*, 129:157–165.

Lamaro, A. A., Marinelarena, A., Torrusio, S. E., and Sala, S. E. (2013). Water surface temperature estimation from Landsat 7 ETM+ thermal infrared data using the generalized single-channel method: Case study of Embalse del Río Tercero (Córdoba, Argentina). *Advances in Space Research*, 51(3):492–500.

Lenters, J. D., Kratz, T. K., and Bowser, C. J. (2005). Effects of climate variability on lake evaporation: Results from a long-term energy budget study of Sparkling Lake, northern Wisconsin (USA). *Journal of Hydrology*, 308(1):168–195.

Lima, M. S., da Motta Marques, D., They, N. H., McMahon, K. D., Rodrigues, L. R., de Souza Cardoso, L., and Crossetti, L. O. (2016). Contrasting factors drive within-lake bacterial community composition and functional traits in a large shallow subtropical lake. *Hydrobiologia*, 778(1):105–120.

Liu, G., Ou, W., Zhang, Y., Wu, T., Zhu, G., Shi, K., and Qin, B. (2015). Validating and mapping surface water temperatures in lake taihu: Results from modis land surface temperature products. *IEEE Journal of Selected Topics in Applied Earth Observations and Remote Sensing*, 8(3):1230–1244.

Liu, H., Blanken, P. D., Weidinger, T., Nordbo, A., and Vesala, T. (2011). Variability in cold front activities modulating cool-season evaporation from a southern inland water in the USA. *Environmental Research Letters*, 6(2):024022.

Liu, H., Zhang, Y., Liu, S., Jiang, H., Sheng, L., and Williams, Q. L. (2009). Eddy covariance measurements of surface energy budget and evaporation in a cool season over southern open water in Mississippi. *Journal of Geophysical Research: Atmospheres (1984–2012)*, 114(D4).

Luz, G. A. d., Guasselli, L. A., and Rocha, D. (2017). Temperature Surface of Guaíba Lake, RS, from time series of MODIS images. *RBRH*, 22.

MacIntyre, S. and Melack, J. M. (1995). Vertical and horizontal transport in lakes: linking littoral, benthic, and pelagic habitats. *Journal of the North American Benthological Society*, 14(4):599–615.

MacIntyre, S., Romero, J. R., and Kling, G. W. (2002). Spatial-temporal variability in surface layer deepening and lateral advection in an embayment of Lake Victoria, East Africa. *Limnology and oceanography*, 47(3):656–671.

McGloin, R., McGowan, H., McJannet, D., and Burn, S. (2014). Modelling sub-daily latent heat fluxes from a small reservoir. *Journal of hydrology*, 519:2301–2311.

Missaghi, S. and Hondzo, M. (2010). Evaluation and application of a three-dimensional water quality model in a shallow lake with complex morphometry. *Ecological Modelling*, 221(11):1512–1525.

Morais, M., Castro, W., and Tundisi, J. G. (2010). Climatologia de frentes frias sobre a Região Metropolitana de São Paulo (RMSP), e sua influência na limnologia dos reservatórios de abastecimento de água. *Revista Brasileira de Meteorologia*, 25(2):205–217.

Munar, A. M., Cavalcanti, J. R., Bravo, J. M., Fan, F. M., Motta-Marques, D. M. L., and Fragroso Jr, C. R. (2017). Coupling large-scale hydrological and hydrodynamic modeling: Toward a better comprehension of shallow lake-watershed processes. *J. Hydrol. (under review)*.

Murphy, S., Wright, R., Oppenheimer, C., and Souza Filho, C. (2013). MODIS and ASTER synergy for characterizing thermal volcanic activity. *Remote sensing of environment*, 131:195–205.

Nash, J. E. and Sutcliffe, J. V. (1970). River flow forecasting through conceptual models part IâA discussion of principles. *Journal of hydrology*, 10(3):282–290.

Nóbrega, M., Collischonn, W., Tucci, C., and Paz, A. (2011). Uncertainty in climate change impacts on water resources in the Rio Grande Basin, Brazil. *Hydrology and Earth System Sciences*, 15(2):585.

Ofir, E., Heymans, J., Shapiro, J., Goren, M., Spanier, E., and Gal, G. (2017). Predicting the impact of Lake Biomanipulation based on food-web modelingâLake Kinneret as a case study. *Ecological Modelling*, 348:14–24.

O'Reilly, C. M., Sharma, S., Gray, D. K., Hampton, S. E., Read, J. S., Rowley, R. J., Schneider, P., Lenters, J. D., McIntyre, P. B., Kraemer, B. M., et al. (2015). Rapid and highly variable warming of lake surface waters around the globe. *Geophysical Research Letters*, 42(24).

O'Sullivan, P. and Reynolds, C. S. (2008). *The lakes handbook: lake restoration and rehabilitation*. John Wiley & Sons.

Paiva, R. C. D., Buarque, D. C., Collischonn, W., Bonnet, M.-P., Frappart, F., Calmant, S., and Bulhões Mendes, C. A. (2013). Large-scale hydrologic and hydrodynamic modeling of the Amazon River basin. *Water Resources Research*, 49(3):1226–1243.

Pereira, F. and Fragoso, C. R. (2013). Pairing multivariate data analysis and ecological modeling in the biomanipulated Lake engelsholm, Denmark. *Journal of Water Management and Research*.

Phillips, R., Saylor, J., Kaye, N., and Gibert, J. (2016). A multi-lake study of seasonal variation in lake surface evaporation using MODIS satellite-derived surface temperature. *Limnology*, 17(3):273–289.

Piccolroaz, S., Toffolon, M., and Majone, B. (2013). A simple lumped model to convert air temperature into surface water temperature in lakes. *Hydrology and Earth System Sciences*, 17(8):3323.

Politi, E., Cutler, M. E., and Rowan, J. S. (2012). Using the NOAA Advanced Very High Resolution Radiometer to characterise temporal and spatial trends in water temperature of large European lakes. *Remote sensing of environment*, 126:1–11.

Pontes, P. R., Collischonn, W., Fan, F. M., Paiva, R. C., and Buarque, D. C. (2015). Modelagem hidrológica e hidráulica de grande escala com propagação inercial de vazões. *Revista Brasileira de Recursos Hídricos*, 20(4):888–904.

Råman Vinnå, L., Wüest, A., and Bouffard, D. (2017). Physical effects of thermal pollution in lakes. *Water Resources Research*.

Recknagel, F., Ostrovsky, I., and Cao, H. (2014). Model ensemble for the simulation of plankton community dynamics of Lake Kinneret (Israel) induced from in situ predictor variables by evolutionary computation. *Environmental modelling & software*, 61:380–392.

Rodríguez, Y. C., El Anjoumi, A., Gómez, J. D., Pérez, D. R., and Rico, E. (2014). Using Landsat image time series to study a small water body in Northern Spain. *Environmental monitoring and assessment*, 186(6):3511–3522.

Roy, D. P., Borak, J. S., Devadiga, S., Wolfe, R. E., Zheng, M., and Descloitres, J. (2002). The modis land product quality assessment approach. *Remote Sensing of Environment*, 83(1):62–76.

Schmid, M., Hunziker, S., and Wüest, A. (2014). Lake surface temperatures in a changing climate: A global sensitivity analysis. *Climatic change*, 124(1-2):301–315.

Schneider, P., Hook, S., Radocinski, R., Corlett, G., Hulley, G., Schladow, S., and Steissberg, T. (2009). Satellite observations indicate rapid warming trend for lakes in California and Nevada. *Geophysical Research Letters*, 36(22).

Schneider, P. and Hook, S. J. (2010). Space observations of inland water bodies show rapid surface warming since 1985. *Geophysical Research Letters*, 37(22).

Schwartzbold, A. and Schafer, A. (1984). Origin and Morphology of the Coastal Lagoons of Rio Grande do Sul, Brazil(Genese e Morfologia das Lagoas Costeiras do Rio Grande do Sul, Brasil). *Amazoniana*, 9(1).

Shao, C., Chen, J., Stepien, C. A., Chu, H., Ouyang, Z., Bridgeman, T. B., Czajkowski, K. P., Becker, R. H., and John, R. (2015). Diurnal to annual changes in latent, sensible heat, and CO2 fluxes over a Laurentian Great Lake: A case study in Western Lake Erie. *Journal of Geophysical Research: Biogeosciences*, 120(8):1587–1604.

Shi, R., Zeng, L., Wang, X., and Sui, D. (2015). High-frequency variability of latent-heat flux in the south china sea. *Aquatic ecosystem health & management*, 18(4):378–385.

Shiflet, A. B. and Shiflet, G. W. (2014). *Introduction to computational science: modeling and simulation for the sciences*. Princeton University Press.

Shuttleworth, W. J. (1993). Evaporation in: Maidment, dr"handbook of hydrology.

Sima, S., Ahmadalipour, A., and Tajrishy, M. (2013). Mapping surface temperature in a hyper-saline lake and investigating the effect of temperature distribution on the lake evaporation. *Remote Sensing of Environment*, 136:374–385.

Siqueira, V. A., Collischonn, W., Fan, F. M., and Chou, S. C. (2016). Ensemble flood forecasting based on operational forecasts of the regional Eta EPS in the Taquari-Antas basin. *RBRH*, 21(3):587–602.

Soulignac, F., Vinçon-Leite, B., Lemaire, B. J., Martins, J. R. S., Bonhomme, C., Dubois, P., Mezemate, Y., Tchiguirinskaia, I., Schertzer, D., and Tassin, B. (2017). Performance Assessment of a 3D Hydrodynamic Model Using High Temporal Resolution Measurements in a Shallow Urban Lake. *Environmental Modeling & Assessment*, pages 1–14.

Steissberg, T. E., Hook, S. J., and Schladow, S. G. (2005). Characterizing partial upwellings and surface circulation at Lake Tahoe, California–Nevada, USA with thermal infrared images. *Remote Sensing of Environment*, 99(1):2–15.

Todini, E. (1996). The ARNO rainfall-runoff model. *Journal of Hydrology*, 175(1):339–382.

Trolle, D., Hamilton, D. P., Pilditch, C. A., Duggan, I. C., and Jeppesen, E. (2011). Predicting the effects of climate change on trophic status of three morphologically varying lakes: Implications for lake restoration and management. *Environmental Modelling & Software*, 26(4):354–370.

Trumpickas, J., Shuter, B. J., and Minns, C. K. (2009). Forecasting impacts of climate change on Great Lakes surface water temperatures. *Journal of Great Lakes Research*, 35(3):454–463.

Tundisi, J., Matsumura-Tundisi, T., Arantes Junior, J., Tundisi, J., Manzini, N., and Ducrot, R. (2004). The response of Carlos Botelho (Lobo, Broa) reservoir to the passage of cold fronts as reflected by physical, chemical, and biological variables. *Brazilian Journal of Biology*, 64(1):177–186.

Tundisi, J., Matsumura-Tundisi, T., Pereira, K., Luzia, A., Passerini, M., Chiba, W., Morais, M., and Sebastien, N. (2010). Cold fronts and reservoir limnology: an integrated approach towards the ecological dynamics of freshwater ecosystems. *Brazilian Journal of Biology*, 70(3):815–824.

Wan, Z. (2008). New refinements and validation of the MODIS land-surface temperature/emissivity products. *Remote Sensing of Environment*, 112(1):59–74.

Wan, Z., Zhang, Y., Zhang, Q., and Li, Z.-L. (2004). Quality assessment and validation of the MODIS global land surface temperature. *International Journal of Remote Sensing*, 25(1):261–274.

Wang, K., Wan, Z., Wang, P., Sparrow, M., Liu, J., and Haginoya, S. (2007). Evaluation and improvement of the MODIS land surface temperature/emissivity products using ground-based measurements at a semi-desert site on the western Tibetan Plateau. *International Journal of Remote Sensing*, 28(11):2549–2565.

Webb, B., Clack, P., and Walling, D. (2003). Water–air temperature relationships in a devon river system and the role of flow. *Hydrological Processes*, 17(15):3069–3084.

Wells, M. G. and Sherman, B. (2001). Stratification produced by surface cooling in lakes with significant shallow regions. *Limnology and Oceanography*, 46(7):1747–1759.

Wloczyk, C., Richter, R., Borg, E., and Neubert, W. (2006). Sea and lake surface temperature retrieval from Landsat thermal data in Northern Germany. *International Journal of Remote Sensing*, 27(12):2489–2502.

Wu, W. (2007). *Computational river dynamics*. CRC Press.

Xu, H., Huang, S., and Zhang, T. (2013). Built-up land mapping capabilities of the ASTER and Landsat ETM+ sensors in coastal areas of southeastern China. *Advances in Space Research*, 52(8):1437–1449.

Zhang, G., Yao, T., Xie, H., Qin, J., Ye, Q., Dai, Y., and Guo, R. (2014). Estimating surface temperature changes of lakes in the Tibetan Plateau using MODIS LST data. *Journal of Geophysical Research: Atmospheres*, 119(14):8552–8567.

Zhong, Y., Notaro, M., Vavrus, S. J., and Foster, M. J. (2016). Recent accelerated warming of the Laurentian Great Lakes: Physical drivers. *Limnology and Oceanography*, 61(5):1762–1786.

Capítulo 4

Can chlorophyll-a in meso-oligotrophic shallow waters be estimated using statistical approaches and empirical models from MODIS imagery?

This chapter is based on the following paper submitted to:
Brazilian Journal of Water Resources

Andrés Mauricio Munar, J. Rafael Cavalcanti, Juan Martin Bravo, David da Motta-Marques and Carlos Ruberto Fragoso Jr.

Abstract

Accurate estimation of chlorophyll-*a* concentration (Chl-*a*) in inland waters through remote-sensing techniques is complicated by local differences in the optical properties of water. In this study, we applied multiple linear regression (MLR), artificial neural network (ANN), nonparametric multiplicative regression (NPMR) and four empirical algorithms (Appel, Kahru, FAI and O14a) to estimate the Chl-*a* concentration from combinations of spectral bands from the MODIS sensor. The multiple linear regression (MLR), NPMR and ANN models were calibrated and validated using *in-situ* chlorophyll-*a* measurements. The results showed that a simple and efficient model, developed and validated through multiple linear regression (MLR) analysis, offered advantages (*i.e.,* better performance and fewer input variables) in comparison with ANN, NPMR and four empirical models (Appel, Kahru, FAI and O14a). In addition, we observed that in a large shallow subtropical lake, where the wind (both velocity and direction) and hydrodynamics are essential factors in the spatial heterogeneity (Chl-*a* distribution), the MRL model adjusted using the specific point dataset, performed better than using the total dataset, which suggest that not be appropriate to generalise a single model to estimate Chl-*a* concentration in these environments from a total dataset. Our approach is a useful tool to estimate Chl-*a* concentrations in meso-oligotrophic shallow waters and corroborates the spatial heterogeneity in these ecosystems.

Keywords: Chl-*a*; MLR; ANN; NPMR; Remote Sensing; Lake Mangueira

Resumo

A estimativa da concentração de Clorofila-a (Chl-*a*) em ambientes aquáticos através de técnicas de sensoriamento remoto é complexa devido as diferenças entre as propriedades óticas da água. O objetivo deste trabalho foi estimar concentrações de Chl-*a* a partir das combinações de bandas espectrais do sensor MODIS, aplicando análise de regressão linear múltipla (MLR), redes neurais artificiais (ANN), regressão multiplicativa não paramétrica e quatro modelos empíricos (Appel, Kahru, FAI e O14a). Os modelos de regressão linear múltipla (MLR, NPMR e ANN) foram calibrados e validados utilizando medições *in-situ* de Chl-*a*. Os resultados demostraram que um simples e eficiente modelo desenvolvido e validado através de regressão linear múltipla (MLR) produz vantagens (*i.e.,* melhor performance e poucas variáveis de entrada) em comparação com modelos ANN, NPMR e quatro modelos empíricos (Appel, Kahru, FAI e O14a). Além disso, foi observado que em um grande lago raso subtropical, no qual o vento (intensidade e direção) e a hidrodinâmica são fatores essenciais na heterogeneidade espacial (distribuição de Chl-*a*), o modelo MLR desenvolvido utilizando um ponto específico do lago teve melhor performance que utilizando o total de dados, sugerindo que não é apropriado generalizar um único modelo para estimar Clorofila-*a* nesses ambientes utilizando o total de dados. Esta abordagem é uma ferramenta útil para estimar concentrações de Chl-*a* em ambientes rasos meso - oligotróficos e corroborar a heterogeneidade espacial desses ecossistemas.

Palavras - chave: Chl-*a*; MLR; ANN; NPMR; Sensoriamento remoto; Lagoa Mangueira

4.1 Introduction

Chlorophyll-a (Chl-*a*) is an important indicator of the trophic state in lakes and reservoirs, showing patterns associated with internal processes and natural stressors (Duka and Cullaj, 2009; Honeywill et al., 2002; Schalles et al., 1998). Detection and quantification of Chl-*a* are essential for assessing water quality in these ecosystems, as the concentration of this compound provides critical knowledge of the phytoplankton community. However, most traditional methods used to retrieve Chl-*a* concentrations are based on *in-situ* measurements, and are time-consuming and difficult to apply to large areas (Gholizadeh et al., 2016; Kasprzak et al., 2008), especially with frequent measurements. In recent years, Chl-a concentrations have often been estimated by remote sensing, which is an effective means of rapid, high-frequency data acquisition (Allan et al., 2011; Olmanson et al., 2011). In addition, this technique allows one to obtain information on remote sites and larger areas.

Currently, empirical or semi-empirical models based on measurements of the reflectance in specific bands of the electromagnetic spectrum are used to retrieve chlorophyll-a concentrations (Duan et al., 2010; Le et al., 2013; Ritchie et al., 2003; Rosa Neto et al., 2015). Limitations of chlorophyll-a detection by remote sensing include atmospheric correction methods and sensor limitations, as well as the influences of detritus, the presence of colored dissolved organic matter (CDOM), and scattering by Total Suspended Matter (TSM), which are difficult to detect because they affect the optical properties of water (Darecki and Stramski, 2004; Hu, 2009; Wu et al., 2009). Another limitation is the light reflected off the bottom, which may affect the accuracy of the empirical algorithm because the signal received by the sensor varies as a function of the wavelength and with the clarity of the water (IOCCG, 2000; Lee et al., 2001).

Recently, data from MODIS (Moderate Resolution Imaging Spectroradiometer) have been used successfully for assessment and continuous monitoring of water quality, including Chl-*a* concentrations, in lakes and reservoirs (Deng et al., 2017; Olmanson et al., 2011; Song et al., 2013; Wu et al., 2014; Zhang et al., 2011). Empirical algorithms based on MODIS data, such as OC3M (O'Reilly, 2000), have been used in different environments (Gilerson et al., 2010; Gurlin et al., 2011; Lesht et al., 2013; Matthews et al., 2012; Ogashawara et al., 2014). Nevertheless, this algorithm has a tendency to overestimate Chl-a concentrations in oligotrophic environments, and to underestimate it in highly productive environments (Komick et al., 2009; Moore et al., 2009).

Recent studies have applied empirical algorithms for retrieving Chl-*a* concentrations in lakes and reservoirs from combinations of MODIS spectral bands (Huang et al., 2014; Wang et al., 2011; Zhang et al., 2016). However, these algorithms have been developed for particular water bodies and for particular seasons, and thus cannot be used everywhere and throughout the year (Matthews, 2011; Palmer and Hunter, 2015). These approaches can be improved from the appropriate spectral remote-sensing reflectance values and combinations of spectral bands. Additionally, few studies have examined a multivariable approach using either regression analysis (Chang et al., 2012; Ogashawara et al., 2014) or an artificial neural network (Wu et al., 2009; Xiang et al., 2015). Of these, only the approach proposed by Ogashawara et al. (2014) was developed in a meso-oligotrophic environment (Itumbiara Reservoir, Brazil). The rest of

studies were developed in eutrophic lakes, such as Lake Okeechobee, USA (Chang et al., 2012) and Lake Chaohu, China (Wu et al., 2009; Xiang et al., 2015).

Monitoring Chl-*a* from remote sensing in freshwater environments such as shallow lakes has limitations (Gholizadeh et al., 2016; Palmer and Hunter, 2015). In addition, in large shallow lakes, which are rarely studied, especially in meso-oligotrophic environments submitted to intense wind regimes, limitations such as scale factors (*e.g.,* representative monitoring at a single point), spatial gradients and hydrodynamics might significantly affect the interpretation of results from remote-sensing data and the performance of the empirical algorithms (Chavula et al., 2009; Ogashawara et al., 2014; Ruiz-Verdú et al., 2016)

In this study, we (1) proposed and compared multivariable empirical models to retrieve Chl-a concentrations, using MODIS data, (2) determined the accuracy of these models in a large shallow subtropical, and (3) verified if generalized models can represent the spatial heterogeneity of the lake. We used multiple linear regression (MLR), artificial neural network (ANN), nonparametric multiplicative regression (NPMR) and four empirical algorithms (Appel, Kahru, FAI and O14a) to retrieve the Chl-*a* concentration in the Lake Mangueira, a large shallow subtropical lake located in Southern Brazil. This approach is the first attempt to assess the application of remote sensing techniques in such a system, which the oligotrophic conditions are common most of the time (Crossetti et al., 2013; Lima et al., 2016), and the spatial heterogeneity has large differences between the littoral and pelagic zones (Cardoso et al., 2012; Crossetti et al., 2013; They et al., 2012).

Differently from previous studies, our approach is a first step towards to obtain comprehensive and reliable empirical models for meso-oligotrophic shallow waters, which may be further tested with remote-sensed data in order to retrieve the Chl-a concentration and help to understanding the shallow lake heterogeneity.

4.2 Methods

4.2.1 Study area

Lake Mangueira is a large shallow subtropical waterbody located in Rio Grande do Sul, Brazil. The lake is 820 km^2 in area and has a mean depth of 2.6 m, a maximum depth of 6.9 m, and is 90 km long and 3-10 km wide (Fig. 1). Its trophic state ranges from oligotrophic to mesotrophic (Crossetti et al., 2013; Fragoso et al., 2011). The regional climate is subtropical with a mean annual temperature of 16^{o}C and annual rainfall between 1,800 and 2,200 mm (Kottek et al., 2006).

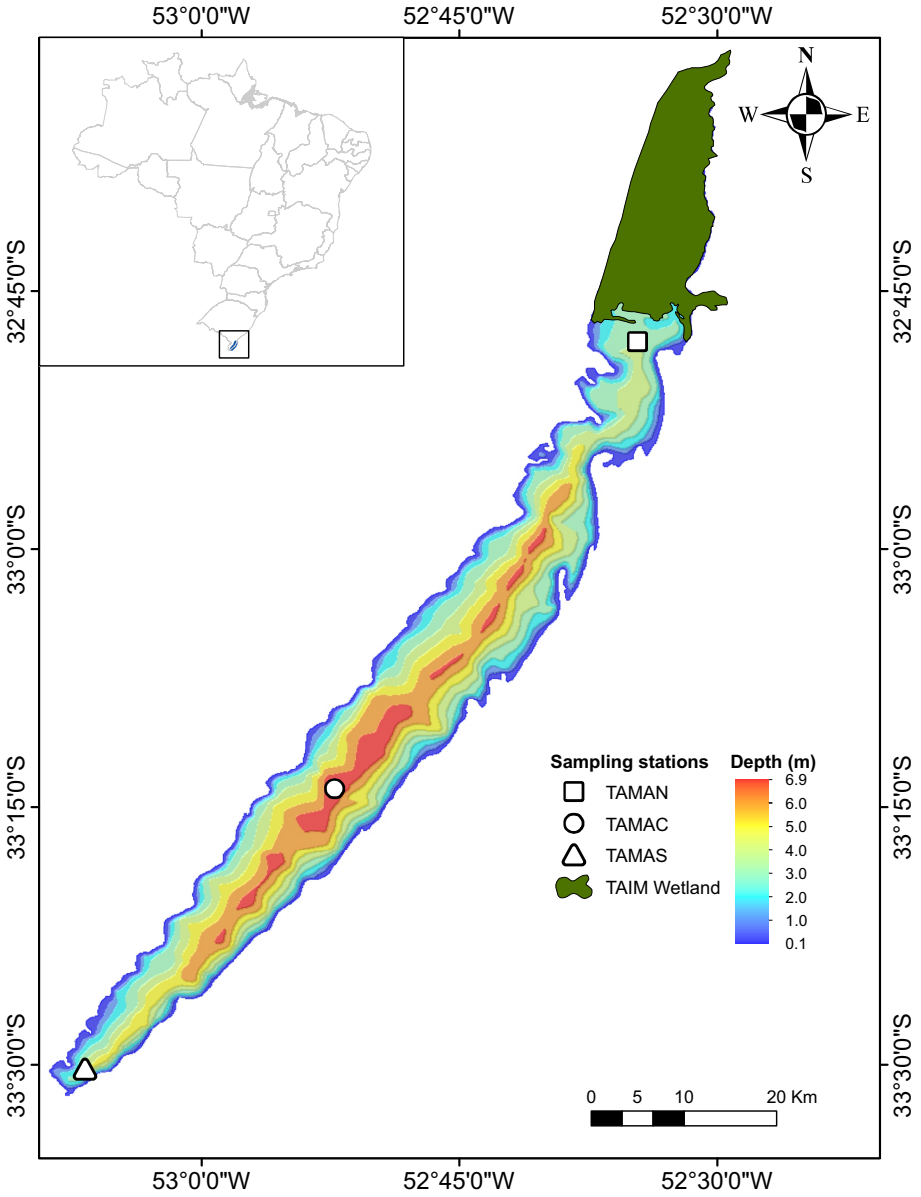

Figure 1 – Bathymetry and locations of sampling stations (North - TAMAN, Central - TAMAC and South -TAMAS) in Lake Mangueira, Rio Grande do Sul, Brazil.

4.2.2 Field Data

The field data were collected over a period of 9 years (2001 to 2009) at three sampling points in the North, Center and South parts of Lake Mangueira, TAMAN, TAMAC and TAMAS respectively, measured two to three times a year. The dataset contained concentrations of Chl-*a*, Secchi disk depth and other limnological variables (*i.e.*, Total Suspended Solids (TSS), Dissolved Oxygen (DO), pH and Depth), collected from the three sampling points, and indicated a wide range of Chl-*a* concentrations at the Central point (Table 1). We used the data from the 2001 - 2005 period for calibration and from the 2006 - 2009 period for model verification.

For Chl-*a* determination, surface water samples were filtered through Whatman GF/F with 90% ethanol and measured by spectrophotometry (Jespersen and Christoffersen, 1987). Dissolved Oxygen (DO), pH and Depth were measured with a multiparameter probe (*YSI 6600*).

Total Suspended Solids (TSS) was assessed gravimetrically by water evaporation in porcelain dishes (APHA, 1992) and the Water Transparency (WT) was measured using a Secchi disk.

Table 1 – Chlorophyll-*a* concentrations and Secchi disk depths, total suspended solids (TSS), dissolved oxygen (DO), pH and Depth measured in 2001-2009 (N=43) at three points (North, Central, South) in Lake Mangueira.

	North	**Central**	**South**
	Mean ± SD (Min-Max)	Mean ± SD (Min-Max)	Mean ± SD (Min-Max)
Chl-*a* ($\mu g.L^{-1}$)	10.88 ± 8.54 (1.04 - 36.9)	13.64 ± 13.52 (0.5 - 63.3)	5.54 ± 4.73 (0.2 - 19.30)
Secchi disk depth (m^{-1})	0.72 ± 0.33 (0.16 - 1.55)	0.79 ± 0.21 (0.55 - 1.36)	1.23 ± 0.40 (0.72 - 1.90)
TSS ($\mu g.L^{-1}$)	33.04 ± 21.03 (3.0 - 80.0)	26.82 ± 14.74 (6.0 - 68.0)	19.85 ± 12.97 (3.0 - 60.0)
DO ($\mu g.L^{-1}$)	9.44 ± 1.50 (6.89 - 13.45)	9.62 ± 1.26 (6.45 - 12.70)	9.94 ± 1.15 (8.12 - 12.70)
pH	8.06 ± 0.42 (7.07 - 8.60)	8.22 ± 0.47 (6.76 - 8.95)	8.25 ± 0.53 (6.84 - 8.92)
Depth (m)	2.88 ± 0.83 (1.60 - 4.30)	2.58 ± 0.74 (1.04 - 3.80)	2.43 ± 0.73 (1.26 - 3.80)

4.2.3 Satellite Data and Image Processing

MODIS-Terra (MOD09GA) and MODIS-Aqua (MYD09GA) Level-2 Surface Reflectance products with a daily frequency and a 500-m spatial resolution were downloaded via the web interface *The Land Processes Distributed Interface Active Archive Center* (LP DAAC), from The US Geological Survey EROS Data Center available at t `http://LPDAAC.usgs.gov`. These products have been successfully used in different inland waters, including oligo- to mesotrophic reservoirs (surface area: 778 km^2) (Curtarelli et al., 2015; Ogashawara et al., 2014), Amazon floodplain lakes (surface area: 2000 km^2) (Moraes Novo et al., 2006), Minnesota lakes (lake surface area > 160 ha) (Knight and Voth, 2012), Poyang Lake (surface area: 3000 km^2) (Qi et al., 2016), and coastal lagoons (900 km^2) (Srichandan et al., 2015). The cloud cover fraction was obtained using a cloud mask product from MODIS product level 2 (named M*D35L2) (Ackerman et al., 1998). In addition, MODIS quality product was also used to assess image quality (Roy et al., 2002). The sinusoidal projection images (ISIN) from the LP DAAC platform were transformed to geographic projection (Lat/Long) using the MODIS Reprojection Tool available at `http://lpdaac2.usgs.gov/landdaac/tools/modis/about.asp`. The MOD09GA, MYD09GA and M*D35L2 products were processed and analysed using a MatLab® routine. To retrieve Chl-*a* concentrations, we used the surface reflectance from the first six spectral bands of the MOD09GA and MYD09GA products, with the centre wavelength location respective (band 1: 648 nm, band 2: 858 nm; band 3: 470 nm; band 4: 555 nm; band 5: 1240 nm; and band 6:1640 nm).

We downloaded a total of 50 MODIS images (32 MODIS-Terra and 18 MODIS-Aqua) matching the *in-situ* measurements of Chl-*a* monitoring days (Table 2).From this total, we selected 16 images for model development and calibration, and 10 images for model verification; the remaining 24 images were discarded due to the presence of clouds, shadows on the measurement sites or to the bad quality of the images from MODIS quality product control.

Table 2 – Number of available MODIS images for calibration/validation periods for the North (N), Central (C), and South (S) points in Lake Mangueira.

Id	Field Campaign Date	Station			Id	Field Campaign Date	Station		
		N	C	S			N	C	S
1	21/03/2001				26	01/02/2004		Calibration	
2	20/04/2001		Calibration	Calibration	27	19/05/2004	Calibration	Calibration	Calibration
3	23/05/2001				28	18/08/2004			
4	19/06/2001				29	18/09/2004	Calibration	Calibration	Calibration
5	17/07/2001				30	10/11/2004			
6	21/08/2001	Calibration	Calibration	Calibration	31	22/03/2005			
7	27/09/2001				32	03/05/2005	Calibration	Calibration	Calibration
8	24/10/2001	Calibration	Calibration	Calibration	33	01/08/2005			
9	20/11/2001	Calibration	Calibration	Calibration	34	01/11/2005	Calibration	Calibration	Calibration
10	19/12/2001				35	01/03/2006			
11	29/01/2002	Calibration	Calibration	Calibration	36	17/05/2006	Validation	Validation	Validation
12	21/02/2002				37	01/08/2006			
13	20/03/2002				38	08/11/2006	Validation		
14	23/04/2002				39	09/11/2006		Validation	Validation
15	27/05/2002				40	30/05/2007	Validation	Validation	Validation
16	19/06/2002	Calibration	Calibration		41	15/08/2007			
17	23/07/2002	Calibration	Calibration	Calibration	42	07/11/2007	Validation	Validation	Validation
18	21/08/2002	Calibration	Calibration	Calibration	43	05/03/2008			
19	30/10/2002	Calibration		Calibration	44	13/08/2008	Validation	Validation	Validation
20	19/11/2002	Calibration	Calibration	Calibration	45	12/11/2008	Validation	Validation	Validation
21	17/12/2002	Calibration	Calibration	Calibration	46	11/03/2009			
22	04/05/2003				47	20/05/2009	Validation	Validation	Validation
23	04/08/2003				48	03/09/2009			
24	01/10/2003				49	10/11/2009		Validation	Validation
25	01/12/2003				50	11/11/2009	Validation		

Discarded Calibration Validation

4.2.4 Multivariable models to retrieve Chl-*a* concentration

Approaches based on multiple linear regression (MLR) models (using exclusion-inclusion sequential models), artificial neural networks (ANN) and nonparametric multiplicative regression (NPMR) were used to retrieve Chl-*a* concentrations, using the MOD09GA and MYD09GA reflectance data products.

An empirical model based on multiple linear regression (MLR) was developed, using two search criteria. The first used a step-wise forward regression from the reflectance for each of the spectral bands from MODIS. This approach was carried out taking into account that the F value was low and the p-value was high. This method generates a multiple linear regression of the bands with the highest correlation. The second development criterion was based on a sequential automatic search of exclusion-inclusion using the Akaike Information Criterion - AIC (Bozdogan, 1987). Using this criterion, an *R* code was developed to fit a sub-model for each of the three datasets (North, Central and South points) and for the total dataset in Lake Mangueira.

An artificial neural network (ANN) was applied using a hidden layer (Fig. 2). The reflectances for each of the spectral bands for three points (North, Central and South) and

the total dataset were the input values and the Chl-*a* concentration was the output node. The training algorithm used was the back-propagation method with heuristic techniques acceleration (Vogl et al., 1988) performed in MatLab®. The Purelin function (Demuth et al., 2008) was used as the activation function in the hidden and output layers.

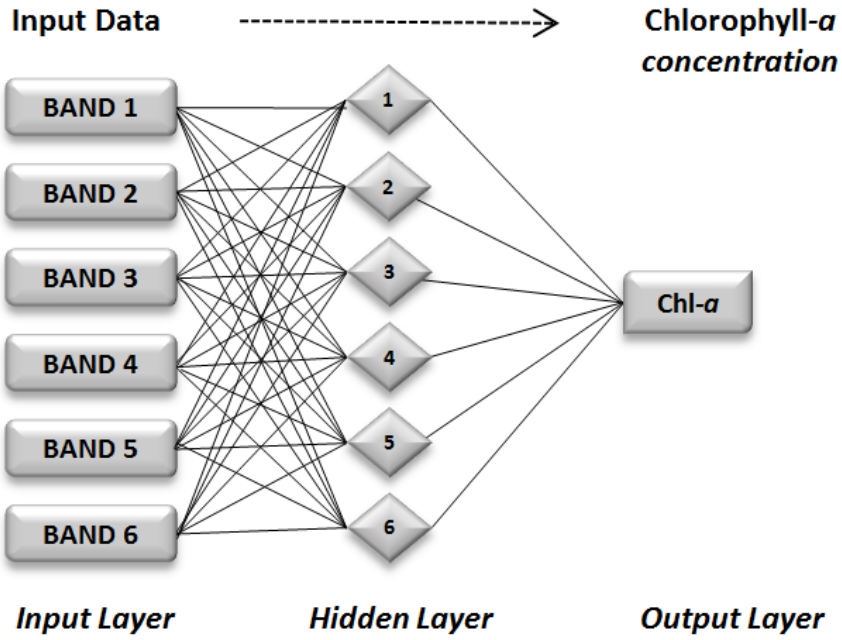

Figure 2 – Schematic diagram of an artificial neural network model.

Non-parametric multiplicative regression (NPMR) using the software *HyperNiche 1.0* was also used to select the best models describing the relationships between Chl-*a* and the reflectance values from the MODIS spectral bands (McCune, 2004, 2006). Two matrices were used as input in NPMR: (1) a matrix of *in-situ* Chl-*a* measurements, and (2) a matrix of reflectance values from the MODIS spectral bands. Here, the Local mean NPMR, uniform weights (Species Occurrence model - "SpOcc") was used (McCune et al., 2003; Peterson, 2000). This model uses a simple kernel function to estimate the response variable (Chl-*a* in our case) and gives equal weight to all sampling points within the window, while all observations outside the window are given zero weight. In addition, we assessed the performance of four empirical models (Kahru, Appel, FAI and O14a, Table 3) that are commonly used to estimate Chl-*a* concentrations in aquatic environments (Curtarelli et al., 2015; Hu et al., 2010; Huang et al., 2014; Tarrant and Neuer, 2009).

Table 3 – *Kahru*, *APPEL*, *FAI*, and *O14a* models to estimate Chl-*a* concentrations in Lake Mangueira.

Model	**Author**
$Kahru = R(\lambda_{b2}) - R(\lambda_{b1})$	*Kahru et al. 2004*
$APPEL = R(\lambda_{b2}) - [(R(\lambda_{b3}) - R(\lambda_{b2})) * R(\lambda_{b2}) + (R(\lambda_{b2}) - R(\lambda_{b1})]$	*El-Alem et al. 2012*
$FAI = R(\lambda_{b2}) - [R(\lambda_{b1}) + (R(\lambda_{b5} - R(\lambda_{b1})) * ((\lambda_{b2} - \lambda_{b1})/(\lambda_{b5} - \lambda_{b1})]$	*Hu and He 2008*
$O14a = 5.6897 + 203.5419 * R(\lambda_{b1}) - (151.0271 * R(\lambda_{b4})$ $+(83.5912 * R(\lambda_{b5})) - (170.4078 * R(\lambda_{b6}))$	*Ogashawara et al. 2014*

* where: $R(\lambda_{b1}), R(\lambda_{b2}), R(\lambda_{b3}), R(\lambda_{b4}), R(\lambda_{b5}), R(\lambda_{b6})$ are the reflectance of bands 1 to 6 respectively with $\lambda_{b1} = 645nm$, $\lambda_{b2} = 859nm$, $\lambda_{b3} = 470nm$, $\lambda_{b4} = 555nm$, $\lambda_{b5} = 1250nm$ and $\lambda_{b6} = 1640nm$

4.2.5 Model accuracy assessment

To evaluate the accuracy of the models, the coefficient of determination (R^2), Bias, Root-Mean-Square-Error (RMSE), and relative RMSE (RMSE%) were calculated between *in situ*-observed and model-estimated Chl-*a* concentrations.

4.3 Results

4.3.1 Model development and calibration

The performance of the multiple linear regression (MLR), artificial neural networks (ANN), and nonparametric multiplicative regression (NPMR) models for the three points (North, Central and South) and the total dataset for Lake Mangueira showed good agreement for the Central and South datasets. In addition, the MLR model performed best for each dataset (Fig. 3).

The MLR model assessment indicated the best performance for the South point (R^2 = 0.83, Bias = 0.00, RMSE% = 10.6%), compared to the Central point (R^2 = 0.77, Bias = -0.31, RMSE% = 14.6%), and the North point (R^2 = 0.61, Bias = 0.00, RMSE% = 19.6%). Also, the MLR model indicated spectral bands 2, 3 and 6 as the most important MODIS channels for the correlation with *in-situ* Chl-*a* values at the North point. For the Central and South points, the best correlations were obtained with the combination of spectral bands 1, 4, 5, 6 and 1, 2, 5, 6 respectively. For the total dataset, spectral bands 1, 3, 5 and 6 were the most important MODIS channels. The MLR models adjusted to the four datasets used are listed as follows:

$$MLR_{north} = 1.13 + (-584.84R(\lambda_{b2})) + (721.14R(\lambda_{b3})) + (33.33R(\lambda_{b6})) \quad (1)$$

$$MLR_{central} = 30.26 + (950.36R(\lambda_{b1})) + (-1032.97R(\lambda_{b4})) + (510.97R(\lambda_{b5})) + (-406.31R(\lambda_{b6})) \quad (2)$$

$$MLR_{south} = -3.12 + (616.28R(\lambda_{b1})) + (-625.52R(\lambda_{b2})) + (127.10R(\lambda_{b5})) + (-33.21R(\lambda_{b6})) \quad (3)$$

$$MLR_{totaldataset} = 9.23 + (36.95R(\lambda_{b1})) + (52.92R(\lambda_{b3})) + (14.47R(\lambda_{b5})) + (-35.73R(\lambda_{b6})) \quad (4)$$

where $R(\lambda_{b1})$, $R(\lambda_{b2})$, $R(\lambda_{b3})$, $R(\lambda_{b4})$, $R(\lambda_{b5})$, $R(\lambda_{b6})$ are the reflectance values of MODIS spectral bands 1, 2, 3, 4, 5, 6 and MLR is the estimated Chl-*a* in $\mu g.L^{-1}$.

The ANN model performed best for the Central point (R^2 = 0.62, Bias = 0.01, RMSE% = 16.0%), compared to the South point (R^2 = 0.41, Bias = -5.19, RMSE% = 18.7%), the North point (R^2 = 0.01, Bias = 2.72, RMSE% = 19.6%), and the total dataset (R^2 = 0.21, Bias = 2.42, RMSE% = 18.4%). The ANN model architecture was composed of 3 layers (input, hidden and output layers): the input layer had the same MODIS channel inputs as the MLR models, the hidden layer had several neurons based on each dataset (North: 12; Central: 4; South: 10), and the

output has one neuron (Chl-*a*). Thus, the ANN architecture was: North: 3-12-1; Central: 4-4-1 and South: 4-10-1.

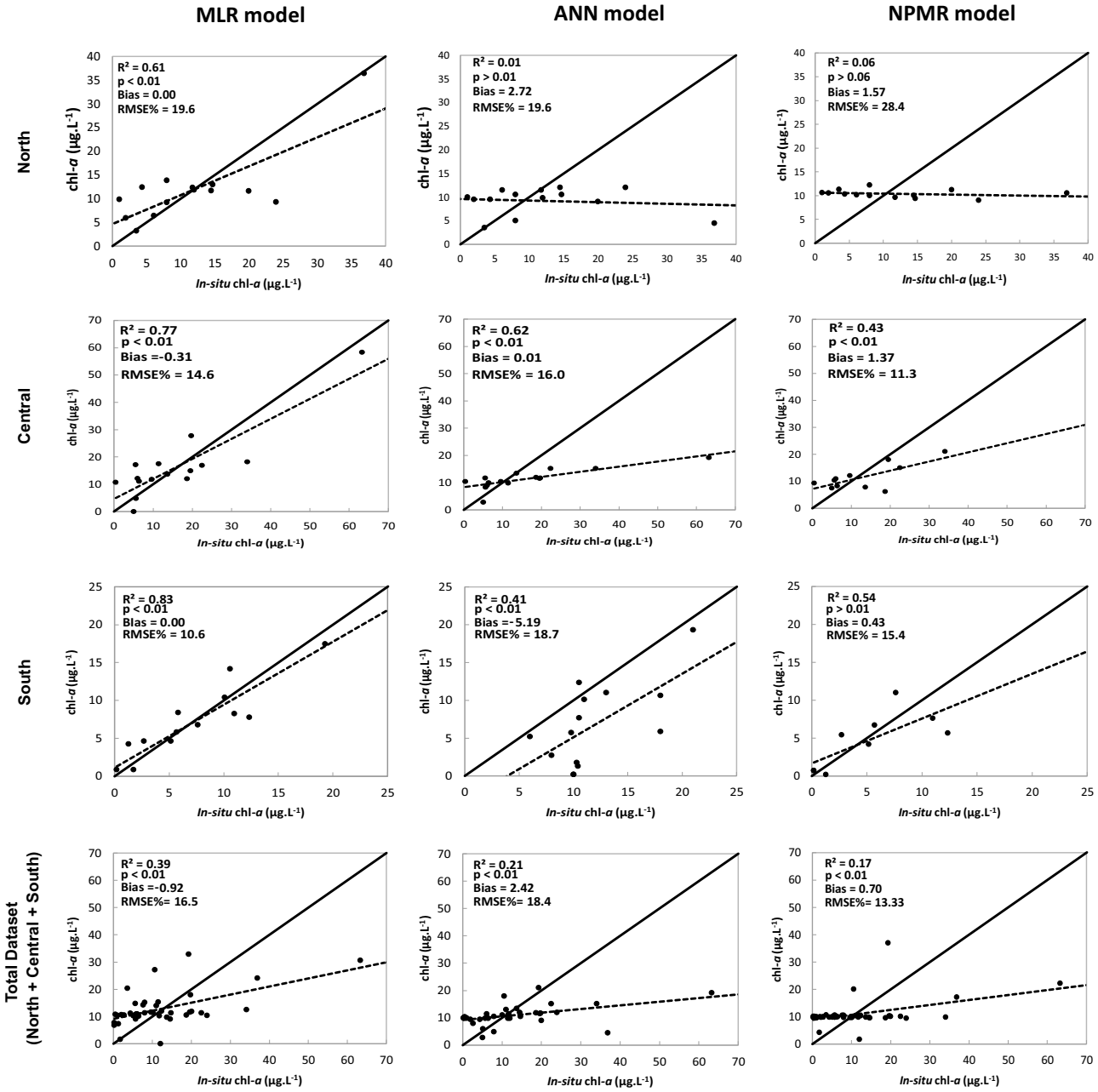

Figure 3 – Chlorophyll-*a* concentrations predicted by MLR, ANN and NPMR models versus *in-situ* chlorophyll-*a* measurements at three points (North, Central and South) and the total dataset in Lake Mangueira during calibration. The solid lines represent the 1:1 (one-to-one) relationship, and the dotted lines represent the best fit.

The results from the NPMR models indicated the best performance for the South point of Lake Mangueira (R^2 = 0.54, Bias = 0.43, RMSE% = 15.4%), compared to the Central point (R^2 = 0.43, Bias = 1.37, RMSE% = 11.3%), the North point (R^2 = 0.06, Bias = 1.57, RMSE% = 28.4%), and the total dataset (R^2 = 0.17, Bias = 0.70, RMSE% = 13.33%). For the three points in the lake, we used as the predictor matrix (input data), the reflectance values from all MODIS spectral

bands (1, 2, 4, 5 and 6). The results indicated that, for the Central and South points, the best performance was obtained with the combination of spectral bands 1, 4 and 5, 6 respectively. For the North and the total dataset, the best performance was obtained with the combination of spectral bands 1, 6 and 1, 2, 5, 6 respectively.

4.3.2 Model validation and comparative assessment

The performance of the different models during the validation phase showed, in general, lower values of the accuracy metrics (Fig. 4). However, the MLR and ANN models showed a smaller loss of performance (R^2 = 0.50, Bias = -1.36, RMSE% = 29.9% and R^2 = 0.46, Bias = -1.78, RMSE% = 24.6%) and maintained satisfactory accuracy compared to the NPMR model (e.g., Central point).

In all cases, the performance of our multivariable models using the total dataset was lower than with the specific point dataset. The same occurred in comparisons against four commonly used empirical models, Appel, Kahru, FAI, and O14a (Table 4). We found that the multiple linear regression model (MLR) was reliable in terms of its estimation of Chl-*a* concentrations for the three points in the lake, although it was less accurate for the South point (R^2 = 0.37, Bias = -3.54, RMSE% = 34.40%). The ANN model performed best for the Central point in Lake Mangueira (R^2 = 0.46, Bias = -1.78, RMSE% = 24.60%), but did not provide satisfactory results for the North and South points. The NPMR model had limitations in retrieving the Chl-*a* concentration for the North (N) Center (C) and South (S) points ($R^2 \leq 0.19$, Bias $\leq$ 5.37, RMSE% $\leq$ 42.50%). The assessment with the four empirical models (Appel, Kahru, FAI and O14a) showed lower accuracy than the MLR model. The Kahru model gave the best Chl-*a* retrieval ($R^2 \leq 0.37$, Bias $\leq$ 9.09, RMSE% $\leq$ 33.50%), followed by the O14a model ($R^2 \leq 0.35$, Bias $\leq$ 5.53, RMSE% $\leq$ 39.97%); the Appel model gave the poorest results ($R^2 \leq 0.26$, Bias $\leq$ 9.07, RMSE% $\leq$ 35.04%). Taking into account the total dataset, the accuracy yielded by the MLR, ANN and NPMR models and the four empirical models (Appel, Kahru, FAI and O14a) also showed low performance compared with the *in-situ* Chl-*a* values.

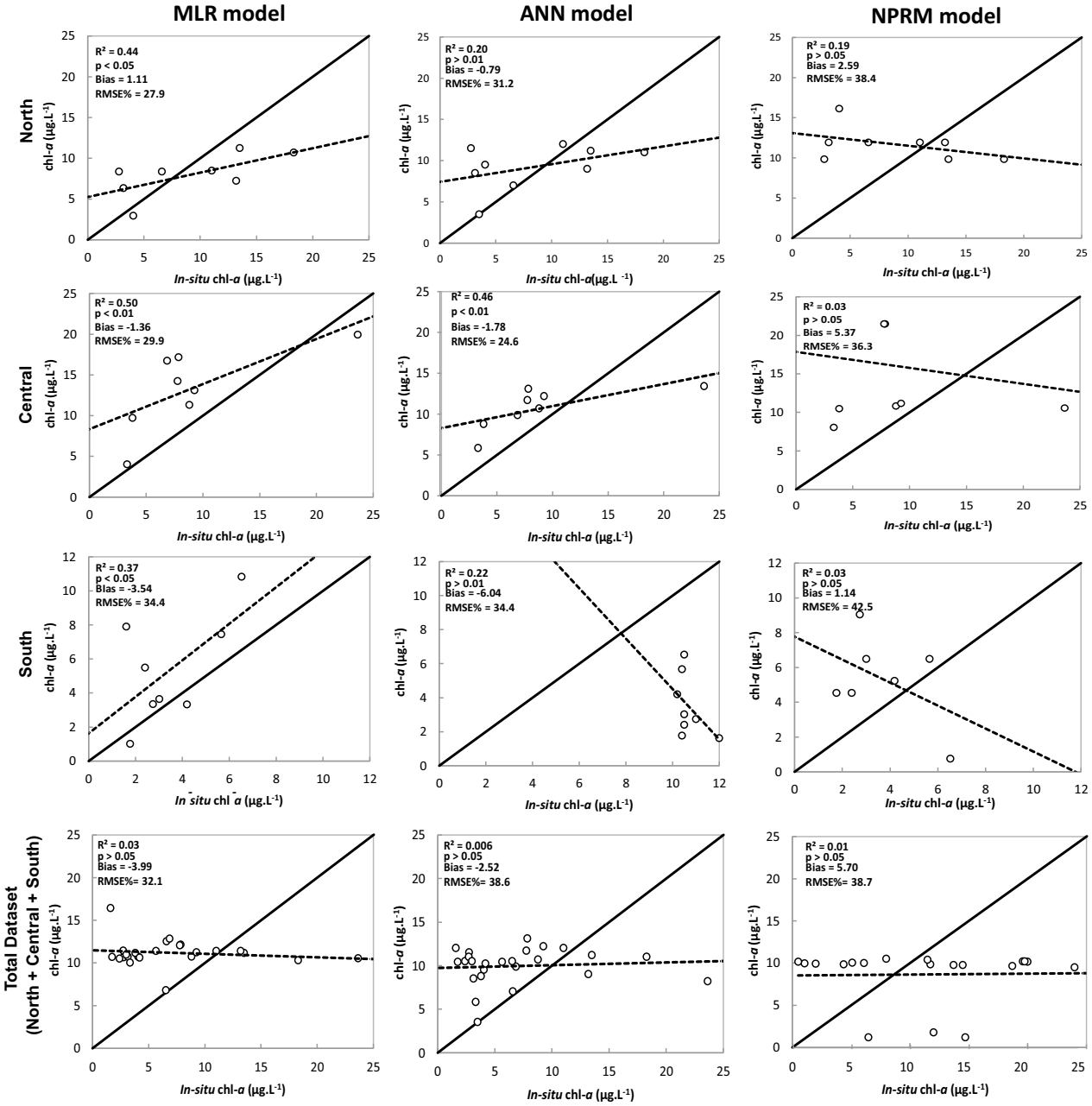

Figure 4 – Chlorophyll-*a* concentrations predicted by MLR, ANN and NPMR models versus *in-situ* chlorophyll-*a* measurements at three points (North, Central and South) and the total dataset in Lake Mangueira during validation. The solid lines represent the 1:1 (one-to-one) relationship, and the dotted lines represent the best fit.

Table 4 – Coefficient of determination (R^2), Bias and Relative RMSE (RMSE%) of multivariable models for the North(N), Central (C) and South (S) points and the Total Dataset (TD) in Lake Mangueira. R^2>0.4 and relative RMSE% <30% are highlighted in bold.

Model	R^2				Bias				RMSE%			
	N	C	S	TD	N	C	S	TD	N	C	S	TD
MLR	**0.44**	**0.50**	0.37	0.03	1.11	-1.36	-3.54	-3.99	**27.90**	**29.90**	34.40	32.10
ANN	0.20	**0.46**	0.22	0.01	-0.79	-1.78	-6.04	-2.52	31.20	**24.60**	34.40	38.60
NPMR	0.19	0.03	0.03	0.01	2.59	5.37	1.14	5.70	38.40	36.30	42.50	38.70
Appel	0.26	0.00	0.22	0.18	9.07	8.92	3.48	5.03	34.41	33.79	35.04	37.20
Kahru	0.30	0.01	0.37	0.02	9.09	8.93	3.50	4.53	33.50	33.48	31.44	36.42
FAI	0.15	0.10	0.33	0.06	9.08	8.93	3.50	4.50	37.00	33.69	32.52	36.95
O14a	0.00	0.22	0.35	0.08	4.18	5.53	3.06	3.89	39.97	**29.81**	31.95	38.65

4.4 Discussion

4.4.1 Performance of Chl-*a* algorithms

For the models proposed here, the MLR and ANN models performed better than other models (R^2 and RMSE%, Table 4), in agreement with the performance found previously for oligo- to meso-trophic waters using MLR models (Curtarelli et al., 2015; Ogashawara et al., 2014) and for eutrophic shallow waters using Back Propagation neural networks (BPs) and Radial Basis Function neural networks (RBFs) (Wu et al., 2009).

Although the NPMR model is generally stronger than the MLR model (McCune et al., 2003; Yost, 2008), our results indicated a significant difference in the performance of the two models. Also, the NPMR model showed lower performance, which was apparent during both the calibration (Fig. 3) and the validation (Fig. 4) periods. This result indicates that the application of NPMR models to retrieve the Chl-*a* concentration from MODIS imagery in Lake Mangueira would not be recommended based on the dataset available. For the four models assessed (Appel, Kahru, FAI and O14a), our findings were consistent with those of El-Alem et al. (2012), who obtained satisfactory results for Chl-*a* > 50 μg.L^{-1} using the Kahru and FAI models.

In Lake Mangueira, the Chl-*a* concentration estimated using the total dataset indicated that the correlation was the lowest for every model proposed and assessed as shown in the calibration (Fig. 3), validation (Fig. 4) and comparison (Table 4). Therefore, it would not be appropriate to generalize a single model to retrieve the Chl-*a* concentration in Lake Mangueira from a total dataset, but rather would be necessary to subdivide the datasets into regions. This can be explained by meso-oligotrophic conditions and the spatial heterogeneity, where the Chl-*a* concentration decreases from north to south, as has been observed or taken into account in other studies (Crossetti et al., 2013; Fragoso et al., 2008, 2011; Rodrigues, 2009). External forcing factors, such as the wind (both speed and direction) also can affect the temporal and spatial distribution of phytoplankton in large shallow lakes (Cardoso et al., 2012; Carrick et al., 1993; Kong and Fao, 2005; Webster and Hutchinson, 1994), In these environments, wind conditions impose stress on the system, in which the biological responses (*e.g.*, Chl-*a*) can be interconnected,

in contrast to environments such as temperate lakes and oceans. In Lake Mangueira, a previous study (Fragoso et al., 2008) showed a trend of phytoplankton aggregation in the southwest and northeast areas, varying with the wind velocity and direction, and coinciding with the orientation of the lake (*i.e.* the fetch). In addition, another key influencing factor is the larger biomass of submerged macrophytes in the South area, which can inhibit phytoplankton production in this area (They et al., 2014) and increases the water transparency (Ferreira, 2009). Regarding the proposed models, our results corroborated the spatial heterogeneity in the Chl-*a* distribution in the Lake Mangueira, as observed previously in other studies (Crossetti et al., 2013; Fragoso et al., 2008, 2011).

The use of models to retrieve Chl-*a* based on multiple linear regression (MLR) from MODIS data is not new. However, our approach showed an improvement over previously published models (*e.g.,* Chang et al., 2012; Ogashawara et al., 2014; Wu et al., 2009) due to the implementation of search criteria based on a sequential automatic search of exclusion-inclusion algorithms for selecting parameters. In addition, the estimation of Chl-*a* concentrations base on MRL presented advantages (*e.g.,* few input variables and explicit calculation of the coefficients of selected independent variables) in comparison with the ANN and NPMR models, which is difficult to interpret the relationship between input and output variables (*"blackbox"* models) (Wu et al., 2014). Furthermore, the MLR model is parsimonious, requiring only a small number of parameters compared to the other empirical models.

4.4.2 Limitations of algorithms for estimating Chl-*a* from MODIS imagery

Several studies (*e.g.,* Carder et al., 2005; Gower and Borstad, 2004) have shown that algorithms may indeed be precluded due to the low signal-to-noise ratio, and the noise-equivalent chlorophyll-*a* concentration of MODIS.

This is a limitation in meso-oligotrophic environments such as Lake Mangueira, which can impede the performance of algorithms based on MODIS imagery, due to low chlorophyll-*a* contents, and the adjacency effects that can be caused by sun glints, as founded in similar environments (Chavula et al., 2009; Matthews and Odermatt, 2015; Watanabe et al., 2016). Furthermore, at the South point, located in the shallow area of the lake, water transparency is high (Table 1), and the light reflected off the bottom (IOCCG, 2000; Lee et al., 2001) also affects the accuracy of the empirical algorithms assessed. Another limitation is associated with the use of satellite remote-sensing techniques, which detect Chl-*a* in surface waters only. However, this limitation may not be applicable to shallow-water systems such as Lake Mangueira, since Chl-*a* concentrations may be relatively uniform throughout the water column.

4.5 Conclusion

This study analyzed the estimates of Chl-*a* concentrations by several models, based on Terra and Aqua MODIS reflectance data in a shallow subtropical lake. A simple model using

multiple linear regression (MLR) provided the most accurate estimates. Our findings indicated that the MLR model was better than the artificial neural networks (ANN) and nonparametric multiplicative regression (NPMR) models.

In addition, the simple model proposed in this study goes beyond the previously reported models, showing two main advantages: better performance and fewer input variables compared with the empirical models that are commonly used (Appel, Kahru, FAI and O14a).

This was the first approach to corroborate the spatial heterogeneity in the Chl-*a* distribution in the Lake Mangueira and the differences into regions (*e.g.,* North, Central and South), using remote sensing techniques.

Finally, although the purpose of this study was not to replace standard monitoring methods, the MRL model using MODIS reflectance data can provide a dynamic, broader-scale view of Chl-*a* concentrations. Further investigation could be focused on MRL model application to analyze in long-term scale, the temporal and spatial distribution of Chl-*a* concentration in Lake Mangueira, in order to understand the seasonal dynamic and the inter-annual variations. The overall methodology proposed here can be used as a tool to help reduce the effort and costs associated with conventional limnological monitoring of shallow waters, and as a data source to support distributed ecological mathematical modelling of these ecosystems.

Acknowledgements: We are grateful to the Coordenação de Aperfeiçoamento de Pessoal de Nível Superior (`CAPES:www.capes.gov.br`) and to the Conselho Nacional de Desenvolvimento Cientifico e Tecnológico (`CNPq:www.cnpq.br`) of Brazil for doctoral scholarships awarded to A. M. Munar and J. R. Cavalcanti. The study is part of the research project *"Impacto das mudanças climáticas em ambientes fluviais e lacustres do Rio Grande do Sul"*, funded by CNPq. We are also grateful to the Global Lake Ecological Observatory Network (`GLEON:www.gleon.org`) for providing a venue and resources for lake-science discussions, and to Dr. Janet W. Reid (Trumansburg, NY, U.S.A.) for revising the English text.

Author Contributions: A.M.M., D.d.M.M and C.R.F.Jr developed the idea for the study, as well as its design. A.M.M., J.R.C., and J.M.B were responsible for the construction and validation of the models and dataset. A.M.M., D.d.M.M., J.M.B and C.R.F.Jr. were responsible for the support in statistical evaluation and paper review. All authors read and approved the manuscript.

Conflicts of Interest: The authors declare no conflict of interest.

Referências

Ackerman, S. A., Strabala, K. I., Menzel, W. P., Frey, R. A., Moeller, C. C., and Gumley, L. E. (1998). Discriminating clear sky from clouds with MODIS. *Journal of Geophysical Research: Atmospheres (1984–2012)*, 103(D24):32141–32157.

Allan, M. G., Hamilton, D. P., Hicks, B. J., and Brabyn, L. (2011). Landsat remote sensing of chlorophyll a concentrations in central North Island lakes of New Zealand. *International Journal of Remote Sensing*, 32(7):2037–2055.

APHA, A. A. P. H. A. (1992). *Standard methods for the examination of water and wastewater*, volume 2. American Public Health Association APHA.

Bozdogan, H. (1987). Model selection and Akaike's information criterion (AIC): The general theory and its analytical extensions. *Psychometrika*, 52(3):345–370.

Carder, K. L., Cannizzaro, J. P., and Lee, Z. (2005). Ocean color algorithms in optically shallow waters: Limitations and improvements. In 5885, P. S., editor, *Remote Sensing of the Coastal Oceanic Environment, 588506*.

Cardoso, L. S., Fragoso Jr, C. R., Souza, R. S., and Motta-Marques, D. (2012). Hydrodynamic control of plankton spatial and temporal heterogeneity in subtropical shallow lakes. In Schulz, H. E., Simões, A. L. A., and Lobosco, R. J., editors, *Hydrodynamics: Natural Water Bodies*, chapter 2, pages 27–48. InTech.

Carrick, H. J., Aldridge, F. J., and Schelske, C. L. (1993). Wind influences phytoplankton biomass and composition in a shallow, productive lake. *Limnology and Oceanography*, 38(6):1179–1192.

Chang, N.-B., Yang, Y. J., Daranpob, A., Jin, K.-R., and James, T. (2012). Spatiotemporal pattern validation of chlorophyll-*a* concentrations in Lake Okeechobee, Florida, using a comparative MODIS image mining approach. *International Journal of Remote Sensing*, 33(7):2233–2260.

Chavula, G., Brezonik, P., Thenkabail, P., Johnson, T., and Bauer, M. (2009). Estimating chlorophyll concentration in Lake Malawi from MODIS satellite imagery. *Physics and Chemistry of the Earth, Parts A/B/C*, 34(13):755–760.

Crossetti, L. O., Becker, V., de Souza Cardoso, L., Rodrigues, L. R., da Costa, L. S., and da Motta-Marques, D. (2013). Is phytoplankton functional classification a suitable tool to investigate spatial heterogeneity in a subtropical shallow lake? *Limnologica-Ecology and Management of Inland Waters*, 43(3):157–163.

Curtarelli, M., Ogashawara, I., Alcântara, E., and Stech, J. (2015). Coupling remote sensing bio-optical and three-dimensional hydrodynamic modeling to study the phytoplankton dynamics in a tropical hydroelectric reservoir. *Remote Sensing of Environment*, 157:185–198.

Darecki, M. and Stramski, D. (2004). An evaluation of MODIS and SeaWiFS bio-optical algorithms in the Baltic Sea. *Remote Sensing of Environment*, 89(3):326–350.

Demuth, H., Beale, M., and Hagan, M. (2008). Neural network toolboxâ 6. *Userâs Guide*.

Deng, Y., Zhang, Y., Li, D., Shi, K., and Zhang, Y. (2017). Temporal and Spatial Dynamics of Phytoplankton Primary Production in Lake Taihu Derived from MODIS Data. *Remote Sensing*, 9(3):195.

Duan, H., Ma, R., Xu, J., Zhang, Y., and Zhang, B. (2010). Comparison of different semi-empirical algorithms to estimate chlorophyll-a concentration in inland lake water. *Environmental Monitoring and Assessment*, 170(1-4):231–244.

Duka, S. and Cullaj, A. (2009). Evaluation of chlorophyll as the primary index for trophic state classification. *Journal of Environmental Protection and Ecology*, 10(2):401–410.

El-Alem, A., Chokmani, K., Laurion, I., and El-Adlouni, S. E. (2012). Comparative analysis of four models to estimate chlorophyll-a concentration in case-2 waters using moderate resolution imaging spectroradiometer (MODIS) imagery. *Remote Sensing*, 4(8):2373–2400.

Ferreira, T. F. (2009). *O papel das macrófitas submersas sobre a qualidade da água, restauração e conservação de lagos rasos subtropicais: estudo de caso, a Lagoa Mangueira, RS*. PhD thesis, Universidade Federal do Rio Grande do Sul, Porto Alegre, Brazil.

Fragoso, C. R., Marques, D. M. M., Collischonn, W., Tucci, C. E., and van Nes, E. H. (2008). Modelling spatial heterogeneity of phytoplankton in Lake Mangueira, a large shallow subtropical lake in South Brazil. *Ecological Modelling*, 219(1):125–137.

Fragoso, C. R., Marques, D. M. M., Ferreira, T. F., Janse, J. H., and van Nes, E. H. (2011). Potential effects of climate change and eutrophication on a large subtropical shallow lake. *Environmental Modelling & Software*, 26(11):1337–1348.

Gholizadeh, M. H., Melesse, A. M., and Reddi, L. (2016). A comprehensive review on water quality parameters estimation using remote sensing techniques. *Sensors*, 16(8):1298.

Gilerson, A. A., Gitelson, A. A., Zhou, J., Gurlin, D., Moses, W., Ioannou, I., and Ahmed, S. A. (2010). Algorithms for remote estimation of chlorophyll-*a* in coastal and inland waters using red and near infrared bands. *Optics Express*, 18(23):24109–24125.

Gower, J. and Borstad, G. (2004). On the potential of MODIS and MERIS for imaging chlorophyll-*a* fluorescence from space. *International Journal of Remote Sensing*, 25(7-8):1459–1464.

Gurlin, D., Gitelson, A. A., and Moses, W. J. (2011). Remote estimation of chl-a concentration in turbid productive watersâReturn to a simple two-band NIR-red model? *Remote Sensing of Environment*, 115(12):3479–3490.

Honeywill, C., Paterson, D., and Hagerthey, S. (2002). Determination of microphytobenthic biomass using pulse-amplitude modulated minimum fluorescence. *European Journal of Phycology*, 37(4):485–492.

Hu, C. (2009). A novel ocean color index to detect floating algae in the global oceans. *Remote Sensing of Environment*, 113(10):2118–2129.

Hu, C. and He, M.-X. (2008). Origin and offshore extent of floating algae in Olympic sailing area. *Eos, Transactions of the American Geophysical Union*, 89(33):302–303.

Hu, C., Lee, Z., Ma, R., Yu, K., Li, D., and Shang, S. (2010). Moderate resolution imaging spectroradiometer (MODIS) observations of cyanobacteria blooms in Taihu Lake, China. *Journal of Geophysical Research: Oceans*, 115(C4).

Huang, C., Li, Y., Yang, H., Sun, D., Yu, Z., Zhang, Z., Chen, X., and Xu, L. (2014). Detection of algal bloom and factors influencing its formation in Taihu Lake from 2000 to 2011 by MODIS. *Environmental Earth Sciences*, 71(8):3705–3714.

IOCCG (2000). Remote Sensing of Ocean Colour in Coastal, and Other Optically-Complex, Waters. Sathyendranath, S. (ed.). *Reports of the International Ocean-Colour Coordinating Group, No. 3, IOCCG, Dartmouth, Canada*, 3:140.

Jespersen, A.-M. and Christoffersen, K. (1987). Measurements of chlorophyllâa from phytoplankton using ethanol as extraction solvent. *Archiv für Hydrobiologie*, 109(3):445–454.

Kahru, M., Michell, B. G., Diaz, A., and Miura, M. (2004). MODIS detects a devastating algal bloom in Paracas Bay, Peru. *Eos, Transactions of the American Geophysical Union*, 85(45):465–472.

Kasprzak, P., PadisÃ¡k, J., Koschel, R., Krienitz, L., and Gervais, F. (2008). Chlorophyll-*a* concentration across a trophic gradient of lakes: An estimator of phytoplankton biomass? *Limnologica-Ecology and Management of Inland Waters*, 38(3):327–338.

Knight, J. F. and Voth, M. L. (2012). Application of MODIS imagery for intra-annual water clarity assessment of Minnesota lakes. *Remote Sensing*, 4(7):2181–2198.

Komick, N., Costa, M., and Gower, J. (2009). Bio-optical algorithm evaluation for MODIS for western Canada coastal waters: An exploratory approach using *in situ* reflectance. *Remote Sensing of Environment*, 113(4):794–804.

Kong, F. and Fao, G. (2005). Hypothesis on cyanobacteria bloom-forming mechanism in large shallow eutrophic lakes. *Acta ecologica sinica/Shengtai Xuebao*, 25(3):589–595.

Kottek, M., Grieser, J., Beck, C., Rudolf, B., and Rubel, F. (2006). World map of the köppen-geiger climate classification updated. *Meteorologische Zeitschrift*, 15(3):259–263.

Le, C., Hu, C., Cannizzaro, J., and Duan, H. (2013). Long-term distribution patterns of remotely sensed water quality parameters in Chesapeake Bay. *Estuarine, Coastal and Shelf Science*, 128:93–103.

Lee, Z., Carder, K. L., Chen, R. F., and Peacock, T. G. (2001). Properties of the water column and bottom derived from Airborne Visible Infrared Imaging Spectrometer (AVIRIS) data. *Journal of Geophysical Research-Oceans*, 106(C6):11639.

Lesht, B. M., Barbiero, R. P., and Warren, G. J. (2013). A band-ratio algorithm for retrieving open-lake chlorophyll values from satellite observations of the Great Lakes. *Journal of Great Lakes Research*, 39(1):138–152.

Lima, M. S., da Motta Marques, D., They, N. H., McMahon, K. D., Rodrigues, L. R., de Souza Cardoso, L., and Crossetti, L. O. (2016). Contrasting factors drive within-lake bacterial community composition and functional traits in a large shallow subtropical lake. *Hydrobiologia*, 778(1):105–120.

Matthews, M. W. (2011). A current review of empirical procedures of remote sensing in inland and near-coastal transitional waters. *International Journal of Remote Sensing*, 32(21):6855–6899.

Matthews, M. W., Bernard, S., and Robertson, L. (2012). An algorithm for detecting trophic status (chlorophyll-*a*), cyanobacterial-dominance, surface scums and floating vegetation in inland and coastal waters. *Remote Sensing of Environment*, 124:637–652.

Matthews, M. W. and Odermatt, D. (2015). Improved algorithm for routine monitoring of cyanobacteria and eutrophication in inland and near-coastal waters. *Remote Sensing of Environment*, 156:374–382.

McCune, B. (2004). Nonparametric multiplicative regression for habitat modeling. *Online at http://www. pcord. com/NPMRintro. pdf*.

McCune, B. (2006). Non-parametric habitat models with automatic interactions. *Journal of Vegetation Science*, 17(6):819–830.

McCune, B., Berryman, S. D., Cissel, J. H., and Gitelman, A. I. (2003). Use of a smoother to forecast occurrence of epiphytic lichens under alternative forest management plans. *Ecological Applications*, 13(4):1110–1123.

Moore, T. S., Campbell, J. W., and Dowell, M. D. (2009). A class-based approach to characterizing and mapping the uncertainty of the MODIS ocean chlorophyll product. *Remote Sensing of Environment*, 113(11):2424–2430.

Moraes Novo, E. M. L., de Farias Barbosa, C. C., de Freitas, R. M., Shimabukuro, Y. E., Melack, J. M., and Pereira Filho, W. (2006). Seasonal changes in chlorophyll distributions in Amazon floodplain lakes derived from MODIS images. *Limnology*, 7(3):153–161.

Ogashawara, I., Alcântara, E. H., Curtarelli, M. P., Adami, M., Nascimento, R. F., Souza, A. F., Stech, J. L., and Kampel, M. (2014). Performance analysis of modis 500-m spatial resolution products for estimating chlorophyll-a concentrations in oligo-to meso-trophic waters case study: Itumbiara reservoir, brazil. *Remote Sensing*, 6(2):1634–1653.

Olmanson, L. G., Brezonik, P. L., and Bauer, M. E. (2011). Evaluation of medium to low resolution satellite imagery for regional lake water quality assessments. *Water Resources Research*, 47(9).

O'Reilly, J. (2000). Ocean color chlorophyll a algorithms for SeaWiFS, OC2, and OC4: Version 4. *SeaWiFS postlaunch calibration and validation analyses*, 3:9–23.

Palmer, S.C.J. Kuster, T. and Hunter, P. D. (2015). Remote sensing of inland waters: Challenges, progress and future directions. *Remote Sensing of Environment*, 157:1–8.

Peterson, E. B. (2000). *Analysis and prediction of patterns in lichen communities over the western Oregon landscape*. PhD thesis, Oregon State University, Corvallis, Oregon.

Qi, H., Lu, J., Chen, X., Sauvage, S., and Sanchez-Pérez, J.-M. (2016). Water age prediction and its potential impacts on water quality using a hydrodynamic model for Poyang Lake, China. *Environmental Science and Pollution Research*, 23(13):13327–13341.

Ritchie, J. C., Zimba, P. V., and Everitt, J. H. (2003). Remote sensing techniques to assess water quality. *Photogrammetric Engineering & Remote Sensing*, 69(6):695–704.

Rodrigues, L. H. R. (2009). *Reguladores da dinâmica das comunidades planctônicas e íctica em ecossistemas límnicos subtropicais*. PhD thesis, Universidade Federal do Rio Grande do Sul, Porto Alegre, Brazil.

Rosa Neto, J. L. R., Fragoso Jr, C. R., Malhado, A. C., and Ladle, R. J. (2015). Spatio-temporal variability of Chlorophyll-A in the Coastal Zone of Northeastern Brazil. *Estuaries and Coasts*, 38(1):72–83.

Roy, D. P., Borak, J. S., Devadiga, S., Wolfe, R. E., Zheng, M., and Descloitres, J. (2002). The MODIS land product quality assessment approach. *Remote Sensing of Environment*, 83(1):62–76.

Ruiz-Verdú, A., Jiménez, J. C., Lazzaro, X., Tenjo, C., Delegido, J., Pereira, M., Sobrino, J. A., and Moreno, J. (2016). Comparison of MODIS and Landsat-8 retrievals of chlorophyll-a and water temperature over Lake Titicaca. In *Geoscience and Remote Sensing Symposium (IGARSS), 2016 IEEE International*, pages 7643–7646. IEEE.

Schalles, J. F., Gitelson, A. A., Yacobi, Y. Z., and Kroenke, A. E. (1998). Estimation of chlorophyll a from time series measurements of high spectral resolution reflectance in an eutrophic lake. *Journal of Phycology*, 34(2):383–390.

Song, K., Li, L., Tedesco, L., Li, S., Duan, H., Liu, D., Hall, B., Du, J., Li, Z., Shi, K., et al. (2013). Remote estimation of chlorophyll-a in turbid inland waters: Three-band model versus GA-PLS model. *Remote Sensing of Environment*, 136:342–357.

Srichandan, S., Kim, J. Y., Kumar, A., Mishra, D. R., Bhadury, P., Muduli, P. R., Pattnaik, A. K., and Rastogi, G. (2015). Interannual and cyclone-driven variability in phytoplankton communities of a tropical coastal lagoon. *Marine pollution bulletin*, 101(1):39–52.

Tarrant, P. and Neuer, S. (2009). Monitoring algal blooms in a southwestern US reservoir system. *Eos, Transactions of the American Geophysical Union*, 90(5):38–39.

They, N. H., da Motta Marques, D., Crossetti, L. O., Becker, V., Canterle, E., Rodrigues, L. R., de Souza Cardoso, L., and Júnior, C. R. F. (2014). Phytoplankton ecological interactions in freshwater ecosystems-integrating relationships in subtropical shallow lakes. In *Phytoplankton*, chapter 4, page 73. Nova Science Publishers.

They, N. H., da Motta Marques, D., and Souza, R. S. (2012). *Lower respiration in the littoral zone of a subtropical shallow lake*, volume 3. Frontiers Media SA, doi:10.3389/fmicb.2012.00434.

Vogl, T. P., Mangis, J., Rigler, A., Zink, W., and Alkon, D. (1988). Accelerating the convergence of the back-propagation method. *Biological Cybernetics*, 59(4-5):257–263.

Wang, M., Shi, W., and Tang, J. (2011). Water property monitoring and assessment for China's inland Lake Taihu from MODIS-Aqua measurements. *Remote Sensing of Environment*, 115(3):841–854.

Watanabe, S., Vincent, W. F., Reuter, J., Hook, S. J., and Schladow, S. G. (2016). A quantitative blueness index for oligotrophic waters: Application to Lake Tahoe, California–Nevada. *Limnology and Oceanography: Methods*, 14(2):100–109.

Webster, I. T. and Hutchinson, P. A. (1994). Effect of wind on the distribution of phytoplankton cells in lakes revisited. *Limnology and Oceanography*, 39(2):365–373.

Wu, G., Liu, L., Chen, F., and Fei, T. (2014). Developing MODIS-based retrieval models of suspended particulate matter concentration in Dongting Lake, China. *International Journal of Applied Earth Observation and Geoinformation*, 32:46–53.

Wu, M., Zhang, W., Wang, X., and Luo, D. (2009). Application of MODIS satellite data in monitoring water quality parameters of Chaohu Lake in China. *Environmental Monitoring and Assessment*, 148(1-4):255–264.

Xiang, B., Song, J.-W., Wang, X.-Y., and Zhen, J. (2015). Improving the accuracy of estimation of eutrophication state index using a remote sensing data-driven method: A case study of Chaohu Lake, China. *Water SA*, 41(5):753–761.

Yost, A. C. (2008). Probabilistic modeling and mapping of plant indicator species in a Northeast Oregon industrial forest, USA. *Ecological Indicators*, 8(1):46–56.

Zhang, Y., Lin, S., Qian, X., Wang, Q., Qian, Y., Liu, J., and Ge, Y. (2011). Temporal and spatial variability of chlorophyll a concentration in Lake Taihu using MODIS time-series data. *Hydrobiologia*, 661(1):235–250.

Zhang, Y., Ma, R., Duan, H., Loiselle, S., Zhang, M., and Xu, J. (2016). A novel modis algorithm to estimate chlorophyll a concentration in eutrophic turbid lakes. *Ecological Indicators*, 69:138–151.

Capítulo 5

Conclusão

Esta tese teve como objetivo principal investigar e compreender o funcionamento hidrológico da Bacia da Lagoa Mirim e o comportamento hidrodinâmico e a qualidade da água da lagoa, a partir da integração da modelagem hidrológica de grande escala e a modelagem hidrodinâmica, assim como o monitoramento de parâmetros de qualidade da água (*e.g.* clorofila-*a*, temperatura da superfície d'água e níveis d'água) utilizando ténicas de sensoriamento remoto. Por tanto, ao longo deste trabalho foram apresentados uma série de estudos (Capítulos 2, 3 e 4) que visaram responder as questões científicas que motivaram o desenvolvimento da tese, e que são apresentadas a seguir:

O acoplamento da modelagem hidrológica - hidrodinâmica de grande escala poderia representar as diferentes variáveis hidrológicas (e.g., vazões, níveis d'água) se comparado com medições in-situ e dados de sensoriamento remoto?

Ao longo deste trabalho foi realizado o acoplamento *offline* do modelo MGB-IPH com o modelo hidrodinâmico/qualidade de água (IPH-ECO). Neste acoplamento, as descargas fluviais dos rios afluentes à lagoa estimadas pelo modelo MGB-IPH, foram utilizadas como *input data* para o modelo IPH-ECO. Esta abordagem foi utilizada para estudar a bacia da Lagoa Mirim em termos da resposta hidrológica e as variações espaciais e temporais dos principais componentes hidrodinâmicos da lagoa (*e.g.,* níveis da água, campos de velocidade, estrutura de fluxo). Os níveis da água simulados no modelo acoplado foram validados utilizando dados altimétricos dos satélites ICESat e ENVISAT e medições *in-situ* na lagoa. Os resultados demostram que o modelo foi capaz de representar as variações temporais (diária, mensal, sazonal, inter-anual) na dinâmica dos níveis da água na Lagoa Mirim, incluindo os períodos máximos, mínimos, anos secos e chuvosos. Além, os resultados da validação dos níveis da água simulados usando dados altimétricos do ICESat, tiveram melhor acurácia ($R^2 \geq 0.66$; RMSE ≤ 29 cm), quando comparados com os do ENVISAT. Embora os níveis da água obtidos a

partir do ENVISAT apresentaram baixa acurácia ($R^2 \geq 0.005$; RMSE $\leq$ 92cm), a tendência e o comportamento sazonal foi bem representada. Esta abordagem pode ser usada para o monitoramento nos níveis da água em lagos e reservatórios, na calibração/validação de modelos hidrodinâmicos ou como fonte alternativa de dados altimétricos.

Qual é a influência das forçantes hidrológicas (descarga pluvial), forçantes externas (vento) e estressores antrópicos (retiradas de água) no comportamento hidrodinâmico da Lagoa Mirim?

O acoplamento da modelagem hidrológica/hidrodinâmica também permitiu analisar o efeito das descargas pluviais, o vento e as retiradas de água no sistema. Os resultados indicaram que durante o período 2000 - 2010, os principais processos hidrodinâmicos são controlados em escala sazonal (meses) pelas descargas pluviais dos principais rios afluentes na lagoa (*e.g.*, Rio Cebollati), e em menor escala (dias) pela influência do vento no sistema (intensidade e direção). Além, foi observado que o stress provocado pelo vento, têm um efeito significativo no comportamento dos principais componentes hidrodinâmicos (*e.g.*, campos de velocidade e níveis da água) na lagoa. Adicionalmente, os níveis da água simulados na lagoa evidenciaram uma queda significativa devido as retiradas de água para irrigação. Por tanto, esta abordagem permitiu estudar em longo prazo os efeitos das descargas pluviais, as retiradas de água e a influência do vento no comportamento hidrodinâmico da lagoa.

Como é a dinâmica da temperatura da superfície d'água e os fluxos de calor da Lagoa Mirim? Será que eventos meteorológicos de pequena escala (e.g. passagem de frentes frias) poderiam influenciar a dinâmica da temperatura da água e os fluxos de calor?

As variações na dinâmica espacial e temporal da temperatura da superfície da água e os fluxos de calor no período 2001-2010 na Lagoa Mirim, foram estudadas a partir da integração entre medições *in situ*, a temperatura superficial da água derivada do produto MODIS LST e o acoplamento do modelo MGB-IPH com o modelo IPH-ECO. Além disso, foi analisado o efeito da passagem de sistemas frontais (*e.g.*, frentes frias) sobre a temperatura superficial da água e os fluxos de calor nesse ecossistema. A sinergia entre essas abordagens, permitiu representar a dinâmica da temperatura superficial da água da Lagoa Mirim e suas variações espaciais e temporais (diurna, mensal, sazonal e inter-anual), incluindo os valores máximos e mínimos. Os resultados mostraram que a temperatura superficial da água simulada foi consistente com a derivada do produto MODIS LST e medições *in-situ*. As simulações permitiram evidenciar distintas regiões térmicas da lagoa, como a região litorânea com temperaturas mais elevadas e a região pelágica com temperaturas mais baixas. Quanto aos fluxos de calor, os resultados mostraram que as perdas de calor na Lagoa

Mirim, foram principalmente ocasionadas por evaporação e saturação atmosférica (calor latente). Ao mesmo tempo, foi evidenciado que a passagem de frentes frias sobre o ecossistema, causa fortes distúrbios na dinâmica da temperatura superficial da água e nos fluxos de calor.

É possível desenvolver modelos empíricos para estimar concentrações de clorofila-a em um lago raso subtropical através de técnicas de sensoriamento remoto?

Modelos empíricos para estimativa de clorofila-*a* em um lago raso subtropical, utilizando a combinação de bandas espectrais do sensor MODIS foram desenvolvidos. Abordagens baseadas em análise de regressão linear múltipla (MLR), redes neurais artificiais (ANN) e regressão multiplicativa não paramétrica (NPMR) foram desenvolvidas e testadas utilizando medições *in-situ* de Clorofila-*a*. Também foram testados quatro modelos empíricos (Appel, Kahru, FAI e O14a) comumente utilizados em ecossistemas aquáticos. Os resultados mostraram que os modelos baseados em análise de regressão linear múltipla (MLR) apresentaram melhor *performance* (*e.g.*, poucas variáveis de entrada) quando comparados com modelos ANN, NPMR e os quatro modelos empíricos testados (Appel, Kahru, FAI and O14a). Além disso, foi observado que em um lago raso subtropical meso-oligotrófico submetido a regime de vento intenso, o modelo MLR desenvolvido utilizando um ponto específico, teve melhor desempenho que usando o total de pontos, indicando que não seria apropriado generalizar um único modelo para estimar Chl-*a* nesse ecossistema. Nesse sentido, os resultados permitiram corroborar a heterogeneidade espacial da distribuição de Chl-*a* na lagoa e as diferenças entre regiões (Norte, Centro e Sul).

Esta pesquisa apresentou uma primeira tentativa para simular o complexo sistema bacia hidrográfica - lagoa como un todo, permitindo uma melhor compreensão da hidrologia da bacia, os principais fatores que controlam a hidrodinâmica e a estrutura e funcionamento ecossistêmico da lagoa. A abordagem proposta nesta tese mostra como é possível integrar modelos hidrológicos/hidrodinâmicos de grande escala baseados em processos para a compreensão do funcionamento hidrológico de grandes bacias e comportamento hidrodinâmico de lagos rasos de grande porte, respondendo a questões cientificas sobre estes sistemas e não servindo somente como ferramentas de suporte em projetos de engenharia como tradicionalmente empregados.

Desta forma, os resultados obtidos, em conjunto com outras pesquisas recentes, apontam para diversas perspectivas de pesquisa e futuros estudos que envolvam a compreensão e previsão da hidrologia de grandes bacias hidrográficas, processos físicos/ecológicos em grandes lagos rasos, integrando novas técnicas de monitoramento de parâmetros de qualidade de água através de sensoriamento remoto, simulação de

cenários de mudança climática e o potencial uso na gestão integrada dos recursos hídricos.

APÊNDICE **A**

Modelo MGB-IPH

A.1 Apresentação

O modelo MGB-IPH ("Modelo Hidrológico de Grandes Bacias") é um modelo de grande escala desenvolvido por Collischonn et al. (2007). O MGB-IPH é similar com outros modelos de grande escala tais como LARSIM (Ludwig and Bremicker, 2006) e VIC (Liang et al., 1994; Nijssen et al., 1997). Estes modelos são baseados em processos que utilizam equações físicas e conceituais para simular o ciclo hidrológico terrestre: balanço de água no solo, balanço de energia e evapotranspiração, interceptação, geração de fluxo superficial, sub-superficial e subterrâneo nos elementos de discretização da bacia hidrográfica; e propagação de vazão na rede de drenagem.

O MGB-IPH tem sido aplicado em diferentes bacias da América do Sul (Collischonn et al., 2005; de Paiva et al., 2013; Tucci et al., 2003). No Brasil foi aplicado nas bacias dos rio Taquari-Antas (RS), com 26.000 km^2, rio Uruguai (75.000 km^2) (Collischonn et al., 2007), no Alto Paraguai (140.000 km^2) (Allasia et al., 2004) e no rio São Francisco (640.000 km^2) (Da Silva et al., 2007; Fan et al., 2014).

A.2 Discretização do modelo, Unidades de Resposta Hidrológica HRU e balanço de água e energia

O MGB-IPH adota uma discretização da bacia hidrográfica em unidades regulares, a partir do Modelo Digital de Elevação MDE denominadas minibacias. Além disso as minibacias que compõem a bacia hidrográfica são subdivididas em Unidades de Resposta Hidrológicas (*Hydrological Response Unit*), que são áreas com comportamento hidrológico similar definidas por uma combinação de mapas de cobertura da terra e de tipo do solo (Kouwen et al., 1993). Em cada minibacia as características de uso de solo, cobertura vegetal e tipo de solo são sintetizadas nas URH. Em cada URH das minibacias são determinados os volumes de escoamentos superficial, sub-superficial (ou interno)

e subterrâneo (Fig. 1a). Dessa forma, o balanço hidrológico é calculado para cada URH em cada minibacia e as vazões estimadas em cada URH são posteriormente somadas e propagadas até a rede de drenagem (Fig. 1b).

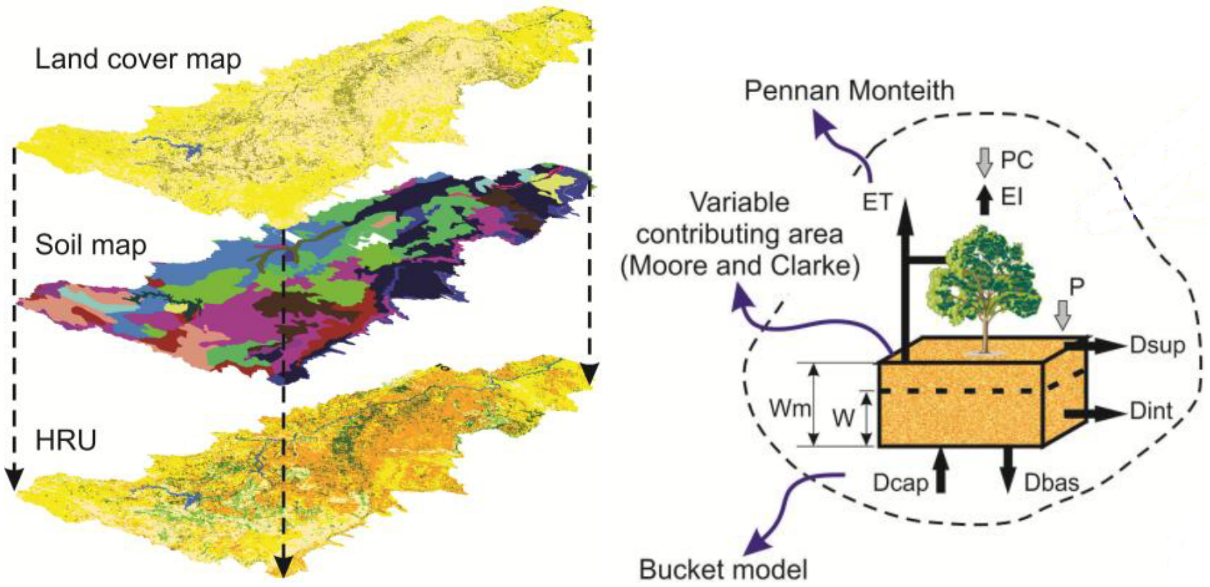

(a) (b)

Figura 1 – **(a)** Representação esquemática da combinação do mapa de cobertura da terra e mapa de solo para geração de Unidades de Resposta Hidrológica (HRU) e **(b)** Balanço de água e energia para uma Unidade de Resposta Hidrológica. Modificado de Collischonn and Tucci (2001).

No modelo MGB-IPH evapotranspiração é estimada pelo método de Penman - Monteith (Monteith, 1965; Shuttleworth, 1993). Já o balanço da água no solo é computado considerando somente uma camada de solo, o qual é descrito da seguinte forma:

$$\frac{dW}{dt} = P - ET - Dsup - Dint - Dbas \tag{3}$$

Onde W [mm] é o armazenamento de água na camada do solo, P [mm. Δt^{-1}] é a precipitação que atinge o solo, ET [mm. Δt^{-1}] é a evapotranspiração a partir do solo, Dsup [mm. Δt^{-1}] é a o fluxo superficial, [mm. Δt^{-1}] é o fluxo sub-superficial e Dbas [mm. Δt^{-1}] é a percolação para o reservatório subterrâneo. A precipitação (PC) é assumida como a precipitação armazenada na superfície da vegetação até atingir a máxima capacidade de interceptação, o qual é determinado para cada Unidade de Resposta Hidrológica baseado no Índice de Área foliar IAF.

A infiltração e o escoamento superficial *Dsup* é baseado no conceito de área de contribuição variável do modelo ARNO (Todini, 1996). O escoamento subsuperficial *Dint* é calculado usando a abordagem proposta por Rawls et al. (1992). A percolação para as camadas do solo *Dbas* é calculada usando uma relação linear simples

entre a capacidade de armazenamento de água no solo e a máxima capacidade de armazenamento.

A.3 Propagação de vazões na rede de drenagem

A propagação de vazão é realizada em duas etapas. Em primeiro lugar é realizada a propagação de vazão no interior da minibacia, utilizando-se modelos de reservatórios lineares simples. Cada minibacia tem três reservatórios lineares que representam a propagação dos escoamentos superficial, subsuperficial e subterrâneo. A vazão de saída dos três reservatórios é somada e propagada pela rede de drenagem utilizando o método Muskingum-Cunge. Nas minibacias de cabeceira, aquelas que não possuem escoamento vindo de montante, o modelo não realiza a propagação de vazão nos trechos de rios correspondentes, mas considera que toda vazão saindo dos reservatórios lineares das minibacias é destinada diretamente ao exutório da mesma. Apenas nas minibacias internas, aquelas que recebem contribuição de montante, é realizada a propagação de vazão em seus respectivos trechos de rio (Fig. 2).

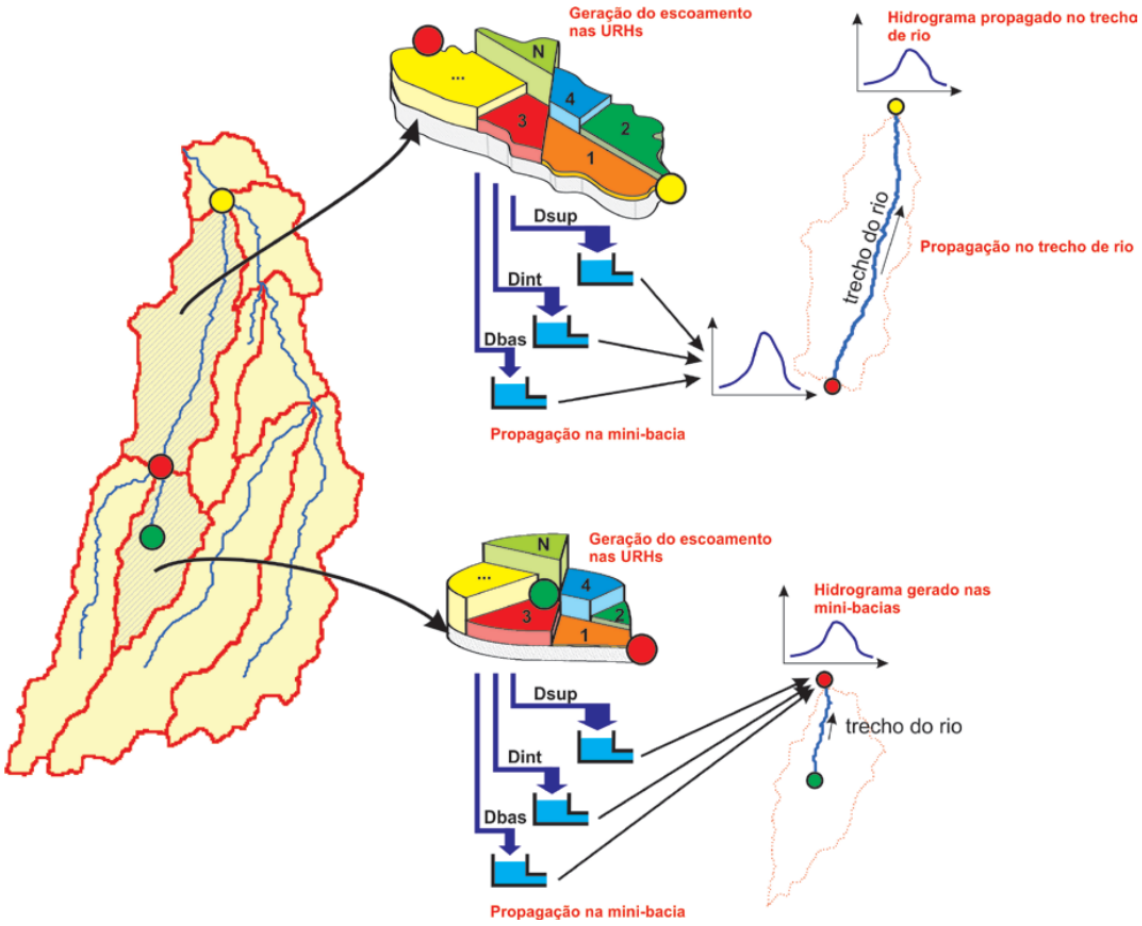

Figura 2 – Representação esquemática dos processos de geração e propagação de escoamentos nas minibacias e propagação de vazão na rede de drenagem. Tomado de Buarque (2015).

No modelo MGB-IPH, para cada trecho de rio são consideradas diversas seções de cálculo, as quais são definidas discretizando o trecho em sub-trechos de acordo com critérios de precisão numérica, de forma que os hidrogramas de saída podem ser avaliados tanto no exutório de cada minibacia (fim do sub-trecho mais de jusante do trecho) como em cada uma dessas seções. Para uma melhor precisão no tempo de viagem e no amortecimento do hidrograma, além da sub-divisão dos trechos de rios, o passo de tempo diário também é sub-divido pelo modelo em intervalos menores durante a propagação (Tucci, 2005).

APÊNDICE **B**

Simulação Hidrológica na Bacia do rio Piratini, RS-Brasil

Este apêndice é baseado no trabalho publicado em anais de: *Congreso Latinoamericano. XII de Hidrogeología - XXVI de Hidráulica. Santiago de Chile, 2014.*
Título: Simulação Hidrológica na Bacia do rio Piratini, RS-Brasil, a partir de dados de chuva observada e dados de chuva derivados do produto MERGE

Andrés Mauricio Munar, David da Motta-Marques, Carlos Ruberto Fragoso Jr. e Walter Collischonn

B.1 Resumo

A complexidade dos diferentes processos do ciclo hidrológico pode ser representada através da modelagem hidrológica, sendo os modelos que simulam o processo de transformação da chuva em vazão os mais utilizados. Estes modelos dependem de uma serie de variáveis de entrada, na qual a precipitação é a variável mais importante. Este trabalho apresenta uma avaliação do Modelo de Grandes Bacias MGB-IPH na bacia do rio Piratini, um dos principais afluentes da Lagoa Mirim, usando bases de dados de postos pluviométricos disponíveis na região e dados da chuva derivados do produto MERGE (combinação chuva observada e chuva estimada por satélite TRMM). Apesar que o modelo MGB-IPH é um modelo distribuído desenvolvido para bacias maiores que 10.000 Km^2, os resultados obtidos são promissores em uma bacia menor (5549 Km^2). O modelo representa satisfatoriamente o processo de transformação chuva-vazão na bacia do rio Piratini para os dados da chuva considerados, obtendo ligeiramente melhores resultados nos critérios de avaliação (coeficiente de Nash e erro de volume) quando foram usados dados de chuva observada.

Palavras-chave: Bacia Hidrográfica, Modelo Hidrológico, MGB-IPH, MERGE

B.2 Introdução

Os modelos hidrológicos que simulam a transformação da chuva em vazão são ferramentas que representam, de forma simplificada, os diversos processos do ciclo hidrológico que interagem numa bacia hidrográfica (Tucci et al., 1998). A modelagem hidrológica, tem se tornado em uma ferramenta bastante utilizada na predição de fluxos ao interior de sistemas hidrológicos, permitindo avaliar processos e fenômenos associados ao fluxos de água.

Nos últimos anos, modelos empíricos tem sido usados em pequenas áreas devido à sua característica concentrada. No entanto, esses modelos são baseados principalmente na análise de observações, usando parâmetros com pouco significado físico, surgindo limitações na hora de representar todos os processos, ignorando a heterogeneidade as características da bacia e fornecendo resultados pouco detalhados (Merritt et al., 2003). Recentemente, modelos conceituais e distribuídos vem sendo usados com sucesso, uma vez que levam em conta os processos físicos e a heterogeneidade espacial, fornecendo resultados mais detalhados. Embora, diante da complexidade desses modelos, existem limitações relacionadas com a pouca disponibilidade de dados, especialmente em grandes bacias hidrográficas, onde o monitoramento é escasso e cujas características físicas, do solo, e da cobertura vegetal geralmente estão disponíveis apenas em escala global (Patro et al., 2009).

Nos modelos hidrológicos, a precipitação é a variável de entrada mais importante (Collischonn et al., 2005). Esta variável normalmente é medida com pluviômetros, o que corresponde a uma estimativa pontual. No entanto, em regiões com monitoramento escasso e baixa densidade de postos pluviométricos, a estimativa de chuva baseada em satélites vem sendo usada com sucesso, sendo uma importante fonte de dados adicionais. A estimativa de chuva por satélite está baseada na medição da radiação emitida ou refletida pela atmosfera, detectada pelos sensores a bordo dos satélites. Diversos produtos de chuva por satélite são disponibilizados por várias agências meteorológicas de diversos países, destacando-se: O Climate Prediction Center Morphing Technique Product (Joyce et al., 2004), Tropical Rainfall Measuring Mission (Huffman et al., 2007) e Remotely Sensed Information using Artificial Neural Networks (Hong, 2003). A utilização dos produtos de estimativa de precipitação proveniente do satélite Tropical Rainfall Measuring Mission (TRMM) tem sido amplamente utilizada para avaliar resultados de modelos numéricos (Rozante and Cavalcanti, 2008; Rozante et al., 2010), como dado de entrada para modelos hidrológicos (Collischonn et al., 2008; Quiroz and Collischonn, 2015), ou na calibração/validação desses modelos (Buarque et al., 2011; Paiva et al., 2011). Embora os produtos do TRMM sejam extremamente úteis para validação de modelos numéricos, alguns erros sistemáticos são verificados, principalmente na faixa leste do nordeste do Brasil (subestimativas associadas às

nuvens quentes e divisas entre a Argentina, Paraguai e sul do Brasil (Rozante and Cavalcanti, 2008). O produto MERGE surgiu de uma técnica que visa combinar os dados do satélite TRMM com os dados de observação de superfície (Surface Synoptic Observations - SYNOP) sobre o continente da América do Sul (Rozante and Cavalcanti, 2008).

Este trabalho, objetivou a avaliação do desempenho de um modelo hidrológico de grande escala, aplicado em uma bacia hidrográfica pequena (5549 Km^2) usando as bases de dados de postos pluviométricos disponíveis na região e a base de dados de chuva derivados do produto MERGE.

B.3 Materiais e Métodos

B.3.1 Área de estudo

A bacia hidrográfica do rio Piratini tem uma área de 5.549 Km^2 e está localizada na região sul do estado do Rio Grande do Sul, Brasil ao norte da bacia da Lagoa Mirim, entre as coordenadas geográficas 31º 00′ a 32º 10′ de latitude Sul e 52º 10′ a 53º 50′ Oeste (Fig. 1). As elevações variam entre 0 e 501 m.s.n.m.

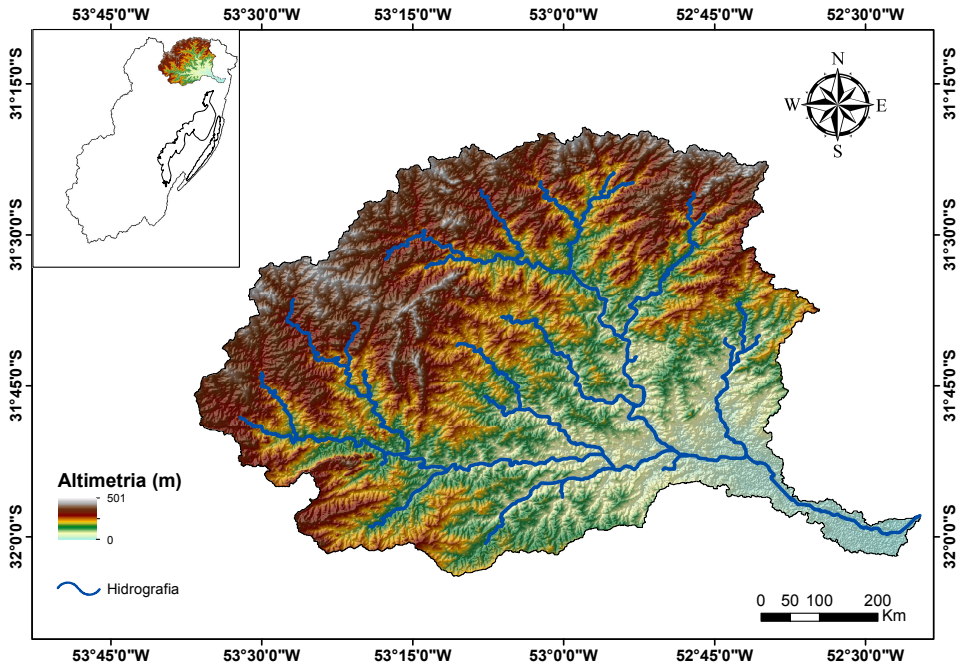

Figura 1 – Bacia do rio Piratini, que faz parte da bacia hidrográfica da Lagoa Mirim. Relevo do STRM DEM

A bacia foi escolhida porque é uma das mais importantes subacias da grande bacia da Lagoa Mirim, principal bacia objeto de estudo da tese. Além, a bacia do rio Piratini, apresenta áreas com monitoramento com baixa densidade de postos pluviométricos por Km^2, no qual o produto MERGE poderia ser testado.

B.3.2 Modelo Hidrológico

O Modelo Hidrológico de Grandes Bacias (MGB-IPH) foi desenvolvido no Instituto de Pesquisas Hidráulicas da Universidade Federal do Rio Grande do Sul (Collischonn et al., 2007). O MGB-IPH é distribuído por minibacias e realiza simulações em nível diário ou horário. Cada minibacia é dividida em blocos de acordo com características como tipo de solo e cobertura vegetal. Cada bloco equivale a uma área hidrológicamente homogênea, denominada Unidade de Resposta Hidrológia URH, ou seja, áreas em que se verifica um comportamento hidrológico semelhante.

Para o cálculo da evapotranspiração potencial por meio do método de Penman-Monteith, o modelo utiliza cinco variáveis climatológicas: temperatura do ar, pressão de vapor, velocidade do vento, radiação líquida e pressão atmosférica. Esta formulação tem uma forte base física, o que permite representar as alterações de evapotranspiração associadas às mudanças de uso do solo, embora para isso sejam necessários dados específicos para cada tipo de vegetação, que não estão normalmente disponíveis (Collischonn et al., 2005). A propagação do escoamento é realizada utilizando o método de Muskingum-Cunge (MC).

O MGB-IPH tem sido aplicado nas bacias dos rio Taquari-Antas (RS), com 26.000 Km^2, e na bacia do rio Uruguai (75.000 Km^2) (Collischonn et al., 2007) . Outras aplicações foram realizadas no Alto Paraguai (140.000 Km^2) (Allasia et al., 2004) e no rio São Francisco (640.000 Km^2) (Da Silva et al., 2007). A preparação de dados e a calibração do modelo seguiram a metodologia adotada nesses trabalhos.

B.3.3 Disponibilidade dos dados

Os dados da precipitação diária sobre a bacia foram obtidos junto ao banco de dados Hidroweb da *Agencia Nacional de Águas* (ANA). Os dados da chuva do produto MERGE foram descarregados da plataforma do *Instituto Nacional de Pesquisas Espaciais* (INPE), e estão disponíveis em pontos de grade. Neste sentido, os dados foram convertidos para pontos de observações nas coordenadas das estações virtuais utilizando uma interpolação destes com as minibacias a serem processadas com MGB-IPH. Foram usados dados de nove postos pluviométricos, com menos de 30% de falhas nas séries temporais, além de dados de duas estações fluviométricas presentes na bacia (Tabela 1).

Tabela 1 – Pontos de controle: estações fluviométricas e exutório da bacia do Rio Piratini

Código	Nome	Rio	Área de drenagem (Km^2)
88575000	Cerro Chato	Arroio Basílio	1050
88641000	Pedro Osório	Rio Piratini	4700
Exutório	Foz Piratini	Rio Piratini	5549

Para a bacia do rio Piratini, dados de normais climatológicas de outras variáveis (temperatura, insolação, velocidade do vento e umidade relativa do ar) foram obtidos de duas estações climatológicas. Na Figura 2 se apresenta a distribuição espacial dos postos pluviométricos, fluviométricos e climatológicos na bacia do Piratini.

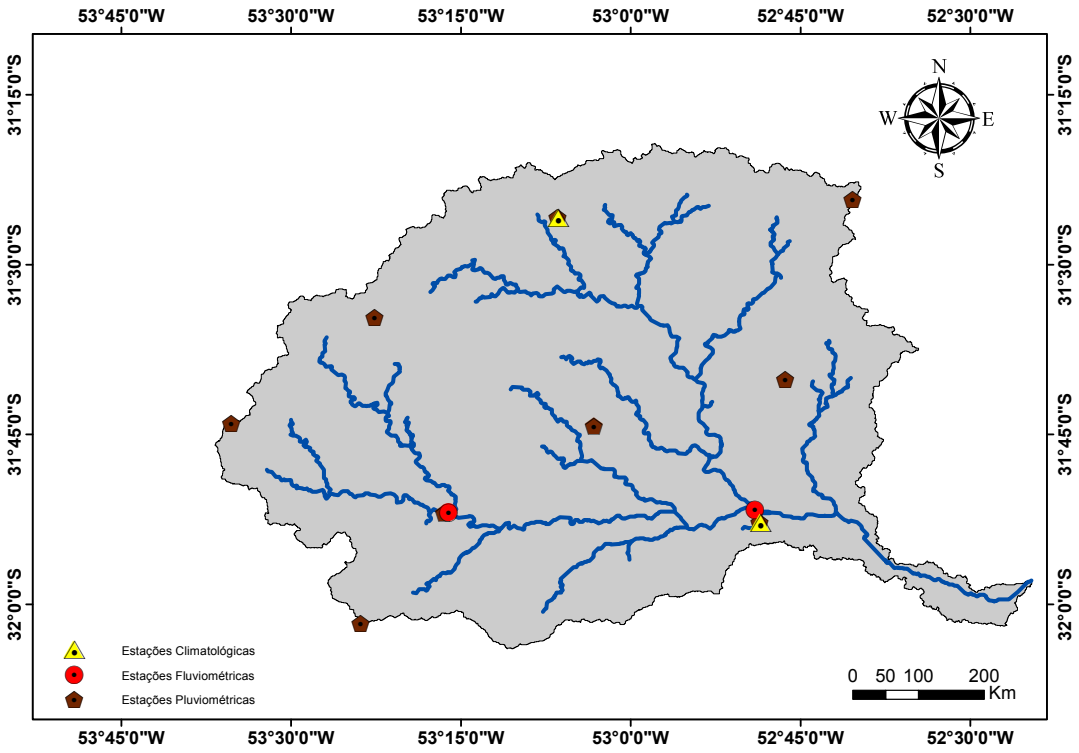

Figura 2 – Localização dos pontos de controle na bacia do rio Piratini

Os mapas de uso de solo e cobertura vegetal foram adquiridos desde a *Empresa Brasileira de Pesquisa Agropecuária* (IBGE-EMBRAPA) e o *Ministério do Meio Ambiente* (MMA).

B.3.4 Processamento dos dados

O trabalho de pré-processamento dos dados foi baseado no uso de ferramentas como geoprocessamento e programas computacionais para a construção dos arquivos de entrada do modelo. O pré-processamento das informações contidas nos mapas (em formato ráster) consistidos nas etapas anteriores, a saber, modelo digital de elevação (sem depressões), direção fluxo, rede de drenagem, mini-bacias, unidades de resposta hidrológicas e sub-bacias foi realizado utilizando as ferramentas *ArcHydro tools* do software ESRI ArcGIS® 10 . A discretização da bacia em células foi utilizada na determinação das direções de fluxo, cálculo da área de drenagem acumulada, delimitação das sub-bacias de acordo com as estações fluviométricas e definição da rede drenagem.

B.3.5 Parametrização e simplificações do modelo

Para a interpolação espacial da precipitação e interpolação temporal das variáveis climatológicas, no modelo MGB-IPH foi necessário interpolar os dados de chuva dos postos pluviométricos da ANA para a posição dos centróides das mini-bacias. Na bacia do rio Piratini, depois de ser observada a disponibilidade temporal dos dados, optou-se por realizar a simulação no período de 2000 a 2006. Para os dados do MERGE, foi realizada a interpolação dos dados da chuva no mesmo período a través da ferramenta Interplu MERGE. Com relação as variáveis climatológicas, foram gerados os dados de clima diários e os dados de clima médios mensais, no mesmo período simulado.

Cada conjunto de dados de precipitação (chuva observada e chuva derivada do MERGE) foi simulado independentemente no modelo MGB. Para a calibração, utilizou-se o período de dados de jan/2000 a dez/2006. Na verificação da modelagem, utilizou-se o período de jan/2011 a out/2013. Os valores dos parâmetros foram atribuídos para cada bloco de tipo de solo e cobertura vegetal. Na aplicação do modelo MGB-IPH foi usado um passo de tempo diário, conforme aos dados de precipitação observada (postos ANA) e dados de chuva derivados do produto MERGE, vazão e dados climatológicos disponíveis neste intervalo.

B.4 Resultados

B.4.1 Discretização da bacia hidrográfica e Unidades de Resposta Hidrológica URH

A bacia do Piratini foi discretizada espacialmente em 53 mini-bacias e três sub-bacias tendo em conta os dois postos fluviométricos da ANA presentes na bacia e a foz do rio (Fig. 3).

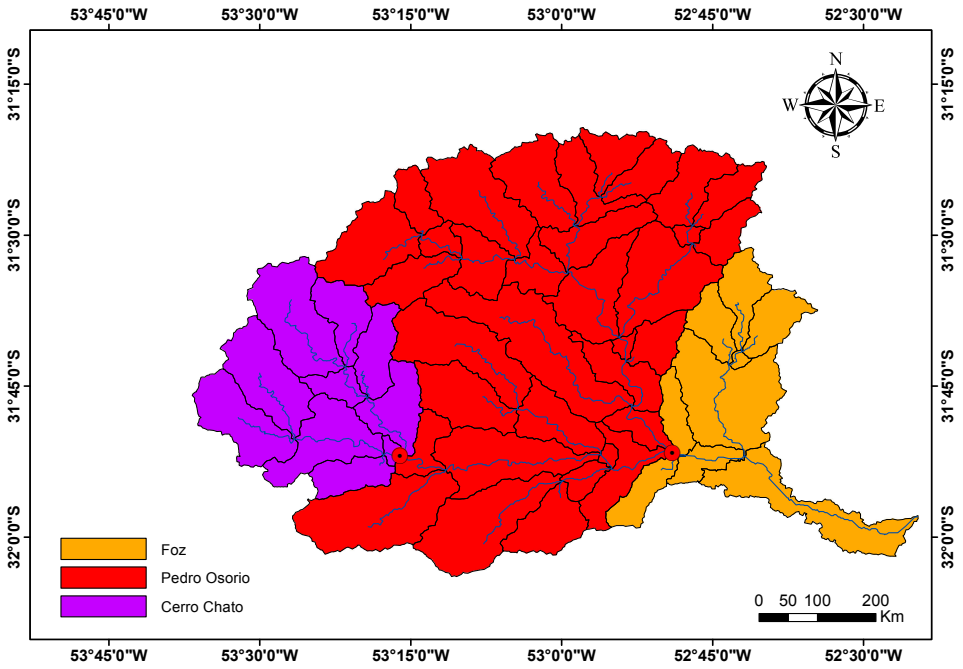

Figura 3 – Sub-bacias e mini-bacias do rio Piratini

Foram definidas seis Unidades de Resposta Hidrológica (URH) (Fig. 4), sendo as matas em solos profundos a maior URH representando mais do que 53% da área da bacia (Tabela 2).

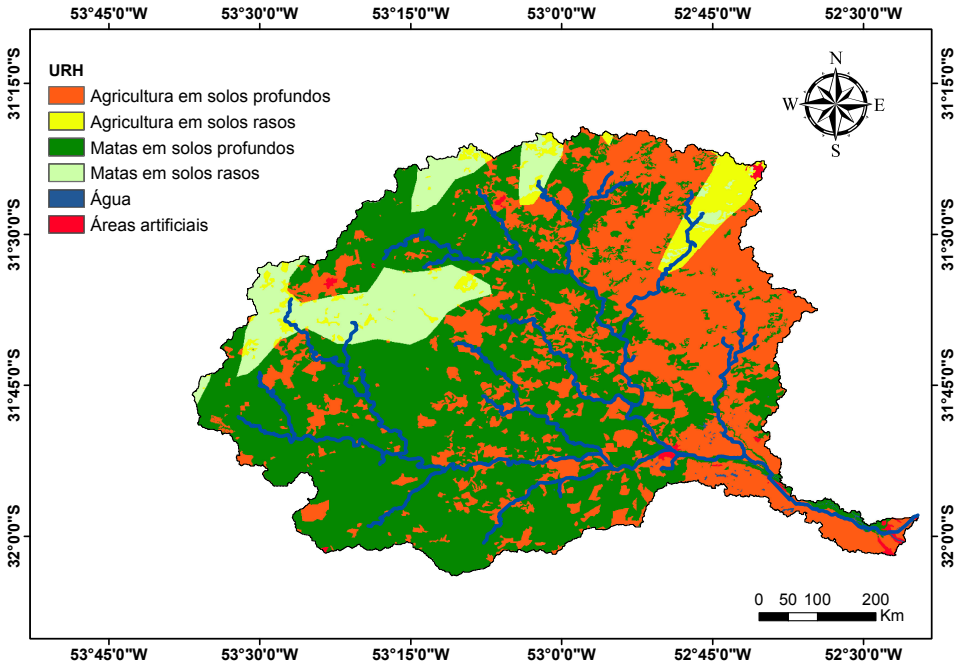

Figura 4 – Unidades de Resposta Hidrológica URH definidas para na bacia do Piratini.

Tabela 2 – Classificação da bacia hidrográfica do rio Piratini em Unidades de Resposta Hidrológica

Id	URH	Área %
1	Matas em solos profundos	53.62
2	Matas em solos rasos	8.52
3	Agricultura em solos profundos	33.63
4	Agricultura em solos rasos	3.40
5	Áreas artificiais	0.46
6	Água	0.37

B.4.2 Calibração dos parâmetros

Os resultados das simulações para a calibração do modelo são mostrados nas Figuras 5 e 6, que correspondem aos hidrogramas das estações Cerro Chato e Pedro Osório respectivamente. Na figura 7 saõ apresentados os resultados das curvas de permanência da estação Cerro Chato (a) e Pedro Osório (b).

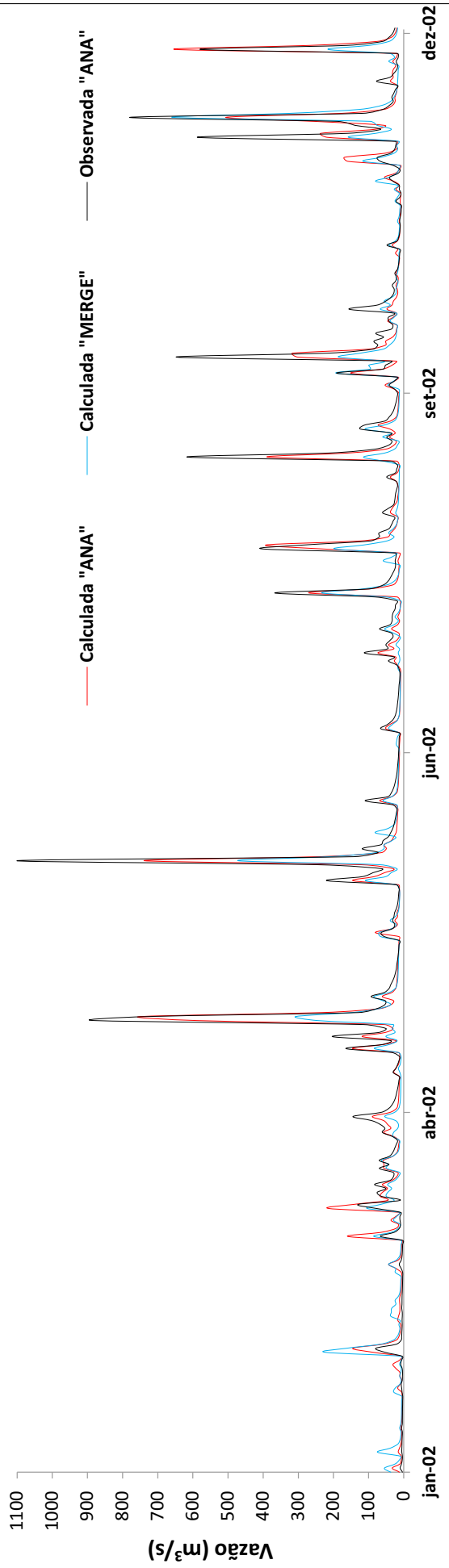

Figura 5 – Comparação de hidrogramas na estação Cerro Chato

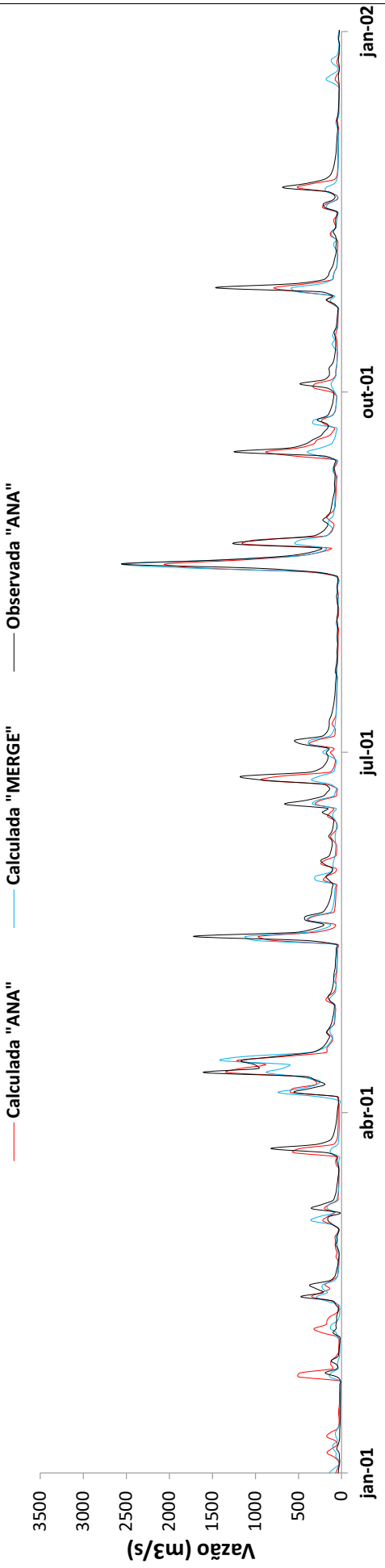

Figura 6 – Comparação de hidrogramas na estação Pedro Osorio

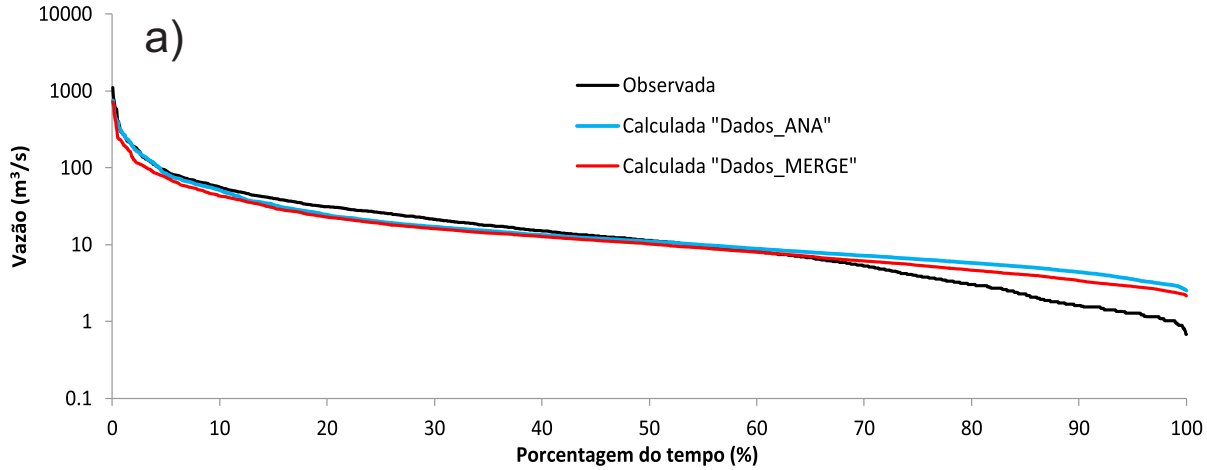

(a)

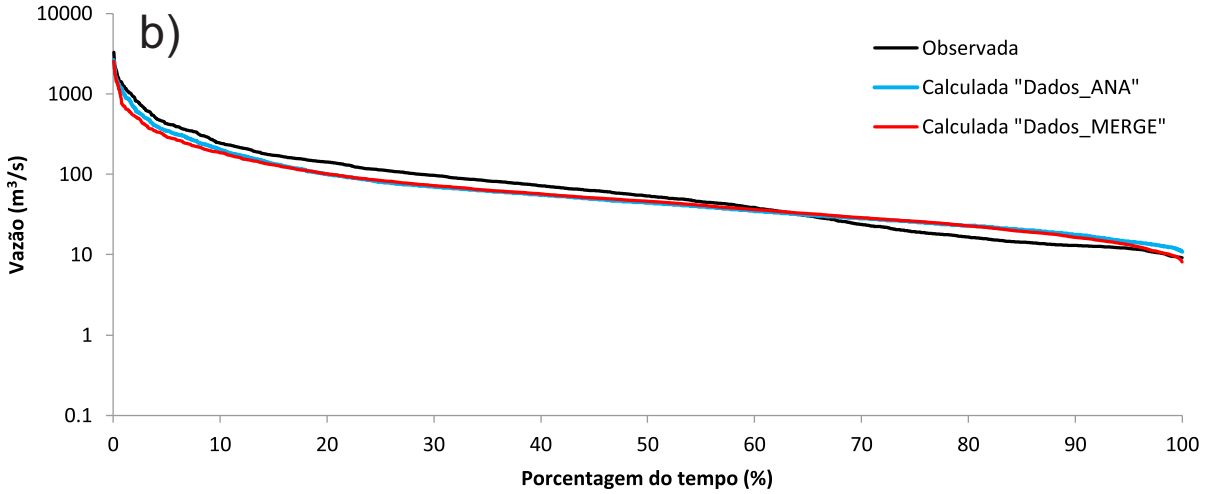

(b)

Figura 7 – Comparação de curvas de permanência nas estações Cerro Chato **(a)** e Pedro Osorio **(b)**

A Tabela 3 apresenta os valores de dois critérios utilizados na avaliação das simulações: coeficiente de Nash (*NS*) e o erro de volume (ΔV em %).

Tabela 3 – Valores dos critérios de avaliação da calibração

3***Sub-bacia**	3***Área de drenagem (Km²)**	**Calibração**				**Validação**			
		Cal. ANA		**Cal. MERGE**		**Cal. ANA**		**Cal. MERGE**	
		NS	ΔV %	*NS*	ΔV %	*NS*	ΔV %	*NS*	ΔV %
Cerro Chato	1050	0.75	-0.186	0.52	-17.22	0.64	14.7	0.51	-38.2
Pedro Osório	4700	0.85	-9.29	0.65	-16.61	0.76	19.85	0.56	-32.5

$$R^2 = 1 - \frac{\sum_{i=1}^{n}(Q_{obs,i} - Q_{cal,i})^2}{\sum_{i=1}^{n}(Q_{obs,i} - \bar{Q}_{obs})^2} \quad (4) \qquad \Delta V = \frac{\sum_{i=1}^{n}(Q_{cal,i} - Q_{obs,i})^2}{\sum_{i=1}^{n} Q_{obs,i}} \quad (5)$$

onde $Q_{obs,i}$ é a vazão observada e $Q_{cal,i}$ é a vazão calculada pelo modelo no tempo i respectivamente.

B.5 Discussão

Os resultados das simulações indicaram que o MGB-IPH representou satisfatoriamente o processo de transformação chuva-vazão na bacia do rio Piratini, usando as bases de dados de chuva observada (dados ANA) e dados de chuva derivados do produto MERGE. Os valores dos critérios apresentados na Tabela 3 mostraram que para as duas sub-bacias (Cerro Chato e Pedro Osório), os hidrogramas observados tiveram bom ajuste com os hidrogramas estimados no MGH-IPH (Figuras 5 e 6), obtendo melhores resultados nos valores dos critérios de avaliação, quando foram usados dados de chuva observada.

Na sub-bacia do Pedro Osório, se obtiveram os melhores resultados na calibração do modelo. Alguns picos de vazão estão bem representados usando dados de chuva observada, em outros, o hidrograma estimado a partir de dados do MERGE mostrou algumas subestimativas. Deve-se destacar, entretanto, que houve uma leve tendência de subestimar vazões máximas e superestimar vazões mínimas a partir do modelo para os diferentes dados de chuva usados (Figura 7a e 7b). Um indicador de subestimação das vazões calculadas é o valor negativo do erro de volume (ΔV), principalmente, quando foram usados dados do produto MERGE.

A superestimativa das vazões mínimas foi maior para a sub-bacia do Cerro Chato (Figura 5a), sendo ligeiramente maior quando foram usados dados da chuva observada. Este comportamento pode ser causado possivelmente a heterogeneidade dos solos nessa sub-bacia.

Os resultados obtidos no modelo destacam que para as duas sub-bacias, o hidrograma observado teve bom ajuste ao hidrograma calculado para os dados da chuva considerados, obtendo melhores resultados quando foram usados dados de chuva observada. Um indicador poder ser o número razoável de postos pluviométricos na bacia. Áreas com alta densidade de observações, o desempenho do produto MERGE é equivalente ao de simplesmente uma média das estações do grade. No entanto, em áreas com observações muito espalhadas, MERGE mostra resultados superiores (Rozante et al., 2010).

B.6 Conclusões

O modelo MGB-IPH, apesar de ser um modelo hidrológico distribuído desenvolvido para bacias maiores que 10.000 Km^2, demonstrou ser capaz de representar

satisfatoriamente o regime hidrológico em uma bacia hidrográfica de pequena escala (5548 Km^2), representando razoavelmente o processo de transformação chuva-vazão.

Em áreas com escassez de dados, a estimativa de precipitação por satélite através do produto MERGE, se torna uma fonte de dados alternativa em modelos hidrológicos, podendo ser usada como *input data*, calibração/validação ou para encontrar fontes de erro.

De maneira geral e considerando os resultados obtidos nos testes de simulação e verificação para os dados de chuva considerados, pode-se afirmar que o modelo permite avaliar resultados e estimar vazões mínimas, médias e máximas de maneira consistente, na bacia hidrográfica do rio Piratini. Além disso, os resultados obtidos já permitem a realização de estudos como a análise dos processos hidrológicos, quantificação da disponibilidade hídrica em sub-bacias e avaliação das consequências de mudanças na cobertura e uso do solo sobre o escoamento na bacia.

Agradecimentos

Os autores agradecem a Coordenação de Aperfeiçoamento de Pessoal de Nivel Superior (CAPES) pelo auxílio em forma de bolsa de doutorado concedida ao primeiro autor.

APÊNDICE C

Modelo IPH-ECO

C.1 Apresentação

O modelo computacional IPH-ECO (Fragoso et al., 2009a, 2008, 2011, 2009b) é um modelo hidrodinâmico e de qualidade da água tridimensional para ecossistemas aquáticos continetais, tais como lagos, reservatórios e estuários, capaz de simular de forma dinâmica, os processos físicos, químicos e biológicos. O modelo vem sendo desenvolvido pelo Grupo de Pesquisa em Ecotecnologia, do Instituto de Pesquisas Hidráulicas da Universidade Federal do Rio Grande do Sul (GPE-IPH/UFRGS)(`http://ipheco.org/`), consistindo em diversas equações diferenciais parciais sendo dividido em dois módulos principais: (a) um módulo hidrodinâmico detalhado, descrevendo fluxos quantitativos (e.g., padrões de circulação, campos de velocidade) e níveis de água; e (b) um módulo de qualidade da água, que lida com o mecanismos de transporte de nutrientes e todas as interações entre a cadeia trófica aquática. As equações diferenciais do módulo hidrodinâmico são solucionadas numericamente aplicando um esquema semi-implícito de diferenças finitas em domínios estruturados (Casulli and Cheng, 1992) ou não-estruturados (Casulli and Walters, 2000). As equações diferenciais para o transporte de substâncias é solucionada com um esquema conservativo baseado em volumes finitos, com os termos fontes nestas equações (e.g., processos capazes de gerar/consumir substâncias) baseados em grande parte no modelo PC-Lake (Janse, 2005).

C.2 Capacidades do Modelo

O modelo IPH-ECO é capaz de simular escoamentos e variáveis de qualidade de água (e.g., nutrientes, biomassa de fitoplâncton) em domínios tri-dimensionais, sendo possível adaptar a resolução do modelo para aplicações bi-dimensionais, unidimensionais e modelos concentrados. É possível utilizar o modelo em diversas

áreas, como segue:

- ❑ Escoamentos derivados por maré, vento e fluviais;
- ❑ Escoamentos sobre estruturas hidráulicas (vertedores);
- ❑ Simulação de Estratificação em lagos, reservatórios e estuários;
- ❑ Entrada de sal em sistemas aquáticos;
- ❑ Simulação com diferentes temperaturas de água e entrada de esgotos;
- ❑ Avaliação de transporte de material dissolvido e poluentes;
- ❑ Transporte de sedimentos e morfologia;
- ❑ Simulação das interações na cadeia trófica aquática;

C.3 Modelo Hidrodinâmico

O módulo hidrodinâmico é baseado no fluxo tridimensional através das equações de Navier- Stokes, descrevendo o escoamento com superfície livre após ponderar sob escalas de tempo turbulentas (*Reynolds Averaged Navier-Stokes Equations*), gerando campos de velocidade nas direções transversal e longitudinal e valores do nível d'água em cada uma das células em cada intervalo de tempo de cálculo. Estas equações expressam os princípios físicos da conservação do volume, da massa e de quantidade de movimento (ou momento). As equações de quantidade de movimento para um fluido incompressível possuem a seguinte forma:

$$\frac{\partial u}{\partial t} + u\frac{\partial u}{\partial t} + v\frac{\partial u}{\partial t} + w\frac{\partial u}{\partial t} - fv = -g\frac{\partial p}{\partial x} + \nu^h\left(\frac{\partial^2 u}{\partial x^2} + \frac{\partial^2 u}{\partial y^2}\right) + \frac{\partial}{\partial z}\left(\nu^v\frac{\partial u}{\partial z}\right) \tag{6}$$

$$\frac{\partial v}{\partial t} + u\frac{\partial v}{\partial t} + v\frac{\partial v}{\partial t} + w\frac{\partial v}{\partial t} + fu = -g\frac{\partial p}{\partial y} + \nu^h\left(\frac{\partial^2 v}{\partial x^2} + \frac{\partial^2 v}{\partial y^2}\right) + \frac{\partial}{\partial z}\left(\nu^v\frac{\partial v}{\partial z}\right) \tag{7}$$

$$\frac{\partial w}{\partial t} + u\frac{\partial w}{\partial t} + v\frac{\partial w}{\partial t} + w\frac{\partial w}{\partial t} = -g\frac{\partial p}{\partial z} + \nu^h\left(\frac{\partial^2 w}{\partial x^2} + \frac{\partial^2 w}{\partial y^2}\right) + \frac{\partial}{\partial z}\left(\nu^v\frac{\partial w}{\partial z}\right) - \frac{\rho}{\rho_0}g \tag{8}$$

onde $u(x,y,z,t)$, $v(x,y,z,t)$ e $w(x,y,z,t)$ são as componentes do vetor velocidade nas direções X, Y e Z, respectivamente; t é o tempo; $p(x,y,z,t)$ é a pressão normalizada definida como a pressão dividida por uma densidade de referência constante ρ_0; f é o parâmetro de Coriolis; g é a aceleração da gravidade e ν^h e ν^v são os coeficientes de viscosidade turbulenta (*eddy viscosity*) na horizontal e vertical, respectivamente. Por último, ρ é a densidade da água e ρ_0 é a densidade de referência da água (constante).

As equações são resolvidas pelo método dos volumes finitos através de um esquema numérico Euleriano-Lagrangiano semi-implicito (Casulli, 1990; Casulli and Cattani, 1994; Casulli and Cheng, 1992; Casulli and Walters, 2000).

A conservação do volume é expressa a partir da condição de incompressibilidade:

$$\frac{\partial u}{\partial t} + \frac{\partial v}{\partial t} + \frac{\partial w}{\partial t} = 0 \tag{9}$$

Integrando a equação da continuidade (Eq. 9) ao longo da profundidade e assumindo uma condição cinemática na superfície obtemos a seguinte relação (Casulli and Cheng 1992):

$$\frac{\partial \eta}{\partial t} + \frac{\partial}{\partial x}\left[\int_{-h}^{\eta} u dz\right] + \frac{\partial}{\partial y}\left[\int_{-h}^{\eta} v dz\right] = 0 \tag{10}$$

onde $h(x, y)$ é a batimetria e $\eta(x, y, t)$ é a elevação da superfície livre. Desta forma, definimos $H(x, y, t) = h(x, y) + \eta(x, y, t)$ como a profundidade total da água (Fig. 8).

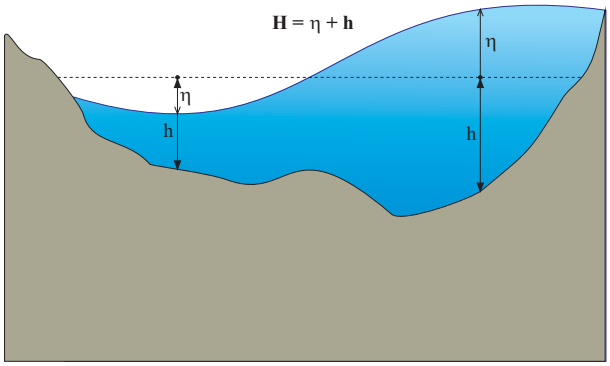

Figura 8 – Relação entre elevação da superfície livre η, batimetria h e profundidade total H. A batimetria é positiva num plano apontando para baixo, o contrário sendo adotado para a elevação da superfície livre. A elevação da superfície livre pode assumir valores positivos e negativos.

A conservação da massa de uma variável escalar é expressa pela seguinte forma diferencial:

$$\frac{\partial C}{\partial t} + \frac{\partial (uC)}{\partial x} + \frac{\partial (vC)}{\partial y} + \frac{\partial (wC)}{\partial z} = \frac{\partial}{\partial x}\left(K^h \frac{\partial C}{\partial x}\right) + \frac{\partial}{\partial y}\left(K^h \frac{\partial C}{\partial y}\right) + \frac{\partial}{\partial z}\left(K^v \frac{\partial C}{\partial z}\right) + S(C) \tag{11}$$

onde $C(x, y, z, t)$ denota a concentração de uma dada quantidade escalar sendo transportada (e.g., Salinidade, temperatura, sólidos suspensos, ou nutrientes); K^h e K^v são as difusividades horizontais e vertical, respectivamente; o termo $S(C)$ engloba os principais processos capazes de produzir ou consumir o escalar sendo transportado.

A equação de movimento leva em consideração forças de ação do vento, resistência do fundo e entradas de tributários. Além disso, a densidade da água é calculada por uma equação de estado em função da temperatura. Logo, correntes desencadeadas por diferenças na densidade da água podem ser capturadas pelo modelo

C.3.1 Transporte de Escalares

O transporte de substâncias escalares (e.g., temperatura, salinidade, biomassa) no modelo IPH-ECO é é realizado utilizando uma versão modificada da Equação (11),

baseado na abordagem proposta por (Gross et al., 1999) levando em conta a dinâmica da superfície livre. A equação de transporte de escalares, ponderada pela profundidade, é dada de maneira compacta da seguinte forma:

$$\frac{\partial HC}{\partial t} + \nabla \cdot (\mathbf{u}HC - \mathbf{\Gamma}\nabla(HC)) = S_C \tag{12}$$

onde $\mathbf{u} = \mathbf{u}(\mathbf{x}, t)$ é o vetor velocidade e $H = H(\mathbf{x}, t)$ é a profundidade total da água, ambos oriundos do modelo hidrodinâmico (Casulli and Walters 2000); Γ é o tensor difusividade, aqui dado como uma matriz diagonal $\mathbf{\Gamma} = (K_x^h, K_y^h, K_z^v)$ e S_C é um termo de perdas e ganhos, capaz de englobar processos específicos de geração/consumo da substância transportada.

C.4 Modelo de Qualidade d´água

O modelo IPH-ECO pode ser utilizado de forma acoplada, onde hidrodinâmica e qualidade da água são avaliados, ou de forma separada, levando-se em conta apenas processos físicos (hidrodinâmica) ou biológicos (qualidade da água). No caso onde a simulação é realizada de forma acoplada, a solução da Equação de Transporte de Escalares (Eq. 11) é computada para cada parâmetro de qualidade da água simulado, alterando apenas o termo fonte em cada equação. Desta forma, o modelo é capaz de simular Temperatura da água, dinâmica de nutrientes (e.g., C, PO_4, NH_4, NH_3, Si), gases (O_2, CO_2 e CH_4), e biomassa de comunidades aquáticas (e.g., fitoplâncton, macrófitas, peixes).

Na simulação da temperatura da água, o modelo utiliza as forçantes meteorológicas na equação de trasporte advectivo-difusivo de calor, considerando o algoritmo de balanço térmico na interface ar-água (Chapra, 2008), que leva em conta o balanço total de calor a partir da primeira lei da termodinâmica para um fluido incompreensível.

$$\frac{\partial T_{agua}}{\partial t} = \underbrace{f_{T_{gua}}^{ROC}(Alb, Rad)}_{Rad.OndasCurtas} + \underbrace{f_{T_{gua}}^{ROL}(Nuv, T_{Ar}, T_{gua})}_{Rad.OndasLongas} + \underbrace{f_{T_{gua}}^{Evap}(Evap)}_{Evaporacao} + \underbrace{f_{T_{gua}}^{Cond}(W, T_{Ar}, T_{gua})}_{Conducao} \tag{13}$$

Os fluxos de calor considerados correspondem a radiações atmosféricas de onda curta e longa (RAOC e RAOL), radiação de onda longa emitida pela água, e os fluxos de calor por condução e evaporação.

Referências

Alcântara, E. H., Stech, J. L., Lorenzzetti, J. A., Bonnet, M. P., Casamitjana, X., Assireu, A. T., and de Moraes Novo, E. M. L. (2010). Remote sensing of water surface temperature and heat flux over a tropical hydroelectric reservoir. *Remote Sensing of Environment*, 114(11):2651–2665.

Allan, M. G., Hamilton, D. P., Hicks, B., and Brabyn, L. (2015). Empirical and semi-analytical chlorophyll a algorithms for multi-temporal monitoring of New Zealand lakes using Landsat. *Environmental monitoring and assessment*, 187(6):1–24.

Allasia, D. G., Collischonn, W., Tucci, C. E. M., Germano, A., Collischonn, B., and Failache, N. (2004). Modelo hidrológico da bacia do Alto Paraguai. *Simpósio Brasileiro de Recursos Hídricos do Centro-Oeste*, 3.

Alsdorf, D. E., Rodriguez, E., and Lettenmaier, D. P. (2007). Measuring surface water from space. *Reviews of Geophysics*, 45(2).

Austin, J. A. and Colman, S. M. (2007). Lake Superior summer water temperatures are increasing more rapidly than regional air temperatures: A positive ice-albedo feedback. *Geophysical Research Letters*, 34(6).

Bergamino, N., Horion, S., Stenuite, S., Cornet, Y., Loiselle, S., Plisnier, P.-D., and Descy, J.-P. (2010). Spatio-temporal dynamics of phytoplankton and primary production in Lake Tanganyika using a MODIS based bio-optical time series. *Remote Sensing of Environment*, 114(4):772–780.

Bonnet, M. and Wessen, K. (2001). ELMO, a 3-D water quality model for nutrients and chlorophyll: first application on a lacustrine ecosystem. *Ecological Modelling*, 141(1):19–33.

Bravo, J., Allasia, D., Paz, A., Collischonn, W., and Tucci, C. (2011). Coupled hydrologic-hydraulic modeling of the Upper Paraguay River basin. *Journal of hydrologic engineering*, 17(5):635–646.

Buarque, D. C. (2015). *Simulação da geração e do transporte do sedimentos em grandes bacias: Estudo de caso do Rio Madera*. PhD thesis, Universidade Federal do Rio Grando do Sul.

Buarque, D. C., de Paiva, R. C. D., Clarke, R. T., and Mendes, C. A. B. (2011). A comparison of amazon rainfall characteristics derived from trmm, cmorph and the brazilian national rain gauge network. *Journal of Geophysical Research: Atmospheres*, 116(D19).

Bukata, R. P. (2013). Retrospection and introspection on remote sensing of inland water quality. *Journal of Great Lakes Research*, 39:2–5.

Burnett, A. W., Kirby, M. E., Mullins, H. T., and Patterson, W. P. (2003). Increasing great lake-effect snowfall during the twentieth century: a regional response to global warming? *Journal of Climate*, 16(21):3535–3542.

Calmant, S., Seyler, F., and Cretaux, J. F. (2008). Monitoring continental surface waters by satellite altimetry. *Surveys in geophysics*, 29(4):247–269.

Carlson, R. E. (1977). A trophic state index for lakes. *Limnology and oceanography*, 22(2):361–369.

Casulli, V. (1990). Semi-implicit finite difference methods for the two-dimensional shallow water equations. *Journal of Computational Physics*, 86(1):56–74.

Casulli, V. and Cattani, E. (1994). Stability, accuracy and efficiency of a semi-implicit method for three-dimensional shallow water flow. *Computers & Mathematics with Applications*, 27(4):99–112.

Casulli, V. and Cheng, R. T. (1992). Semi-implicit finite difference methods for three-dimensional shallow water flow. *International Journal for numerical methods in fluids*, 15(6):629–648.

Casulli, V. and Walters, R. A. (2000). An unstructured grid, three-dimensional model based on the shallow water equations. *International journal for numerical methods in fluids*, 32(3):331–348.

Chapra, S. C. (2008). *Surface water-quality modeling*. Waveland press.

Chavula, G., Brezonik, P., Thenkabail, P., Johnson, T., and Bauer, M. (2009). Estimating chlorophyll concentration in Lake Malawi from MODIS satellite imagery. *Physics and Chemistry of the Earth, Parts A/B/C*, 34(13):755–760.

Chen, J. and Quan, W. (2013). An improved algorithm for retrieving chlorophyll-a from the yellow river estuary using modis imagery. *Environmental monitoring and assessment*, 185(3):2243–2255.

Chipman, J. and Lillesand, T. (2007). Satellite-based assessment of the dynamics of new lakes in southern Egypt. *International Journal of Remote Sensing*, 28(19):4365–4379.

Cole, T. M. and Wells, S. A. (2006). CE-QUAL-W2: A two-dimensional, laterally averaged, hydrodynamic and water quality model, version 3.5.

Collischonn, B., Collischonn, W., Silva, B. C., and Tucci, C. E. (2005). Simulação hidrológica da bacia do rio São Francisco usando precipitação estimada pelo satélite TRMM: resultados preliminares. *Anais do XVI Simpósio Brasileiro de Recursos Hídricos, ABRH, João Pessoa (PB)*.

Collischonn, B., Collischonn, W., and Tucci, C. E. M. (2008). Daily hydrological modeling in the amazon basin using trmm rainfall estimates. *Journal of Hydrology*, 360(1):207–216.

Collischonn, W., Allasia, D., Da Silva, B. C., and Tucci, C. E. (2007). The MGB-IPH model for large-scale rainfall-runoff modelling. *Hydrological Sciences Journal*, 52(5):878–895.

Collischonn, W. and Tucci, C. (2001). Hydrological simulation of large drainage basins. *Brazilian J. Water Resour*, 6(1):15–35.

Crosman, E. T. and Horel, J. D. (2009). MODIS-derived surface temperature of the Great Salt Lake. *Remote Sensing of Environment*, 113(1):73–81.

Curtarelli, M., Ogashawara, I., Alcântara, E., and Stech, J. (2015). Coupling remote sensing bio-optical and three-dimensional hydrodynamic modeling to study the phytoplankton dynamics in a tropical hydroelectric reservoir. *Remote Sensing of Environment*, 157:185–198.

Curtarelli, M. P., Alcântara, E., Rennó, C. D., Assireu, A. T., Bonnet, M. P., and Stech, J. L. (2014). Modelling the surface circulation and thermal structure of a tropical reservoir using three-dimensional hydrodynamic lake model and remote-sensing data. *Water and Environment Journal*, 28(4):516–525.

Da Silva, B. C., Collischonn, W., Tucci, C. E. M., Clarke, R. T., and Corbo, M. D. (2007). Previsão hidroclimática de vazão de curto prazo na bacia do rio São Francisco. *Revista Brasileira de Recursos Hídricos*, 12:31–47.

Dargahi, B. and Setegn, S. G. (2011). Combined 3D hydrodynamic and watershed modelling of Lake Tana, Ethiopia. *Journal of Hydrology*, 398(1):44–64.

de Paiva, R. C. D., Buarque, D. C., Collischonn, W., Bonnet, M.-P., Frappart, F., Calmant, S., and Bulhões Mendes, C. A. (2013). Large-scale hydrologic and hydrodynamic modeling of the Amazon River basin. *Water Resources Research*, 49(3):1226–1243.

Debele, B., Srinivasan, R., and Parlange, J.-Y. (2008). Coupling upland watershed and downstream waterbody hydrodynamic and water quality models (SWAT and CE-QUAL-W2) for better water resources management in complex river basins. *Environmental Modeling & Assessment*, 13(1):135–153.

Dessie, M., Verhoest, N. E., Pauwels, V. R., Adgo, E., Deckers, J., Poesen, J., and Nyssen, J. (2015). Water balance of a lake with floodplain buffering: Lake Tana, Blue Nile Basin, Ethiopia. *Journal of Hydrology*, 522:174–186.

Dias, J., Sousa, M., Bertin, X., Fortunato, A., and Oliveira, A. (2009). Numerical modeling of the impact of the Ancão Inlet relocation (Ria Formosa, Portugal). *Environmental Modelling & Software*, 24(6):711–725.

Dronkers, J. (1996). The influence of buoyancy on transverse circulation and on estuarine dynamics. *Buoyancy Effects on Coastal and Estuarine Dynamics*, pages 341–356.

El-Alem, A., Chokmani, K., Laurion, I., and El-Adlouni, S. E. (2012). Comparative analysis of four models to estimate chlorophyll-a concentration in case-2 waters using moderate resolution imaging spectroradiometer (MODIS) imagery. *Remote Sensing*, 4(8):2373–2400.

EPA (2000). Environmental Protection Agency. *National water quality inventory report. Washington, DC: US EPA.*

ERM (2006). GEMSS-HDM Hydrodynamic and Transport Module. Technical Documentation. *Surface Modeling Group (SMG). ERM Inc., Exton, PA, USA.*

Fan, F. M., Collischonn, W., Meller, A., and Botelho, L. C. M. (2014). Ensemble streamflow forecasting experiments in a tropical basin: The São Francisco river case study. *Journal of Hydrology*, 519:2906–2919.

Fragoso, C., Ferreira, T. F., and da Motta-Marques, D. (2009a). *Modelagem ecológica em ecossistemas aquáticos*. Modelagem Ecológica.

Fragoso, C. R., Marques, D. M. M., Collischonn, W., Tucci, C. E., and van Nes, E. H. (2008). Modelling spatial heterogeneity of phytoplankton in Lake Mangueira, a large shallow subtropical lake in South Brazil. *Ecological Modelling*, 219(1):125–137.

Fragoso, C. R., Marques, D. M. M., Ferreira, T. F., Janse, J. H., and van Nes, E. H. (2011). Potential effects of climate change and eutrophication on a large subtropical shallow lake. *Environmental Modelling & Software*, 26(11):1337–1348.

Fragoso, C. R., van Nes, E. H., Janse, J. H., and da Motta Marques, D. (2009b). IPH-TRIM3D-PCLake: A three-dimensional complex dynamic model for subtropical aquatic ecosystems. *Environmental Modelling & Software*, 24(11):1347–1348.

Giardino, C., Bartoli, M., Candiani, G., Bresciani, M., and Pellegrini, L. (2007). Recent changes in macrophyte colonisation patterns: an imaging spectrometry-based evaluation of southern lake garda (northern italy). *Journal of Applied Remote Sensing*, 1(1):011509–011509.

Gross, E. S., Koseff, J. R., and Monismith, S. G. (1999). Evaluation of advective schemes for estuarine salinity simulations. *Journal of Hydraulic Engineering*, 125(1):32–46.

Guzman, J. A., Moriasi, D., Gowda, P., Steiner, J., Starks, P., Arnold, J. G., and Srinivasan, R. (2015). A model integration framework for linking SWAT and MODFLOW. *Environmental Modelling & Software*, 73:103–116.

Hong, Y. (2003). Precipitation Estimation from Remotely Sensed Information using Artificial Neural Network-Cloud Classification System.

Horne, A. and Glodman, C. (1994). *Limnology*. McGraw-Hill.

Huang, C., Li, Y., Yang, H., Sun, D., Yu, Z., Zhang, Z., Chen, X., and Xu, L. (2014). Detection of algal bloom and factors influencing its formation in Taihu Lake from 2000 to 2011 by MODIS. *Environmental Earth Sciences*, 71(8):3705–3714.

Huffman, G. J., Bolvin, D. T., Nelkin, E. J., Wolff, D. B., Adler, R. F., Gu, G., Hong, Y., Bowman, K. P., and Stocker, E. F. (2007). The TRMM multisatellite precipitation analysis (TMPA): Quasi-global, multiyear, combined-sensor precipitation estimates at fine scales. *Journal of Hydrometeorology*, 8(1):38–55.

Huot, Y., Babin, M., Bruyant, F., Grob, C., Twardowski, M., and Claustre, H. (2007). Does chlorophyll a provide the best index of phytoplankton biomass for primary productivity studies? *Biogeosciences discussions*, 4(2):707–745.

Hutter, K., Wang, Y., and Chubarenko, I. P. (2010). *Physics of Lakes: Volume 1: Foundation of the Mathematical and Physical Background*. Springer Science & Business Media.

Janse, J. H. (2005). *Model studies on the eutrophication of shallow lakes and ditches*. Wageningen University, Ph.D. thesis.

Jay, D. A. (1990). Residual circulation in shallow estuaries: shear, stratification and transport processes. In *Residual currents and long-term transport*, pages 49–63. Springer.

Jensen, J. R. (2009). *Remote sensing of the environment: An earth resource perspective 2/e*. Pearson Education India.

Ji, Z.-G. (2017). *Hydrodynamics and water quality: modeling rivers, lakes, and estuaries*. John Wiley & Sons.

Joyce, R. J., Janowiak, J. E., Arkin, P. A., and Xie, P. (2004). CMORPH: A method that produces global precipitation estimates from passive microwave and infrared data at high spatial and temporal resolution. *Journal of Hydrometeorology*, 5(3):487–503.

Ke, L. and Song, C. (2014). Remotely sensed surface temperature variation of an inland saline lake over the central Qinghai–Tibet Plateau. *ISPRS Journal of Photogrammetry and Remote Sensing*, 98:157–167.

Kouwen, N., Soulis, E., Pietroniro, A., Donald, J., and Harrington, R. (1993). Grouped response units for distributed hydrologic modeling. *Journal of Water Resources Planning and Management*, 119(3):289–305.

Kragt, M. E., Robson, B. J., and Macleod, C. J. (2013). Modellers' roles in structuring integrative research projects. *Environmental modelling & software*, 39:322–330.

Kuo, A. Y., Hamrick, J. M., and Sisson, G. M. (1990). Persistence of residual currents in the james river estuary and its implication to mass transport. In *Residual Currents and Long-Term Transport*, pages 389–401. Springer.

Li, Y., Zhang, Q., Yao, J., Werner, A. D., and Li, X. (2013). Hydrodynamic and hydrological modeling of the Poyang Lake catchment system in China. *Journal of Hydrologic Engineering*, 19(3):607–616.

Liang, X., Lettenmaier, D. P., Wood, E. F., and Burges, S. J. (1994). A simple hydrologically based model of land surface water and energy fluxes for general circulation models. *Journal of Geophysical Research: Atmospheres*, 99(D7):14415–14428.

Liu, G., Ou, W., Zhang, Y., Wu, T., Zhu, G., Shi, K., and Qin, B. (2015). Validating and Mapping Surface Water Temperatures in Lake Taihu: Results From MODIS Land Surface Temperature Products. *Selected Topics in Applied Earth Observations and Remote Sensing, IEEE Journal of*, 8(3):1230–1244.

Longstaff, B. J. and Nauman, E. (2010). *Integrating and Applying Science: A practical handbook for effective coastal ecosystem assessment*. IAN Press.

Ludwig, K. and Bremicker, M. (2006). *The water balance model LARSIM: design, content and applications*. Institut fur Hydrologie der Universitat Freiberg i. Br.

Martin, J. L. and McCutcheon, S. C. (1998). *Hydrodynamics and transport for water quality modeling*. CRC Press.

Martin, J. L., Wool, T., and Olson, R. (2002). A dynamic one-dimensional model for hydrodynamics and water quality. *EPDRiv1 Version*, 1.

Merritt, W. S., Letcher, R. A., and Jakeman, A. J. (2003). A review of erosion and sediment transport models. *Environmental Modelling & Software*, 18(8):761–799.

Miranda, L. B. (2002). *Princípios de Oceanografia Física de Estuários Vol. 42*. Edusp.

Monteith, J. (1965). Evaporation and environment. The state and movement of water in living organisms. Symposium of the society of experimental biology, Vol. 19 (pp. 205-234).

Nickus, U., Bishop, K., Erlandsson, M., Evans, C., Forsius, M., Laudon, H., Livingstone, D., Monteith, D., and H., T. (2010). Direct impacts of climate change on freshwater ecosystems. *M. Kernan, R. Battarbee, B. Moss (Eds.), Climate Change Impacts on Freshwater Ecosystems.*, 38(4).

Nijssen, B., Lettenmaier, D. P., Liang, X., Wetzel, S. W., and Wood, E. F. (1997). Streamflow simulation for continental-scale river basins. *Water Resources Research*, 33(4):711–724.

Olmanson, L. G., Brezonik, P. L., and Bauer, M. E. (2011). Evaluation of medium to low resolution satellite imagery for regional lake water quality assessments. *Water Resources Research*, 47(9).

Paiva, R. C. D., Buarque, D. C., Clarke, R. T., Collischonn, W., and Allasia, D. G. (2011). Reduced precipitation over large water bodies in the Brazilian Amazon shown from TRMM data. *Geophysical Research Letters*, 38(4).

Panosso, R. d. F., Attayde, J., Muehe, D., and Esteves, F. (1998). Morfometria das lagoas Imboassica, Cabiúnas, Comprida e Carapebus: Implicações para seu funcionamento e manejo. *Ecologia das Lagoas Costeiras do Parque Nacional da Restinga de Jurubatiba e do Município de Macaé (RJ). Rio de Janeiro: NUPEM/UFRJ*, pages 91–108.

Patro, S., Chatterjee, C., Singh, R., and Raghuwanshi, N. S. (2009). Hydrodynamic modelling of a large flood-prone river system in india with limited data. *Hydrological Processes*, 23(19):2774–2791.

Quiroz, K. and Collischonn, W. (2015). Método de combinação de dados de precipitação estimados por satélite e medidos em pluviômetros para a modelagem hidrológica. *Revista Brasileira de Recursos Hídricos*, 20(1):202–217.

Rawls, W. J., Ahuja, L. R., Brakensiek, D. L., Shirmohammadi, A., Maidment, D., et al. (1992). *Infiltration and soil water movement.* McGraw-Hill Inc.

Rolim, S. B. A., Degrazia, G. A., Xavier, M. B., Hackmann, C. L., and Pereira Filho, W. (2015). Remote Surface Temperature Measurements of a Coastal Lagoon in Southern Brazil: Periods of Winter and Summer. *American Journal of Environmental Engineering*, 5(1A):78–84.

Rozante, J. R. and Cavalcanti, I. F. A. (2008). Regional eta model experiments: SALLJEX and MCS development. *Journal of Geophysical Research: Atmospheres (1984–2012)*, 113(D17).

Rozante, J. R., Moreira, D. S., de Goncalves, L. G. G., and Vila, D. A. (2010). Combining TRMM and surface observations of precipitation: technique and validation over South America. *Weather and Forecasting*, 25(3):885–894.

Ruiz-Verdú, A., Koponen, S., Heege, T., Doerffer, R., Brockmann, C., Kallio, K., Pyhälahti, T., Peña, R., Polvorionos, A., Heblinski, J., et al. (2008). Development of MERIS lake water algorithms: Validation results from Europe. In *Proceedings of theâ 2nd MERIS/(A) ATSR User Workshopâ, Frascati, Italy, 22– 26 September 2008 (ESA SP-666, November 2008)*. Citeseer.

Schalles, J. F. (2006). Optical remote sensing techniques to estimate phytoplankton chlorophyll a concentrations in coastal. In *Remote sensing of aquatic coastal ecosystem processes*, pages 27–79. Springer.

Shuttleworth, W. J. (1993). Evaporation in: Maidment, dr"handbook of hydrology.

Sima, S., Ahmadalipour, A., and Tajrishy, M. (2013). Mapping surface temperature in a hyper-saline lake and investigating the effect of temperature distribution on the lake evaporation. *Remote Sensing of Environment*, 136:374–385.

Steissberg, T. E., Hook, S. J., and Schladow, S. G. (2005). Characterizing partial upwellings and surface circulation at Lake Tahoe, California–Nevada, USA with thermal infrared images. *Remote Sensing of Environment*, 99(1):2–15.

Stocker, T. F., Qin, D., Plattner, G. K., Tignor, M., and Allen, S. K. (2013). Summary for policymakers, in: Clima te Change 2013: The Physical Science Basis. Contribution of Working Group 1 to the Fifth Assessment Report of the Intergovernmental Panel on Climate Change. *Cambridge Univ. Press, Cambridge, U. K.*, 38(4).

Tebbs, E., Remedios, J., and Harper, D. (2013). Remote sensing of chlorophyll-a as a measure of cyanobacterial biomass in lake bogoria, a hypertrophic, saline–alkaline, flamingo lake, using landsat etm+. *Remote Sensing of Environment*, 135:92–106.

Todini, E. (1996). The ARNO rainfall-runoff model. *Journal of Hydrology*, 175(1):339–382.

Tucci, C. (2005). Modelos Hidrológicos. Associação Brasileira de Recursos Hídricos/ABRH.

Tucci, C. E. et al. (1998). *Modelos hidrológicos*. UFRGS.

Tucci, C. E. M., Clarke, R. T., Collischonn, W., da Silva Dias, P. L., and de Oliveira, G. S. (2003). Long-term flow forecasts based on climate and hydrologic modeling: Uruguay River basin. *Water Resources Research*, 39(7).

Uncles, R. and Stephens, J. (1996). Buoyancy phenomena in the Tweed estuary. *Buoyancy Effects on Coastal and Estuarine Dynamics*, pages 175–193.

Wang, M., Shi, W., and Tang, J. (2011). Water property monitoring and assessment for China's inland Lake Taihu from MODIS-Aqua measurements. *Remote Sensing of Environment*, 115(3):841–854.

Warren, I. and Bach, H. (1992). Mike 21: a modelling system for estuaries, coastal waters and seas. *Environmental Software*, 7(4):229–240.

Wool, T. A., Ambrose, R. B., Martin, J. L., Comer, E. A., and Tech, T. (2006). Water quality analysis simulation program (WASP). *Userâs Manual, Version*, 6.

Wooster, M., Patterson, G., Loftie, R., and Sear, C. (2001). Derivation and validation of the seasonal thermal structure of Lake Malawi using multi-satellite AVHRR observations. *International Journal of Remote Sensing*, 22(15):2953–2972.

Wynne, T. T., Stumpf, R. P., Tomlinson, M. C., Fahnenstiel, G. L., Dyble, J., Schwab, D. J., and Joshi, S. J. (2013). Evolution of a cyanobacterial bloom forecast system in western lake erie: Development and initial evaluation. *Journal of Great Lakes Research*, 39:90–99.

Xiao, F., Ling, F., Du, Y., Feng, Q., Yan, Y., and Chen, H. (2013). Evaluation of spatial-temporal dynamics in surface water temperature of Qinghai Lake from 2001 to 2010 by using MODIS data. *Journal of Arid Land*, 5(4):452–464.

Xu, Z., Godrej, A. N., and Grizzard, T. J. (2007). The hydrological calibration and validation of a complexly-linked watershed–reservoir model for the Occoquan watershed, Virginia. *Journal of Hydrology*, 345(3):167–183.

Zhang, G., Yao, T., Xie, H., Qin, J., Ye, Q., Dai, Y., and Guo, R. (2014). Estimating surface temperature changes of lakes in the Tibetan Plateau using MODIS LST data. *Journal of Geophysical Research: Atmospheres*, 119(14):8552–8567.